"RADIOMICS BASED ASSESSMENT OF PULMONARY NODULES DETECTED ON HIGH RESOLUTION COMPUTED TOMOGRAPHY OF THE CHEST: A ONE YEAR HOSPITAL BASED OBSERVATION STUDY"

BY

REGISTRATION NUMBER. BS0121012

Dissertation

Submitted to
KAHER, Belagavi, Karnataka,
In partial fulfilment of the requirements for the degree of

M.D.

In

RADIO-DIAGNOSIS

J. N. MEDICAL COLLEGE,
BELAGAVI -590010. KARNATAKA

DEC – 2024/JAN – 2025

KLE ACADEMY OF HIGHER EDUCATION AND RESEARCH,

BELAGAVI, KARNATAKA

Endorsement by the HOD/Principal/ Head of the Institution

This is to certify that the dissertation **"RADIOMICS BASED ASSESSMENT OF PULMONARY NODULES DETECTED ON HIGH RESOLUTION CHEST TOMOGRAPHY: A ONE YEAR, HOSPITAL BASED, OBSERVATIONAL STUDY"** is a bonafide research work done by **REG NO BS0121012**.

Dr. SANTOSH D. PATIL
M.D.(Radio-Diagnosis)
Professor & HOD
Dept. of Radio-diagnasis
J.N. Medical College, BELAGAVI-10.
KMC Reg No. 58456

Dr. SANTOSH D PATIL
M.D. RADIO-DIAGNOSIS

Professor and Head,
Department of Radio Diagnosis,
J. N. Medical College,
Nehru Nagar, Belagavi – 590010

Date: 26/06/24
Place: Belagavi

KAHER
J.N. MEDICAL COLLEGE
BELAGAVI

Dr. N.S. MAHANTASHETTI
M. D. PEDIATRICS

Principal,
J. N. Medical College,
Nehru Nagar, Belagavi – 590010

PRINCIPAL
J.N. Medical College,
BELAGAVI- 590 010

26/06/24
Place : Belagavi

UNDERTAKING

I, Reg. No. BS0121012, hereby declare that the information and the data mentioned in my dissertation entitled **"RADIOMICS BASED ASSESSMENT OF PULMONARY NODULES DETECTED ON HIGH RESOLUTION COMPUTED TOMOGRAPHY OF THE CHEST: A ONE YEAR HOSPITAL BASED OBSERVATION STUDY"** belongs to me and is original. I am aware of the definition of plagiarism as detailed below:

- An act or instance of using or closely imitating the language and thoughts of another author without authorization and the representation of that author's work as one's own, as by not crediting the original author.
- A piece of writing or other work reflecting such unauthorized use or imitation.
- The deliberate or reckless representation of another's words, thoughts or ideas as one's own without attribution in connection with submission of academic work, whether graded or otherwise.

I hereby declare that the dissertation prepared by me is original one and does not involve plagiarism anywhere. In case at a later stage, it is found that I have indulged in plagiarism, then I am solely responsible for the same and the institution is at liberty to take any disciplinary action against me including cancellation of dissertation or any other penalties imposed by the University.

Date:26/06/2024

Place: Belagavi **(REG. NO. BS0121012,)**

PLAGIARISM CERTIFICATE

KLE JAWAHARLAL NEHRU MEDICAL COLLEGE
(A constituent unit of KLE Academy of Higher Education & Research Deemed-to-be-University)
(Recognized by National Medical Commission, New Delhi)
Accredited 'A+' Grade by NAAC (3rd Cycle) Placed in Category 'A' by MoE (GoI)
Nehru Nagar, Belagavi- 590 010, Karnataka, INDIA
0831 - 2471350 0831 - 2470759 www.jnmc.edu principal@jnmc.edu

Ref No: MDC/PG/ Date: 25-06-2024

"ACCEPTANCE LETTER"

The softcopy of thesis entitled: **"RADIOMICS BASED ASSESSMENT OF PULMONARY NODULES DETECTED ON HIGH RESOLUTION CHEST TOMOGRAPHY: A ONE YEAR HOSPITAL OBSERVATIONAL STUDY"** has been submitted for anti-plagiarism check through Turnitin software. The scan has been carried out and the scanned output reveals a match percentage of **07%** which is within the acceptable limits of **10%** as per the guidelines given by UGC.

Guide.

KAHER BELAGAVI J.N. MEDICAL COLLEGE

Dr. (Mrs.) N.S. Mahantashetti.
Chairperson-Antiplagiarism Committee &
Principal,
J. N. Medical College, Belagavi.

PRINCIPAL
J.N. Medical College,
BELAGAVI- 590 010

To,
Reg. No. BS0121012
Postgraduate Student,
2021-22 Batch,
Department of Radio-Diagnosis
J. N. Medical College, Belagavi.

ETHICAL CLEARANCE CERTIFICATE

Accredited "A" Grade by NAAC in 3rd Cycle Placed in Cat. 2017 "A" by MHRD (Govt.)

JNMC INSTITUTIONAL ETHICS COMMITTEE
JAWAHARLAL NEHRU MEDICAL COLLEGE,
NEHRU NAGAR, BELAGAVI-590010 (KARNATAKA-INDIA)

Website: http//www.jnmc.edu
E-Mail : dome@jnmc.edu

Phone: (+91-(0)831 Office : 2472550
Principal: 2471701
Fax No. +91 (0)831 - 2470759

Ref No.MDC/JNMCIEC/ 237 **Date: 7/10/2022**

To,

REGISTRATION NUMBER. BS0121012

PG Student in Radio-diagnosis,
J. N. Medical College,
BELAGAVI.

Sub: Institutional Ethical Clearance for the study.

With reference to the above, we wish to inform you that your proposed research project titled **"RADIOMICS BASED ASSESSMENT OF PULMONARY NODULES DETECTED ON HIGH RESOLUTION CHEST TOMOGRAPHY: A ONE YEAR, HOSPITAL BASED, OBSERVATIONAL STUDY"** is ethical and justifiable. The proposed research project has been cleared by the JNMC Institutional Ethics Committee.

(Dr. Smita Sonoli)
Member Secretary
JNMC Institutional Ethics Committee
J.N.Medical College, Belagavi.

for **(Dr. Harsha Hegde)**
Chairman,
JNMC Institutional Ethics Committee
J.N.Medical College, Belagavi

LIST OF CONTENTS

ABSTRACT

BACKGROUND

Pulmonary nodules are a frequent incidental finding on thoracic CT scans, observed in approximately 30-50% of adult scans and 0.2% of chest radiographs. While most pulmonary nodules stem from previous infections or benign causes, their clinical significance varies based on size, growth rate, and malignancy potential. Small nodules typically follow a benign course and require no intervention, whereas larger or suspicious nodules necessitate histopathological evaluation to exclude malignancy (Swensen et al., 2000).

The diagnostic challenge posed by pulmonary nodules is significant due to overlapping imaging features between benign and malignant lesions, variations in nodule characteristics over time, and limitations of imaging modalities in detecting small or subtle lesions. Conventional imaging relies on visual interpretation of descriptive parameters such as size, shape, and borders, but these subjective assessments are prone to inter- and intra-observer variability, leading to potential misdiagnosis (McWilliams et al., 2013).

Radiomics, an emerging field, offers a promising solution by extracting a plethora of quantitative features from medical images. This data-driven approach aims to enhance diagnostic accuracy, prognosis, and therapy response predictions. Radiomics transforms standard medical images into high-dimensional data, capturing details about pixel intensity distributions, texture patterns, and spatial relationships within the imaged tissue that are not discernible by visual inspection alone (Aerts et al., 2014).

In the context of pulmonary nodules, several studies have demonstrated the potential of radiomics in pulmonary nodule evaluation. For instance, Hawkins et al. (2016) showed that machine learning models incorporating radiomic features achieved sensitivities of up to 90% and specificities of 85% in distinguishing malignant from benign nodules. Additionally, McWilliams et al. (2013) developed a risk prediction model based on nodule characteristics, patient demographics, and smoking history, providing valuable insights into the likelihood of malignancy in early-stage nodules.

Radiomics represents a paradigm shift in medical imaging, transforming conventional images into high-dimensional data that reveal detailed tissue characteristics. The extraction and analysis of quantitative imaging features allow for a comprehensive evaluation of pulmonary nodules beyond what is discernible through traditional visual inspection.

By examining features related to texture, shape, and intensity, radiomics provides an in-depth understanding of the nodule's biological behavior. This research aims to harness the full potential of radiomics, emphasizing its role in differentiating between benign and malignant nodules with greater precision.

The objective of this study is to use IBEX, a radiomics based open-source software for the evaluation and qualitative assessment of pulmonary nodules on high resolution chest tomography over a period of one year

OBJECTIVES

The primary objective of this research is to explore and validate the use of radiomics in the evaluation and qualitative assessment of pulmonary nodules through the utilization of the Imaging Biomarker Explorer (IBEX), an open-source radiomics software.

This study is based on IBEX, a robust and versatile platform for radiomic analysis. IBEX facilitates the extraction, quantification, and visualization of complex imaging data, making it an ideal tool for this research. The objective is to leverage IBEX to analyze various radiomic features of pulmonary nodules, providing a detailed and objective assessment.

This study aims to discuss the principles of radiomics, methodologies for feature extraction and analysis, current advancements, and emerging trends, as well as future directions and challenges in the field.

In summary, this study seeks to advance the field of radiomics in the evaluation of pulmonary nodules, leveraging the capabilities of IBEX to enhance diagnostic and prognostic accuracy, streamline clinical workflows, and contribute to precision medicine.

MATERIALS & METHODS:

The study will employ a 128-slice Computed Tomography Revolution EVO Wipro (GE Healthcare USA) machine. All patients referred to the radiology department will undergo a standard high-resolution computed tomography scan of the thorax. The scans will be thoroughly evaluated for pulmonary nodules, and all findings will be systematically recorded and analyzed. Informed consent will be obtained from all participants before their inclusion in the study.

Radiomic analysis will be performed using IBEX. DICOM files will be imported into IBEX, radiomic features extracted and visualized through histograms and scatter plots. Subsequently, statistical analysis will be conducted to identify features correlated with nodule malignancy. The analysis results will be exported and compiled into a detailed report in Excel or CSV format.

EXAMPLE WORKFLOW

- Import DICOM Files: Navigate to the import or load section in IBEX and load DICOM files of lung CT scans into IBEX.
- Perform segmentation to outline lung nodules i.e. establishing region of interest
- Select radiomic features like texture and shape for extraction.
- Extract features and visualize the data using histograms and scatter plots.
- Export the analysis results as an excel/ csv file.
- Validate the findings through cross-validation

RESULTS:

The study focuses on the application of radiomics to the evaluation of pulmonary nodules using the Imaging Biomarker Explorer (IBEX) to derive comprehensive radiomic features extracted from computed tomography (CT) scans, offering insights into the quantitative characterization of pulmonary nodules. This section presents the findings and statistical outcomes derived from the data.

The observed bimodal and multimodal patterns in Surface Area, Volume, and Kurtosis suggest distinct subpopulations within the dataset, likely due to varied data collection methods or inherent attribute variability. The left-skewed distributions for F4-IntensityDirect and F5-IntensityDirect indicate a predominance of lower intensity values, reflecting specific sample traits that warrant further investigation for deeper insights.

Correlation heatmaps show moderate relationships among certain intensity measures, implying potential interactions, but the generally weak correlations suggest overall independence among these measures due to diverse influencing factors or measurement conditions. Box plots and density plots reveal significant variability in

Global Entropy, Kurtosis, and Skewness, indicating a diverse dataset with a wide range of characteristics. Analysis of energy and correlation measures across various angles highlights unique directional properties, suggesting further investigation into these specific patterns. To better understand the underlying patterns and relationships, cluster analysis techniques could identify distinct subgroups within the data, revealing latent structures.

DISCUSSION

Radiomics extracts numerous quantitative features from medical images, offering detailed tissue characterization not visible through traditional methods. In pulmonary nodules, these features act as biomarkers for predicting malignancy, assessing treatment response, and forecasting outcomes. This method identifies subtle patterns and heterogeneities crucial for distinguishing between benign and malignant nodules.

Traditional imaging focuses on size, shape, and border characteristics, which are subjective and often fail to capture tumor heterogeneity. Radiomics addresses this by providing a comprehensive, objective assessment through quantitative analysis.

Clinically, radiomics enhances the management of pulmonary nodules by facilitating early and accurate diagnosis, timely intervention, and personalized treatment planning, thus improving patient outcomes and reducing unnecessary procedures.

Radiomics is transformative in pulmonary nodule evaluation, utilizing platforms like IBEX to enable detailed data analysis, fostering innovation, and improving precision medicine. It integrates clinical and molecular data to advance patient care.

In conclusion, radiomics through IBEX enhances diagnostic accuracy and personalized treatment. Continued research and collaboration are crucial to fully realize its potential in clinical practice.

INTRODUCTION

Pulmonary nodules are a common incidental finding on CT scans of the thorax, in approximately 30-50% of adult CT scans and 0.2% of chest radiographs. (1)

The majority of pulmonary nodules are the result of old infections, scar tissue, or secondary to other asymptomatic causes, which follow a benign course. The clinical implications depend on size, rate of growth and probability of malignant transformation. Small nodules are usually benign and require no intervention, larger nodules or those with concerning features warrant histopathological diagnosis to rule out malignancy. (2)

In their study Swensen et al., 2000 (3) developed and validated a predictive model to estimate the probability of malignancy in solitary pulmonary nodules based on clinical and radiographic features. Another study by McWilliams, A., et al. (2013) (3) assessed the likelihood of malignancy in pulmonary nodules detected during initial screening CT scans based on nodule characteristics, patient demographics, and smoking history, providing insights into probability of malignancy in early-stage nodules, particularly among high-risk individuals

The diagnosis of pulmonary nodules can be challenging due to overlapping imaging features between benign and malignant lesions, temporal variability in nodule and the poor performance of conventional imaging modalities to detect small or subtle lesions.

Conventional imaging techniques relies on visual interpretation of descriptive parameters (quantitative parameters) such as size, shape, nature of extent, borders, positional relationship to surrounding tissue, and relative vascularity of a lesion.

However, these subjective assessments can suffer from large inter & intra-observer variability.

Conventional imaging techniques based on quantitative parameters have limited sensitivity and specificity, leading to unnecessary interventions or missed diagnoses. Hence, it is imperative to adopt more objective methods for evaluating pulmonary nodules. This necessity arises from the limitations of current subjective approaches, which can lead to significant variability in assessment and diagnosis. By integrating objective techniques, we can enhance the accuracy and consistency of pulmonary nodule evaluation, ultimately improving patient outcomes.

Additionally in oncology imaging, the critical implications of tumor heterogeneity are often overlooked, despite its significant impact for diagnosis and treatment. Tumor heterogeneity describes the observation that different tumor cells within the same patient can exhibit distinct morphological and phenotypic profiles, including variations in cellular morphology, gene expression, metabolism, motility, proliferation, and metastatic potential. (5)

Tumor heterogeneity suggests that different regions within a single tumor, as well as different tumors in the same patient can show substantial differences. Consequently, random samples of tumor tissues obtained through invasive biopsy for molecular characterization may fail to accurately represent the full extent of biological variation within tumors, *(7)* On the other hand, the entire tumor can be sampled non-invasively and repeatedly with medical imaging.

Additionally, tumor variability can significantly affect how tumors respond to treatments and influence patient outcomes. The assimilation of data on heterogeneity measures can be used to identify longitudinal trends in the development of disease, develop novel targeted therapies and predict clinical outcomes.

Furthermore, there is comprehensive literary evidence indicating that medical images contain detailed information on phenotypic patterns, which explain the underlying molecular and genetic biology of tumors. These qualitative aspects extend beyond the limited parameters currently used in clinical practice. (8-10)

Thus, there is an imperative need for a combined approach that optimally utilizes both qualitative and quantitative features extracted from medical images, which can be achieved through the application of radiomics. This fusion of methodologies can lead to a more comprehensive understanding and management of tumor heterogeneity.

RADIOMICS

Radiomics enables the characterization of tissue properties that may otherwise not be discernible by visual inspection alone. Radiomics aims to transform medical images into mineable data by extraction and analysis of quantitative imaging features from medical images for the purpose of disease diagnosis, prognosis, and treatment response prediction. These imaging features capture information about the spatial distribution of pixel intensities, texture patterns, shape characteristics, and spatial relationships within the imaged tissue.

Radiomics has been extensively investigated and validated across multiple domains of medicine. In the field of oncology, radiomics has been extensively studied

in oncology for tumor characterization, prediction of treatment response, and prognostication.

(Kumar et al., 2012*)* have showed that radiomics can help in monitoring the response to therapies such as chemotherapy, radiotherapy, and immunotherapy by analyzing changes in imaging features over time (12). For example, radiomics features have been used to predict the aggressiveness of lung cancer and patient survival in the study by (Hawkins et al., 2016) (5).

In cardiology, (Li et al., 2021) have explored the use of radiomics in the assessment of myocardial tissue characteristics, prediction of cardiac events, and evaluation of treatment outcomes in diseases such as heart failure and coronary artery disease (13).

In neurology, radiomics has been tested for differentiation of brain tumor subtypes, prediction of treatment response in glioblastoma, and the assessment of neurological diseases such as Alzheimer's and multiple sclerosis (14)

The field of radiomics has seen significant advancements due to the development of specialized software platforms. These tools are designed to facilitate the analysis and visualize complex imaging data, enabling researchers and clinicians to identify and quantify patterns that may not be discernible through conventional methods. Among the numerous radiomics platforms available IBEX, 3D Slicer, PyRadiomics, CaPTk, LIFEx, Radiomics.io, ITK-SNAP have gained considerable popularity within the medical imaging community.

These platforms are open-source, making them freely accessible for use and modification. This openness fosters a collaborative environment that promotes innovation and development in radiomics.

IMAGING BIOMARKER EXPLORER

The Imaging Biomarker Explorer (IBEX) is a specialized tool or platform designed to facilitate the identification, analysis, and exploration of imaging biomarkers. Imaging biomarkers are quantitative indicators derived from medical images that can be used to assess biological processes, pathological changes, or responses to therapy.

IBEX integrates various types of imaging data (CT, MRI, PET) and associated clinical data, providing a comprehensive platform for biomarker discovery and validation. The platform typically includes tools for extracting quantitative features from medical images, such as texture, shape, and intensity metrics. It allows for advanced visualization capabilities, allowing researchers to explore and interpret the extracted features and their correlations with clinical outcomes. It also includes built-in statistical and machine learning tools to analyse the extracted features, helping to identify significant biomarkers and their associations with disease states or treatment responses.

IBEX WORKFLOW:

The workflow of radiomics encompasses several key steps, each crucial for the extraction of quantitative data from medical images and the subsequent analysis to derive clinically relevant insights.

Image Acquisition:

The process begins with the acquisition of medical imaging data, such as CT scans, MRI, PET scans, or others, depending on the clinical indication and modality availability.

Image Preprocessing:

Preprocessing is essential to standardize images and correct for variations introduced during acquisition, ensuring uniformity across datasets.

Common preprocessing steps include noise reduction, intensity normalization, spatial resampling, and image registration to align images from different time points or modalities.

Region of Interest (ROI) Segmentation:

ROI segmentation involves delineating the region of interest within the medical image that corresponds to the pathology or anatomical structure of interest.

Manual or automated segmentation techniques may be employed, depending on the complexity of the region and the available tools.

Feature Extraction:

A wide range of imaging features can be extracted from pulmonary nodule images using radiomics analysis. These features capture information about nodule intensity, texture, shape, and spatial relationships, which are potentially relevant for distinguishing between benign and malignant nodules.

Shape features quantify geometric properties of the nodule, such as volume, surface area, sphericity, and irregularity.

Texture features capture spatial patterns and relationships between adjacent pixels, including entropy, energy, contrast, homogeneity, and correlation.

Intensity-based features describe the distribution of pixel intensities within the ROI, such as mean, median, standard deviation, skewness, and kurtosis.

Spatial features capture spatial relationships and interactions between different regions within the nodule, such as distance-based features, neighborhood intensity difference features, and fractal-based features.

The detailed descriptions of the feature sets used in this study are provided below.

GREY LEVEL COOCURRENCE MATRIX

The Gray Level Co-occurrence Matrix (GLCM) is a statistical approach to analyze texture for pattern recognition for medical imaging. The GLCM examines the spatial relationship between pixels and derives various texture features describing the image's characteristics (4,15). Several peer-reviewed studies have demonstrated a high correlation between GLCM (Gray Level Co-occurrence Matrix) analysis based on computed tomography (CT) and the identification of malignant pulmonary nodules which highlight the effectiveness of GLCM in distinguishing malignant nodules from benign ones by analyzing texture features. The study published by (15) evaluated the diagnostic value of artificial intelligence (AI) combined with GLCM-based texture analysis for distinguishing between benign and malignant pulmonary nodules. The study found that AI models, which included GLCM features, had a sensitivity of 94.69% in detecting pulmonary nodules, outperforming traditional physician readings which had a sensitivity of 85.40%.

The GLCM is a matrix where the number of rows and columns corresponds to the number of gray levels (intensities) in the image. Each element of the matrix (i,j)(i, j)(i,j) indicates the frequency with which two pixels, separated by a specific spatial relationship (defined by distance and angle), occur with gray levels iii and jjj.

The steps involved to construct a GLCM include quantifying the image to reduce the number of grey levels, define parameters about distance and direction (e.g., 0°, 45°, 90°, 135°) of spatial relationship, followed by estimating the frequencies for each pair of pixel values at a given distance and direction.

Few examples of the features extracted from GLCM include – Contrast, Correlation, Energy.

CONTRAST

Contrast is a measure that computes the local variations in the GLCM. Contrast as a feature can extract information at various contrast levels, namely low contrast images wherein the differences between gray levels are minimal. Medium contrast images have more noticeable differences in gray levels in which contrast and correlation features can be effectively used to identify patterns and structures and high contrast images have significant differences between gray levels wherein features like contrast and energy become more prominent as they highlight sharp variations and edges (15).

Aerts et al. (2014) demonstrated the utility of contrast features in non-invasive tumor characterization, highlighting their role in distinguishing malignant from benign nodules with high accuracy. Their study indicated that contrast features, as part of a comprehensive radiomic analysis, could significantly improve diagnostic workflows(4).

It is calculated using the formula

Contrast=∑i,j(i−j)2P(i,j)\text{Contrast} = \sum_{i,j} (i - j)^2 P(i, j),

Contrast=i,j∑(i−j)2P(i,j)

CORRELATION

Measures the degree to which a pixel is correlated to its neighbor. Lambin et al. (2015) provided a comprehensive overview of radiomics, emphasizing the importance of correlation features in understanding the heterogeneity of lung tumors(16). It is calculated by:

Correlation=∑i,j(i−μi)(j−μj)P(i,j)σiσj\text{Correlation} = \frac{\sum_{i,j} (i - \mu_i)(j - \mu_j) P(i, j)}{\sigma_i \sigma_j}Correlation=σiσj∑i,j(i−μi)(j−μj)P(i,j)

ENERGY:

Represents the sum of squared elements in the GLCM, also known as uniformity or the angular second moment (4). (Kumar et al. 2015) focused on the role of energy features in the comprehensive characterization of lung tumors. Their study underscored the potential of energy features in improving the precision of radiomic analyses and supporting personalized treatment strategies (17). It is calculated by:

Energy=∑i,jP(i,j)2\text{Energy} = \sum_{i,j} P(i, j)^2Energy=i,j∑P(i,j)2

BUSYNESS

Busyness is a texture feature derived from Neighbor Intensity Difference (NID) matrices. It quantifies the rate of change of intensity between neighboring pixels and provides an indication of the local variability or heterogeneity of the image, capturing the complexity of the texture. Busyness indicates the heterogeneity within a tumor, often linked to its aggressiveness. Higher busyness values suggest greater complexity and variability within the tissue texture, which correlates with increased risk of malignancy. It is calculated using the NGTDM, which compares the gray level of a pixel to the average gray level of its neighbors

To calculate busyness, a neighborhood around each pixel is defined, typically using a fixed-size window (e.g., 3x3 or 5x5) centered on each pixel following which difference between its gray level and the average gray level of its surrounding neighbors is determined using:

d(i, j) = |I(i, j) - \bar{I}(i, j)|]

Where I(i,j)I(i, j)I(i,j) is the gray level of the pixel at position (i,j)(i, j)(i,j) and I¯(i,j)\bar{I}(i, j)I¯(i,j) is the average gray level of its neighbors.

Subsequently NGTDM is constructed where element represents the sum of the absolute differences for a particular gray level. Finally, busyness of a pixel of interest can be estimated using the formula

{Busyness} = \frac{\sum_{i=1}^{N} \sum_{j=1}^{N} |I(i, j) - \bar{I}(i, j)|}{\sum_{i=1}^{G} P(i) \times N}]

Here, NNN is the total number of pixels, GGG is the number of gray levels, and P(i)P(i)P(i) is the number of pixels with gray level iii.

COARSENESS

Coarseness is a texture feature derived from Neighbor Intensity Difference (NID) matrices. It quantifies the level of spatial variation in pixel intensity values within an image i.e. it measures the granularity of the texture, indicating how smooth or rough an image appears.

Coarseness helps in analyzing the texture of tumors, which often exhibit different textural properties compared to normal tissues. By quantifying coarseness, radiologists can gain insights into the nature of the tumor (19).

Malignant tumors may have a more heterogeneous and coarse texture compared to benign tumors or healthy tissue (20). A high coarseness value corresponds to a smoother texture while a low coarseness value indicates a rougher texture with frequent intensity changes.

Changes in the coarseness value can indicate alterations in the tumor's texture, which linearly correlates with the treatment efficacy (8). Studies have shown that texture features, including coarseness, are associated with patient outcomes. Tumors with higher coarseness values might be associated with a better prognosis (20).

To estimate coarseness, a 3*3 or 5*5 neighborhood is defined around each pixel, following which the average intensity of a pixel with its neighboring pixels is estimated. The absolute difference between the intensity of the central pixel and the average intensity of its neighbors is computed and the absolute differences for all pixels in the image are summed.

Coarseness=1∑i=1GP(i)·|i−I¯|\text{Coarseness} = \frac{1}{\sum_{i=1}^{G} P(i) \cdot |i - \bar{I}|}Coarseness=∑i=1GP(i)·|i−I¯|1

Here, GGG is the number of gray levels, P(i)P(i)P(i) is the number of pixels with gray level iii, and I¯\bar{I}I¯ is the average intensity of the neighborhood.

COMPLEXITY:

Complexity is a texture feature derived from Neighbourhood Intensity Difference (NID) matrices which measures the level of structural variation within an image. Essentially, complexity captures the local variations in pixel intensity and their spatial arrangement, providing insight into the heterogeneity of the tissue.

Complexity is typically calculated using the Neighbourhood Gray-Tone Difference Matrix (NGTDM). The steps involved in estimating complexity include defining a neighbourhood, calculating the average intensity of a pixel relative to its neighbourhood, computing the absolute difference between all the pixel intensities based on which a NGTDM is built where each element corresponds to the sum of absolute differences for a particular gray level. Complexity is calculated using the formula:

$$\text{Complexity}=\sum_{i=1}^{G} P(i) \cdot \sum_{j=1}^{G} |i - j| \cdot P(j) \cdot \left(\frac{|i - \bar{I}| + |j - \bar{I}|}{2}\right)$$

Here, GGG is the number of gray levels, P(i)P(i)P(i) and P(j)P(j)P(j) are the probabilities of gray levels iii and jjj respectively, and Iˉ\bar{I}Iˉ is the average intensity of the neighborhood.

Complexity has been clinical in analysis of CT scans for purposes of tumor characterization, differentiating tumor types, monitoring treatment response and prognosis (12).

CONTRAST

In radiomics, contrast is a texture feature derived from Neighbourhood Intensity Difference (NID) matrices. It measures the local variations in pixel intensity within an image essentially quantifying the intensity difference between neighboring pixels and reflecting how much intensity values change over a small area. High contrast indicates significant intensity differences, suggesting a heterogeneous or complex texture, while low contrast indicates smoother, more homogeneous textures. Contrast in radiomics has found application in tumor characterization and distinguishing tumor types (20), monitoring response (21) and prognosis (19).

The steps for calculation of contrast as same as those for complexity, (except in constructing a NGTDM, each element corresponds to sum of absolute differences for a particular gray level) the formula for calculation of contrast is:

Contrast=∑i=1GP(i)·(∑j=1G(i−j)2·P(j))\text{Contrast} = \sum_{i=1}^{G} P(i) \cdot \left(\sum_{j=1}^{G} (i - j)^2 \cdot P(j) \right)Contrast=i=1∑GP(i)·(j=1∑G(i−j)2·P(j))

Here, GGG is the number of gray levels, and P(i)P(i)P(i) and P(j)P(j)P(j) are the probabilities of gray levels iii and jjj respectively.

GLOBAL ENTROPY IN NEIGHBOURHOOD INTENSITY DIFFERENCE

Global entropy is a texture feature derived from the Neighbourhood Intensity Difference (NID) matrices that measures the randomness or complexity of pixel intensity distributions within an image.

It quantifies the amount of disorder or unpredictability in the texture of the image. High entropy values indicate a highly complex and varied texture, while low entropy values suggest a more uniform texture. The steps for calculation of contrast as same as those for complexity, (except each element corresponds to the sum of the absolute differences for a particular grey level) the formula for calculation of entropy is:

Entropy=−∑i=1GP(i)log 2(P(i))\text{Entropy} = -\sum_{i=1}^{G} P(i) \log_2(P(i))Entropy=−i=1∑GP(i)log2(P(i))

Here, GGG is the number of gray levels, and P(i)P(i)P(i) is the probability of occurrence of gray level iii.

INTENSITY DIRECT

Intensity direct refers to a set of features that describe the direct measurements of pixel intensity values in an image. These features capture the distribution and variation of intensity levels, providing insights into the overall brightness and contrast of the image.

Intensity direct features help characterize the brightness and contrast of tumors in CT scans. Malignant tumors often exhibit distinct intensity patterns compared to benign ones, aiding in their differentiation.

Intensity direct features serve as prognostic indicators too. Higher intensity variations within a tumor might be associated with a more aggressive behavior and a poorer prognosis.

Intensity direct features are calculated directly from the pixel intensity values within a specified region of interest (ROI). The steps involved in estimating intensity direct features include: Define and segment the ROI within the image on which various statistical measures are computed (mean, median, standard deviation, minimum, maximum, and percentiles) and a intensity histogram is generated to analyze the frequency distribution of pixel intensities.

KURTOSIS

Kurtosis is a statistical measure used to describe the "tailedness" of the probability distribution of pixel intensity values in an image (4). It quantifies the extent to which the distribution has heavy tails or outliers compared to a normal distribution.

Malignant tumors often exhibit higher kurtosis due to their heterogeneous structure and the presence of extreme intensity values, compared to benign tumors which tend to have more uniform textures (22). Variation in kurtosis can be monitored over time to assess the effectiveness of treatment. A decrease in kurtosis might indicate a reduction in tumor heterogeneity, suggesting a positive response to treatment (22). High kurtosis in tumors has been associated with poor prognosis due to the presence of extreme intensity variations, indicating aggressive tumor behavior.

Kurtosis is calculated using the pixel intensity values within a specified region of interest (ROI) in the image.

The formula for kurtosis is:

Kurtosis=N∑i=1N(xi−μ)4(∑i=1N(xi−μ)2)2−3\text{Kurtosis}=\frac{N\sum_{i=1}^{} (x_i - \mu)^4}{(\sum_{i=1}^{N} (x_i - \mu)^2)^2} - 3Kurtosis=(∑i=1N(xi−μ)2)2N∑i=1N(xi−μ)4−3

NNN is the number of pixels,

xix_ixi is the intensity of the iii-th pixel,

μ\muμ is the mean intensity,

The term −3-3−3 adjusts the result so that a normal distribution has a kurtosis of zero.

Continuation of IBEX workflow

Feature Selection:

Feature selection techniques are employed to identify the most relevant and informative features that are most discriminative for the clinical task at hand either selected based on domain knowledge about the type of malignancy or by various statistical methods, machine learning algorithms.

Machine learning models are commonly used in radiomics analysis to classify pulmonary nodules as benign or malignant based on extracted imaging features. Supervised learning algorithms, such as support vector machines (SVM), random forests, decision trees, logistic regression, and artificial neural networks (ANN), are trained on labeled datasets to learn the relationship between imaging features and nodule pathology.

Unsupervised learning algorithms, such as clustering algorithms (k-means clustering, hierarchical clustering) and dimensionality reduction techniques (PCA, t-

SNE), are used for exploratory analysis and pattern recognition without labeled training data.

Model Building and Validation:

The selected features are used to build predictive models or classifiers that relate radiomic signatures to clinical outcomes, such as diagnosis, prognosis, or treatment response. Machine learning algorithms, logistic regression, support vector machines, random forests, or deep learning models, may be employed for model building.

The performance of the developed models is evaluated using appropriate validation techniques, such as cross-validation, bootstrapping, or independent validation on external datasets.

RADIOMICS IN PULMONARY NODULE EVALUATION

Radiomics features extracted from pulmonary nodule images can serve as quantitative imaging biomarkers for predicting nodule malignancy, treatment response, and patient prognosis. Several studies (23,24) have demonstrated the potential of radiomics-based biomarkers in differentiating between benign and malignant nodules, assessing tumor heterogeneity, predicting patient survival, and guiding personalized treatment strategies.

Radiomics analysis can be integrated with clinical and molecular data to improve the accuracy and robustness of pulmonary nodule evaluation. Molecular data such as genetic mutations, gene expression profiles, and protein biomarkers can provide insights into tumor biology, treatment response, and patient prognosis. Integrating radiomics with clinical and molecular data through multi-omics approaches

enables a more comprehensive and personalized evaluation of pulmonary nodules, leading to improved diagnostic accuracy, prognostication, and treatment selection.

COMPARATIVE ANALYSIS OF RADIOMICS WITH CONVENTIONAL METHODS

The significant advantages of radiomics over conventional imaging methods in providing detailed, quantitative analyses that enhance diagnostic accuracy and inform clinical management.

Yip and Aerts (2016) conducted a review comparing radiomics with traditional imaging approaches in oncology. They concluded that radiomics offers a more detailed and quantitative assessment of tumor biology, which can lead to better individualized treatment plans. They also emphasized the need for standardized methodologies to ensure the reproducibility and reliability of radiomic analyses.

Parmar et al. (2018) evaluated the predictive power of radiomic features in comparison to standard clinical parameters in a large cohort study. Their findings indicated that radiomics provided superior prognostic information, particularly in stratifying patients based on risk and predicting survival outcomes. This study underscored the added value of radiomics in clinical decision-making (26).

CLINICAL UTILITY AND IMPACT ON PATIENT MANAGEMENT FOR RADIOMICS BASED MODELS FOR PULMONARY NODULES

The clinical utility of radiomics-based models for pulmonary nodules has been a significant area of research, demonstrating their impact on patient management and clinical decision-making. Aerts et al. (2014) pioneered the use of radiomics for non-invasive tumor characterization, showing that quantitative image features could predict patient outcomes more accurately than traditional methods (4).

Rios Velazquez et al. (2017) explored the integration of radiomic features with clinical and genomic data to enhance the prediction of lung cancer prognosis. Their study found that radiomics, when combined with other data types, provided a more comprehensive assessment of patient risk, allowing for more tailored treatment strategies. This holistic approach underscores the importance of radiomics in the broader context of precision medicine (27).

AIMS & OBJECTIVES

The primary objective of this dissertation is to leverage IBEX, an open-source software grounded in radiomics, to qualitatively evaluate pulmonary nodules. This involves a comprehensive examination of the foundational principles of radiomics, the methodologies employed for feature extraction and analysis, the latest advancements and emerging trends, and the prospective directions and challenges confronting the field.

Additionally, this study seeks to enhance the existing clinical workflow for evaluating pulmonary nodules, addressing both diagnostic and prognostic aspects.

REVIEW OF LITERATURE

DIAGNOSTIC CHALLENGES

1. **Imaging ambiguity**:

Pulmonary nodules are often detected incidentally and often pose a diagnostic dilemma due to their nonspecific radiologic appearance. Benign and malignant nodules can have overlapping imaging characteristics, making differentiation challenging (28). The Fleischner Society guidelines provide criteria for follow-up and management of nodules based on size and appearance, yet these criteria still lead to clinical decisional ambiguity (29).

2. False Positives and Overdiagnosis:

Advances in imaging technology have increased the sensitivity for detecting smaller pulmonary nodules, but consequently also led to a higher rate of false positives and overdiagnosis. A study by (Gould et al.2015) highlighted that many detected nodules are benign, leading to unnecessary follow-ups and interventions (30). Overdiagnosis can cause psychological stress for patients and lead to potentially harmful diagnostic procedures.

3. Stratification Challenges:

Various risk prediction models have been developed to stratify pulmonary nodules, such as the Mayo Clinic model and the Brock University model. However, these models have limitations in accuracy and generalizability across different populations (3,31).

The accuracy of these models is often influenced by patient demographics and nodule characteristics, necessitating a more personalized approach to risk assessment.

The integration of biomarkers and genetic testing into risk stratification shows promise but remains underutilized. Biomarkers such as circulating tumor DNA and specific gene mutations could enhance the accuracy of nodule classification but require further validation in clinical practice (32).

4. High Risk of Unnecessary Biopsies

Unnecessary biopsies of benign nodules expose patients to the risks of invasive procedures, including bleeding, infection, and pneumothorax.

A study by Wiener et al. (2012) found that a significant proportion of patients undergoing biopsies for pulmonary nodules had benign results, indicating a high rate of unnecessary procedures (33).

The morbidity associated with these procedures underscores the need for improved diagnostic accuracy to avoid unnecessary interventions. The financial burden of unnecessary biopsies and follow-up imaging is substantial. An economic analysis by Pyenson et al. (2014) estimated that the cost of follow-up and diagnostic procedures for incidentally detected nodules could exceed billions of dollars annually in the United States alone (34).

The psychological impact on patients diagnosed with pulmonary nodules, particularly when follow-up and additional testing are required, is significant. The uncertainty and prolonged surveillance can lead to anxiety and reduced quality of life (35).

This highlights the need for more cost-effective strategies in the management of pulmonary nodules. Better communication strategies and patient-centered care approaches are necessary to mitigate these effects.

Adherence to established guidelines for the management of pulmonary nodules is variable among clinicians. A study by Wiener et al. (2013) found discrepancies in guideline adherence, with some practitioners opting for more aggressive diagnostic approaches (33). Standardizing practice patterns and ensuring guideline adherence can improve patient outcomes and reduce unnecessary procedures.

PULMONARY NODULES & RISK OF MALIGNANCY

This review by (Gould, M. K., et al. 2013) provides an overview of the current guidelines and strategies for evaluating pulmonary nodules, including risk assessment tools and imaging modalities. It discusses the importance of incorporating clinical factors, nodule characteristics, and patient risk factors in determining the likelihood of malignancy.

The Fleischner Society guidelines offer evidence-based recommendations for the management of incidental pulmonary nodules detected on CT imaging (29)**.** The guidelines provide risk stratification criteria based on nodule size, morphology, and patient characteristics, helping clinicians determine the appropriate follow-up and management strategies.

This study Devaraj, A., et al. (2018) highlights the significance of qualitative and quantitative analyses of low-dose CT scans in assessing indeterminate pulmonary nodules (37). It discusses the role of radiomic features, such as size, density, texture, and shape, in predicting the risk of malignancy and guiding clinical management decisions.

The study by (Li, F., et al. 2016**)** investigates the utility of semi-automated volumetric measurement on chest CT scans for predicting the malignancy of solitary pulmonary nodules. It demonstrates that volumetric analysis, combined with radiomic features and clinical variables, improves the accuracy of malignancy prediction compared to traditional size-based criteria (38).

LIMITATIONS OF QUALITATIVE ASSESSMENT

1. Subjectivity and Variability:

The studies by Nixon et al., 2013 (39) and Warfield et al., 2004 (40) suggested that qualitative analysis of radiological scans was inherently subjective, relying on the radiologist's experience and interpretative skills resulting in significant inter- and intra-observer variability, which can lead to inconsistent diagnoses and treatment plans

2. Reproducibility Issues:

A review by (Balassy et al. 2003) (41) concluded that even experienced radiologists might arrive at different conclusions when interpreting the same images at different times, thus undermining the reproducibility and the reliability of radiological diagnoses and to track disease progression accurately over time.

3. Limited Sensitivity and Specificity:

Qualitative methods lack the sensitivity and specificity required for early detection of subtle abnormalities. Yankelevitz et al. (2000) found that quantitative measurements of lung nodules provided a more precise assessment of nodule growth compared to qualitative evaluations (42).

IMPERATIVE FOR INTEGRATION OF QUANTITATIVE AND QUALITATIVE EVALUATION OF MEDICAL IMAGES

1. Enhanced Diagnostic Accuracy:

Quantitative measures provide objective data that enhance the accuracy of radiological diagnoses. Automated volumetric analysis, for example, offers precise measurements of tumor size and growth rates, which are crucial for staging and treatment planning (43).

Studies such as those by Reeves et al. (2007) have demonstrated that integrating quantitative metrics like nodule volume and growth rates improves the detection and characterization of lung cancer (44).

2. **Standardization and Reproducibility**:

Quantitative methods contribute to reducing variability and improving reproducibility. Automated image analysis algorithms provide consistent outputs, mitigating the subjectivity inherent in qualitative evaluations (45).

The use of computer-aided detection (CAD) systems in mammography has been shown to increase the detection rate of breast cancer, providing a second, unbiased opinion that complements the radiologist's assessment (46).

3. Quantitative Biomarkers for Disease Monitoring:

Quantitative imaging biomarkers enables the precise monitoring of disease progression and response to therapy. Tumor volume, perfusion rates, and metabolic activity, quantified through imaging techniques like MRI and PET, offered insights into the biological behavior of diseases (47). Quantitative imaging biomarkers are particularly valuable in oncology, in assessing the efficacy of treatments and making informed decisions about treatment changes accordingly (46).

PRINCIPLES OF RADIOMICS AND THE STANDARD WORKFLOW

1. Image Acquisition and Reconstruction:

Standardized protocols for image acquisition and reconstruction are crucial to ensure the quality and reproducibility of radiomics features (6).

2. Segmentation:

Accurate and reproducible segmentation of ROIs is a critical step. Segmentation can be performed manually, semi-automatically, or fully automatically using advanced algorithms (19).

3. Feature Extraction:

A variety of algorithms are used to extract hundreds to thousands of features from the segmented ROIs. These features capture different aspects of the image data (26).

4. Data Preprocessing and Normalization:

Preprocessing steps such as resampling, intensity normalization, and feature selection are applied to ensure that the extracted features are comparable across different images and patients (50).

5. Model Building and Validation:

Statistical and machine learning methods are employed to build predictive models based on radiomics features. These models must be rigorously validated using independent datasets to assess their generalizability and robustness (22).

VALIDITY OF RADIOMICS

1. Reproducibility and Repeatability:

Ensuring the reproducibility and repeatability of radiomics features is essential for their clinical application. Studies have highlighted the need for standardized imaging protocols and robust feature extraction methods to achieve reliable results (51).

2. Biological and Clinical Relevance:

Validating the biological and clinical relevance of radiomics features involves correlating them with underlying genetic, histopathological, and clinical data. This step is crucial to demonstrate that the extracted features are meaningful and can provide valuable insights into disease processes (4)

RADIOMICS FOR QUANTITATIVE ESTIMATION OF PULMONARY NODULES

This seminal paper by (Aerts et al., 2014) demonstrates the potential of radiomics in decoding tumor phenotype using quantitative imaging features extracted from CT scans. The study highlights the ability of radiomic features to capture tumor heterogeneity and predict patient outcomes in lung cancer, including pulmonary nodules (4).

Coroller et al. investigated the predictive value of radiomic phenotype features derived from CT imaging in predicting pathological response in non-small cell lung cancer (NSCLC). The study demonstrates that radiomic features can serve as biomarkers for treatment response assessment and outcome prediction in patients with pulmonary nodules (52).

The study by (Ganeshan, B., et al. 2013) explores the histopathologic correlates of texture parameters derived from CT imaging in non-small cell lung cancer (NSCLC). The findings elucidate the relationship between radiomic features, tumor histology, and patient outcomes, providing insights into the underlying biological characteristics of pulmonary nodules (53).

The work by Huang, Y., et al. (2016) focused on colorectal adenocarcinoma, this study showcases the development of a CT-based radiomics signature for discriminating between high-grade and low-grade tumors (54). The principles of radiomics employed in this study can be applied to pulmonary nodules for phenotype characterization and outcome prediction.

ROLE OF RADIOMICS IN MEDICAL IMAGING

In the field of Oncology, radiomics has been extensively studied in oncology for tumor characterization, prediction of treatment response, and prognostication. For example, radiomics features have been used to predict the aggressiveness of lung cancer and patient survival (55).

Radiomics can help in monitoring the response to therapies such as chemotherapy, radiotherapy, and immunotherapy by analyzing changes in imaging features over time (12).

In cardiology, radiomics is being explored for the assessment of myocardial tissue characteristics, prediction of cardiac events, and evaluation of treatment outcomes in diseases such as heart failure and coronary artery disease (56).

Radiomics applications in neurology include the differentiation of brain tumor subtypes, prediction of treatment response in glioblastoma, and the assessment of neurological diseases such as Alzheimer's and multiple sclerosis (57).

MATERIALS AND METHODS

SOURCE OF DATA:

Participants over 18 years old visiting the Radiology Department at KLE's Dr. Prabhakar Kore Hospital for high resolution computed tomography of thorax.

STUDY DESIGN:

Observational study conducted from May 2023 to May 2024.

SAMPLE SIZE:

The formula used for sample size calculation is the minimum sample size formula based on prevalence rate-

$$n = (Za)2\text{-}P(1\text{-}P)/d2$$

n=estimated sample size

Za=level of significance (for a level of significance at 5%, the Zvalue is1.96)

P= prevalence

d= percentage likely difference in prevalence

Considering an 85% power and a 5% significance level, the sample size was determined to be 100 subjects.

SAMPLING TECHNIQUE: Convenient sampling.

SAMPLING METHOD:

Each patient will first receive a clinical evaluation, followed by undergoing a high-resolution computed tomography (HRCT) thorax scan using a 128-slice CT scanner (Revolution EVO Wipro GE) from GE Healthcare. This sequence ensures comprehensive assessment and precise imaging for accurate diagnosis.

INCLUSION CRITERIA:

All incidentally diagnosed or clinically suspected cases for pulmonary nodules. Individuals aged 18 to 80, regardless of sex in all Clinically suspected cases.

EXCLUSION CRITERIA:

Proven cases of pulmonary nodules.

Cases that have received any type of treatment or procedure for managing a pulmonary nodule

Unfit patients for examination/ clinically unstable patients.

Patients who refuse to participate.

METHODOLOGY:

The study will be conducted using 128 slice Computed Tomography Revolution EVO Wipro (GE HEALTHCARE, USA) machine manufactured by GE Healthcare. Standard scan protocol for high resolution tomography of chest will be implemented for all patients referred to the department of radiology. Subsequently, their scans will be meticulously evaluated for the presence of pulmonary nodules. The findings will be systematically documented and analyzed. Additionally, informed consent will be obtained from each patient to ensure ethical compliance and transparency throughout the study.

IBEX WORKFLOW

Visit the IBEX Website: Go to the official IBEX website to download the source code version (http://bit.ly/IBEXSrc_MDAnderson)/ the standalone version (http://bit.ly/IBEX_MDAnderson)

1. Install Software:

Follow the installation guide provided on the website. This may include installing dependencies such as MATLAB Runtime if required by IBEX.

2. Loading DICOM Files

Launch IBEX and import DICOM files:

Open the Application and start IBEX from your applications menu or command line. Use the file menu or import button to access the import dialog.

Select DICOM files and load images:

Browse and select the DICOM files from your local storage. Click on 'Load' to import the selected DICOM files into IBEX. The images will be displayed for further processing.

3. Preprocessing

Quality Check:

Examine the imported images to ensure they are of good quality and free from artifacts that could affect analysis. Modify settings like windowing, contrast, and brightness to enhance image clarity.

Image Segmentation to define ROI:

Use segmentation tools to outline the region of interest (ROI) within the images. This can be done manually or using automated/semi-automated segmentation algorithms. Once segmentation is complete, save the ROI for feature extraction.

4. Feature Extraction

Choose Feature Sets:

IBEX offers a variety of radiomic features. Select those relevant to your study, such as shape based features (e.g., volume, surface area). which quantify the geometry of the ROI. Texture within ROI can be analysed using features like GLCM (Gray Level Co-occurrence Matrix). The intensity distribution/ features can be extracted using features like mean, standard deviation

Run Extraction

Start the feature extraction process. IBEX will compute and display the selected features.

5. Data Analysis

Perform Analysis:

Use statistical tools within IBEX/ third party software to analyze the data. This could involve:

Descriptive Statistics: Summarize basic features of the dataset.

Correlation Analysis: Identify relationships between features.

Regression Analysis: Explore predictive relationships.

Machine Learning: Apply classification or clustering algorithms.

6. Exporting Results

Export Data: Save the extracted features and analysis results in various formats (CSV, Excel, etc.) for further use.

Generate Reports: Compile a comprehensive report that includes images, feature tables, statistical findings, and interpretation

RESULTS

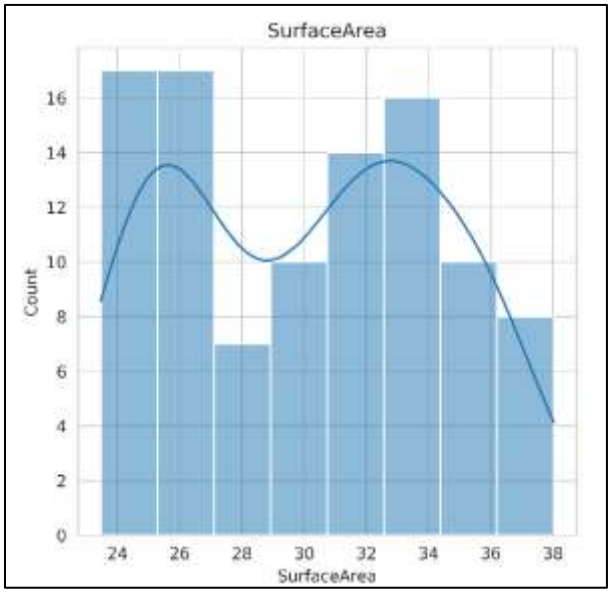

Image 1: Histogram for Surface Area

Surface Area: Surface Area values are depicted on X axis and the count of occurrences on Y axis which shows a bimodal distribution with peaks at the lower end (24-26) and mid-range (30-32), with fewer occurrences at higher values (36-38).

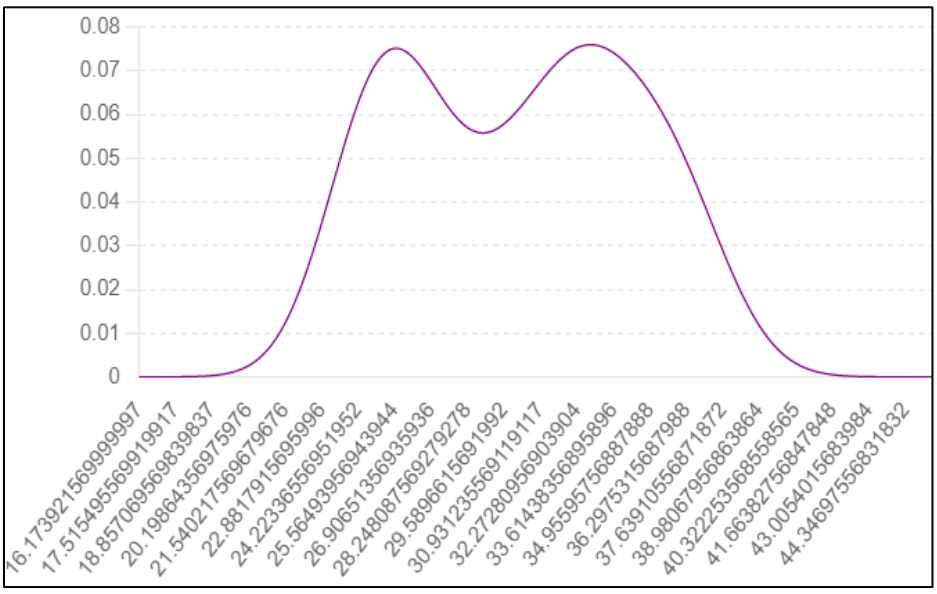

Image 2: Density Plot for Surface Area

The curve (image 2) represents the estimated density of surface area values. The height of the curve points the relative frequency of surface area values in that range.

The x-axis represents the range of surface area values which appear cluttered and y axis depicts density values i.e. how concentrated the data points are around specific surface area values on y axis dataset.

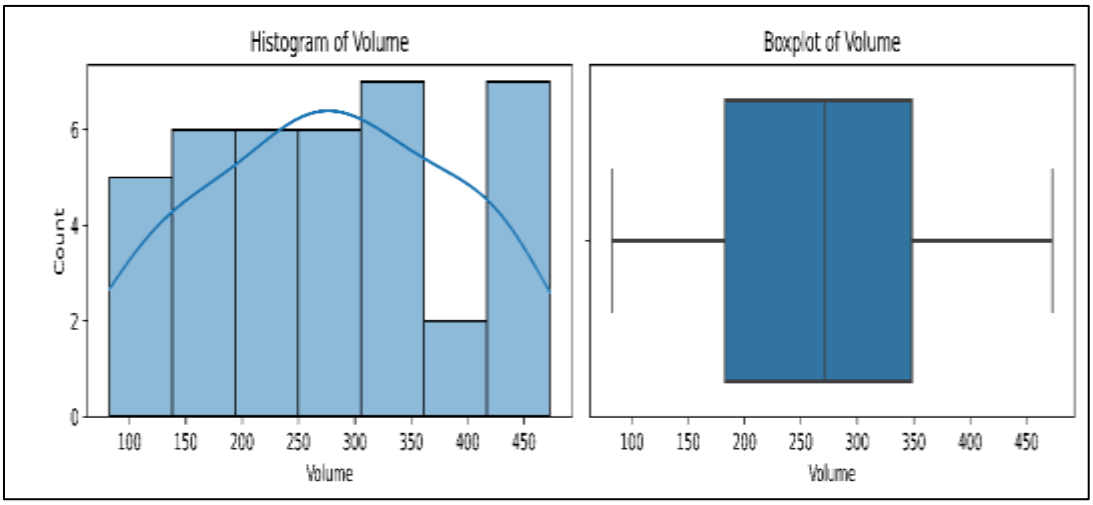

Image 3: Histogram and Boxplot for volume

The above histogram depicts volume values on x axis and count of occurrences on Y axis. The bimodal distribution indicates two main groups of volume values, with peaks around 200 and 450.

The above boxplot for volume depicts volume values on x axis and volume values on Y axis. The boxplot shows the central tendency and spread, with some potential outliers indicating variability in volume values.

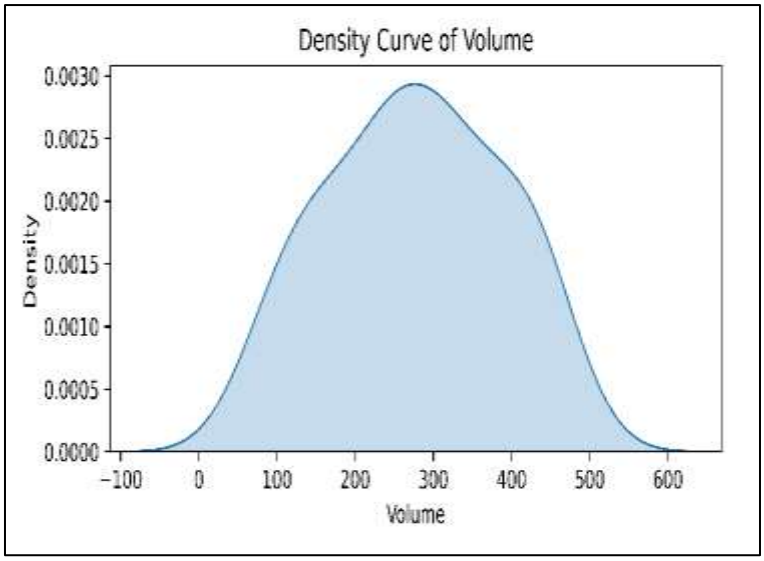

Image 4: Density curve for volume

The above density curve for volume depicts volume values on x axis and density on Y axis. The density curve supports the histogram findings, with clear peaks and a gradual decline, indicating the overall distribution pattern.

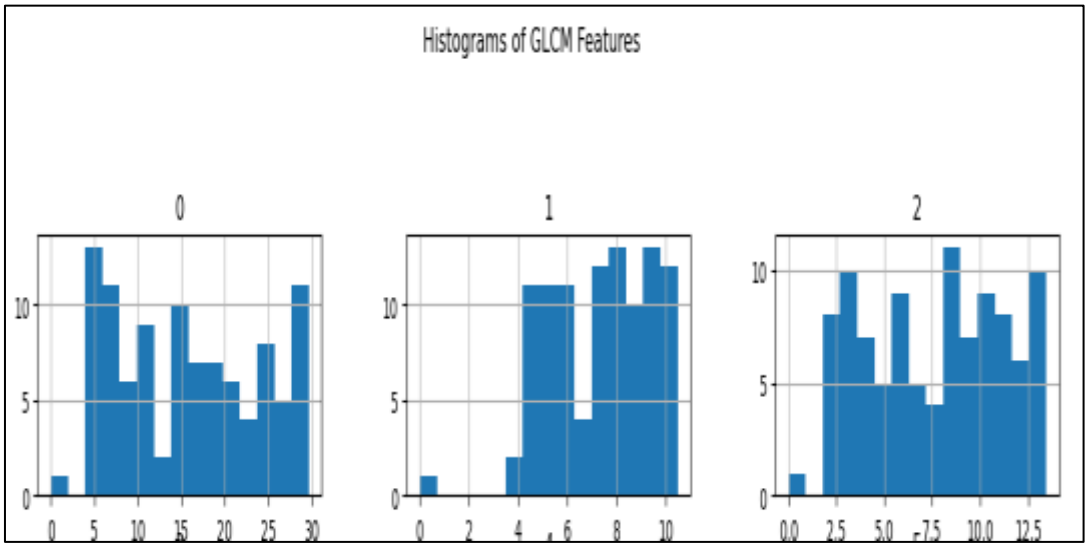

Image 5: Histogram for GLCM features (-333 to -1, 0-1, 45-1)

Histogram 1 for -333-1 contrast shows a unimodal distribution with a peak around the middle value. The distribution is slightly skewed to the right.

Histogram 2 for 0-1 contrast displays a bimodal distribution with two prominent peaks, suggesting the presence of two distinct groups within the data.

Histogram 3 for 45-1 contrast displays unimodal distribution that is symmetric around the central value, indicating a normal distribution.

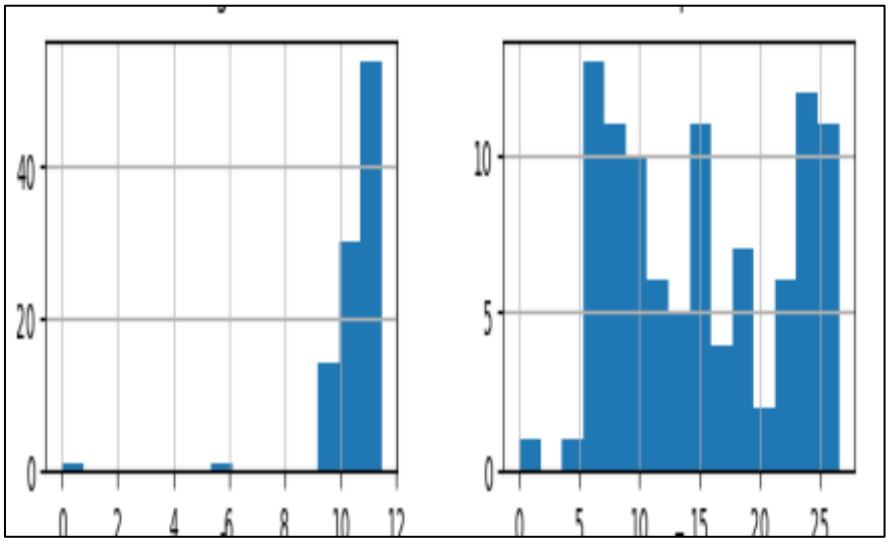

Image 6: Histograms for (90 to1, 135-1)

Histogram 4 for 90-1 contrast is slightly skewed to the left, with a single, broad peak indicating a central tendency towards higher values.

Histogram 5 for 135-1 contrast shows a very skewed distribution with a long tail to the right, suggesting that most data points are concentrated on the lower end.

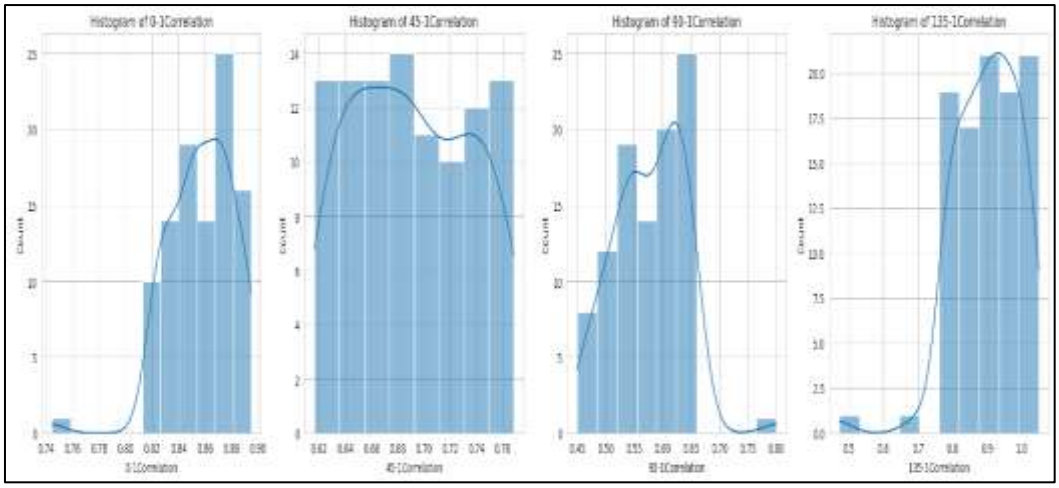

Image 7: Histogram for 0-1 correlation, 45-1 correlation, 90-1 correlation and 135-1 correlation depicts a skewed distribution pattern with some values being more frequent, indicating specific patterns of relationships.

The histogram for 0-1 correlation with correlation values plotted on x axis and frequency plotted on y axis shows a right-skewed distribution with most values between 0.82 and 0.88, indicating high correlation values are common.

The histogram for 45-1 correlation with correlation values plotted on x axis and frequency plotted on y axis shows a evenly distributed set of values between 0.62 and 0.76, suggesting a moderate spread of correlation values.

The histogram for 90-1 correlation with correlation values plotted on x axis and frequency plotted on y axis shows a right-skewed distribution with a concentration of values between 0.55 and 0.75, indicating these correlation values are frequent

The histogram for 135-1 correlation with correlation values plotted on x axis and frequency plotted on y axis, shows a strong right-skew with most values around 0.9 to 1.0, indicating very high correlation values are common.

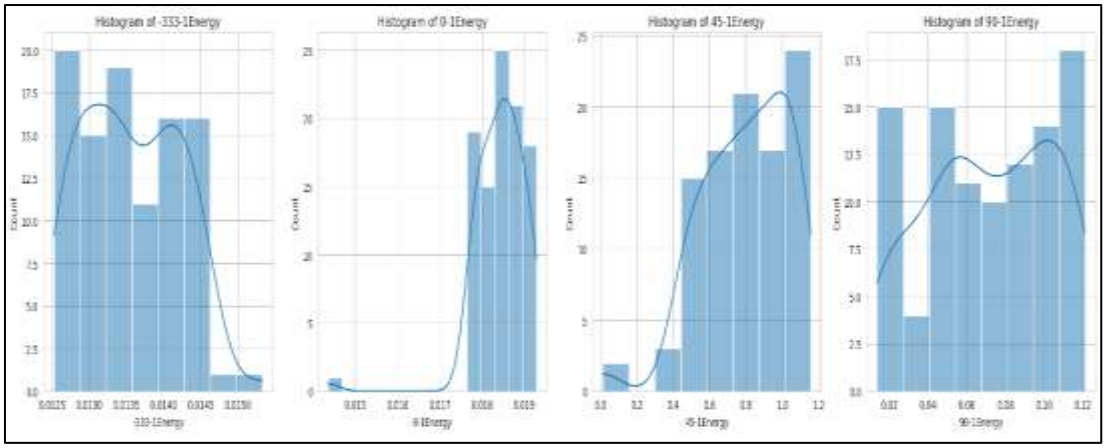

Image 8: Histogram for -333 to -1 energy, 0-1 energy, 45-1 energy, 90-1 energy values.

The histogram for -333 to -1 energy, 0-1 energy, 45-1 energy, 90-1 energy variables shows evenly distributed data points with distinct peaks, suggesting variability in energy measures.

The histogram for -333-1 energy values with energy values plotted on x axis and frequency plotted on y axis shows a bimodal distribution of energy values with peaks around 0.013 and 0.015, suggesting two distinct groups.

The histogram for 45-1 energy values with energy values plotted on x axis and frequency plotted on y axis shows distribution with a peak around 1.0 with a spread from 0.4 to 1.2, indicating higher energy values are more frequent.

The histogram for 0-1 energy values with energy values plotted on x axis and frequency plotted on y axis shows a peak in energy values around 0.018, with a right-skewed distribution indicating higher frequency at lower values.

The histogram for 90-1 energy values with energy values plotted on x axis and frequency plotted on y axis shows the bimodal distribution of energy values with peaks around 0.06 and 0.1, suggesting two distinct groups of energy values.

The histogram for 135-1 energy values with energy values plotted on x axis and frequency plotted on y axis shows a right-skewed distribution of 135-1 energy values with most values between 0.002 and 0.005, indicating low energy values are more common.

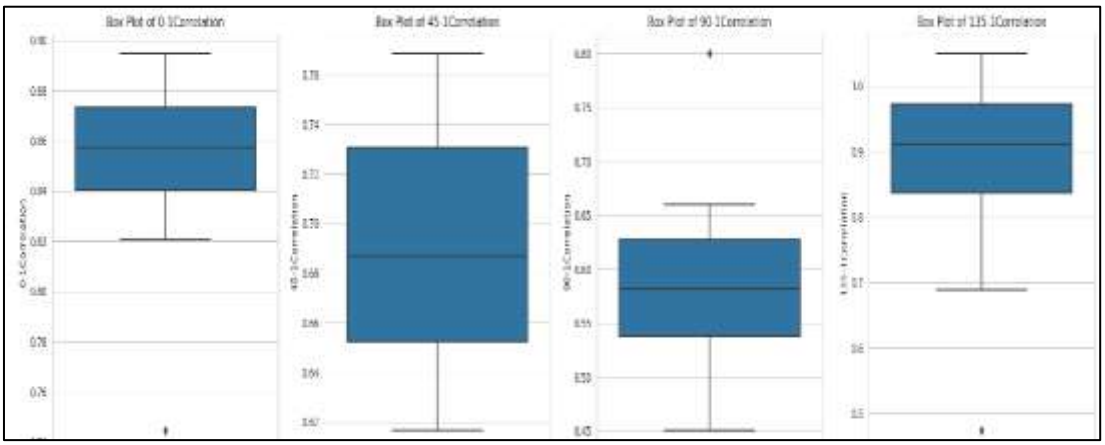

Image 9: Box Plots for Correlation (0 to1, 45 to1, 90 to 1, 135 to 1)

Box Plot of 0.1 Correlation: The data is tightly clustered around the median, indicating low variability, median is approximately 0.82 with a slight negative skew, as indicated by the longer lower whisker.

Box Plot of 45.1 Correlation shows a wider spread compared to the 0.1 correlation, with the median around 0.68, slightly positively skewed

Box Plot of 90.1 Correlation shows the data points being more spread out. The median is near 0.58.

Box Plot of 135.1 Correlation shows data with a slightly higher central tendency. Median is around 0.75. with a moderate spread of date, similar to the 45.1 correlation with a slightly negative skew

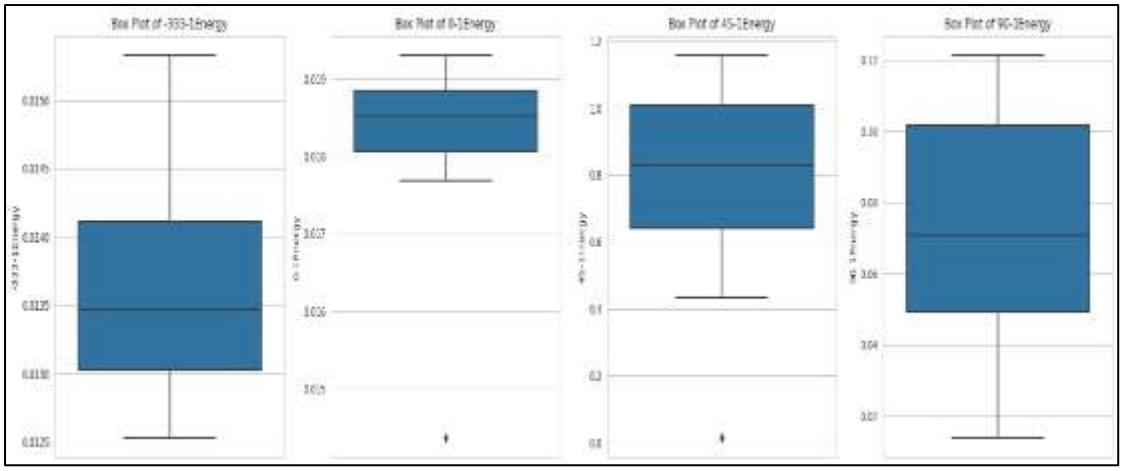

Image 10: Box Plots for Energy (-333 to 1, 0 to 1, 45 to 1, 90 to 1)

Box Plot of -333.1 Energy, shows very tight clustering of data points. The median is approximately 0.1315 with a symmetrical distribution.

Box Plot of 0.1 Energy shows the data points being moderately distributed which appears symmetrical.

Box Plot of 45.1 Energy, shows a distribution pattern similar to the 0.1 energy but with a slightly lower central tendency with a slight positive skew. The median is close to 0.09.

Box Plot of 90.1 Energy Distribution shows the data points being tightly clustered with a symmetrical data distribution. The median is around 0.165.

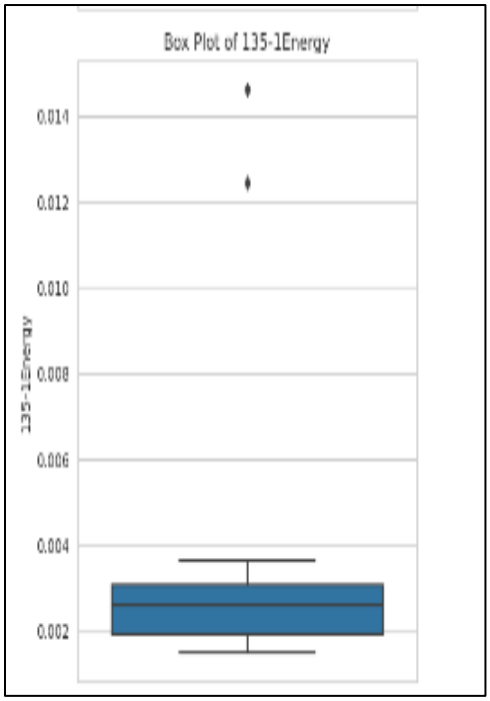

Image 11: Box Plots for Energy (135 to 1)

Box Plot of 135.Energy shows very tight clustering similar to -333.1 energy with symmetrical distribution of data. Median is approximately 0.004.

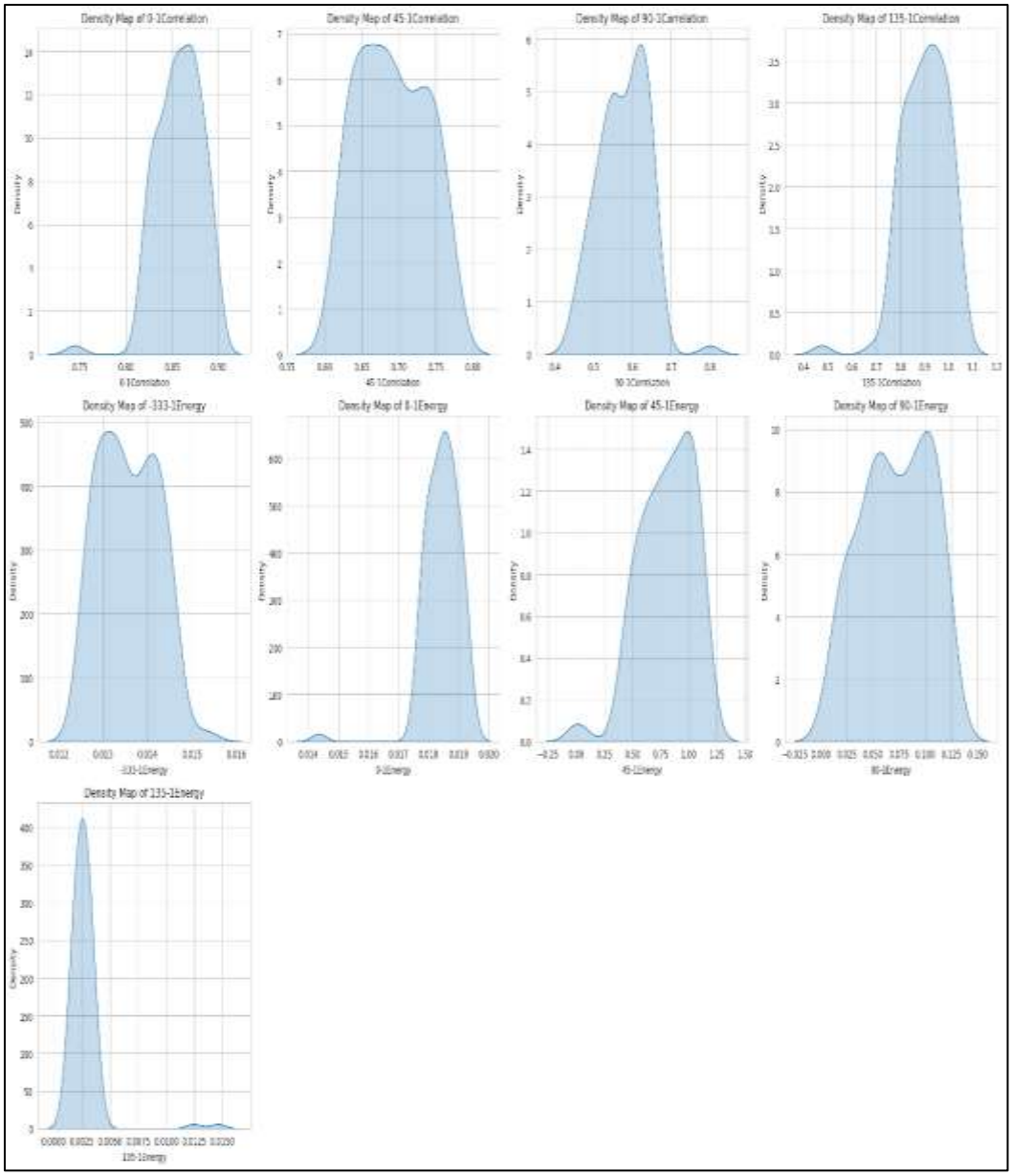

Image 12: Density plots for Energy (-333 to 1, 0 to 1, 45 to 1, 90 to 1) and Density maps for Correlation (0 to1, 45 to1, 90 to 1, 135 to 1).

Density maps for correlation values depicted by values on x axis and frequency plotted on Y axis. Density maps for Energy values depicted by values on x axis and frequency plotted on Y axis.

For 0.1 Correlation, the data appears to be narrowly distributed suggesting a low variability and a slight negative skew, with the “mode” being (peak)

For 45.1 Correlation, the mode is around 0.68, with a spread wider than the 0.1 correlation, indicating moderate variability and a slightly positive skewed distribution.

For 90.1 Correlation, the mode is approximately 0.58 with a spread wider than 0.1 correlation with moderate variability

For 135.1 Correlation, the mode is around 0.48, spread similar to 90.1 correlation with a slightly negatively skewed distribution.

For 0.1 Energy, the data is highly concentrated around 0.015 (mode) and the spread of data appears to be very narrow indicating low variability.

For 45.1 Energy, the peak is around 0.09 (mode) with a narrow spread and a slightly positively skewed distribution

For 90.1 Energy, the mode is around 0.075 with a narrow spread, indicating low variability.

For 135.1 Energy, the data shows a sharp peak near 0.005 (mode) with an extremely narrow indicating very low variability.

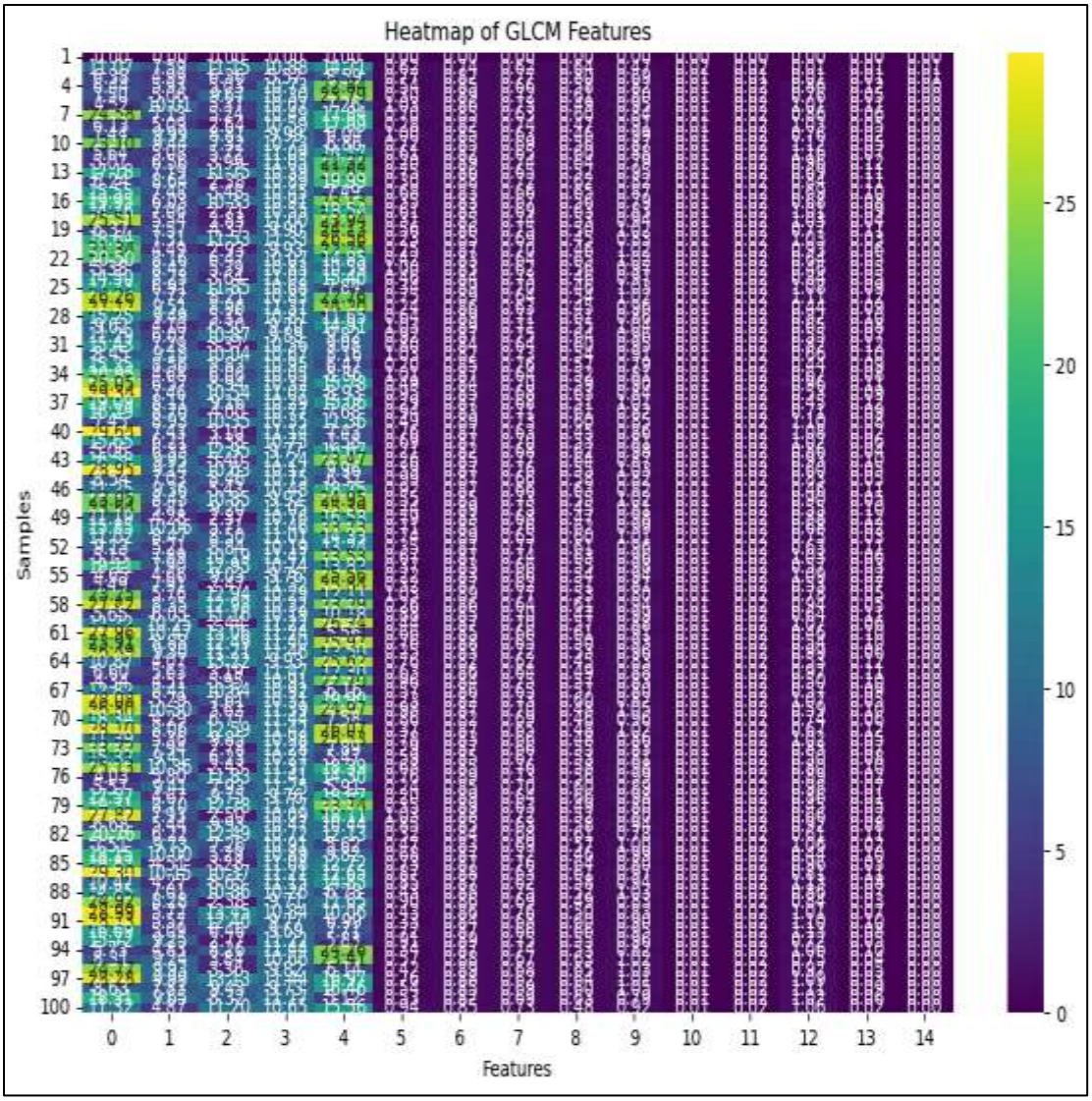

Image 13: Heatmap for GLCM (Grey level coocurrence matrix)

The heatmap shows the intensity of the GLCM features across different samples. Each cell within the heatmap contains a numerical value, representing the specific measurement of a GLCM feature for a sample. On the right side of the heatmap, there is a vertical color scale ranging from 0 to 25.

X- axis plots the different GLCM features being analyzed from 0 to 14 and Y axis plots the different data points analyzed for those features from 0 to 100. The colors transition from purple (low values) to yellow (high values), indicating the intensity or magnitude of the GLCM features.

Image 14: Pairplots for all the GLCM (Grey level coocurrence matrix) features

The pairplot provides scatter plots for each pair of features, along with histograms on the diagonal.

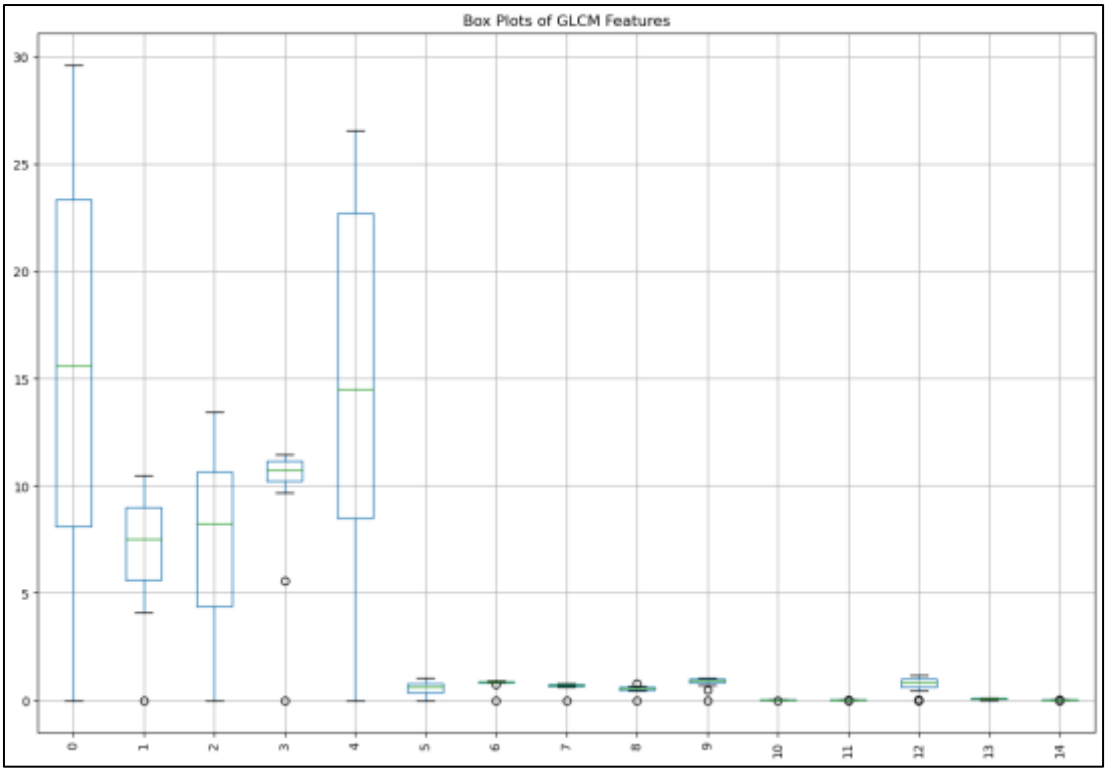

Image 15: Box Plots for all the GLCM (Grey level coocurrence matrix) features

The plots (index 0-2) show a wide range of values with a relatively high median, especially index 0 which has a median above 15. The spread is large, indicating high variability in the data. Outliers are present, particularly in index 2.

The plots (index 3-5) show significantly narrow spread, indicating less variability. The medians are lower compared to indices 0-2. Index 4 shows a very tight distribution with a small IQR and no outliers, suggesting very consistent data.

These indices (6-14) show extremely low variability with most data points appearing as a line at the bottom, suggesting that the values for these features are close to zero. The medians are at or near zero, and there are no outliers, indicating uniformity and possibly less informative features compared to others.

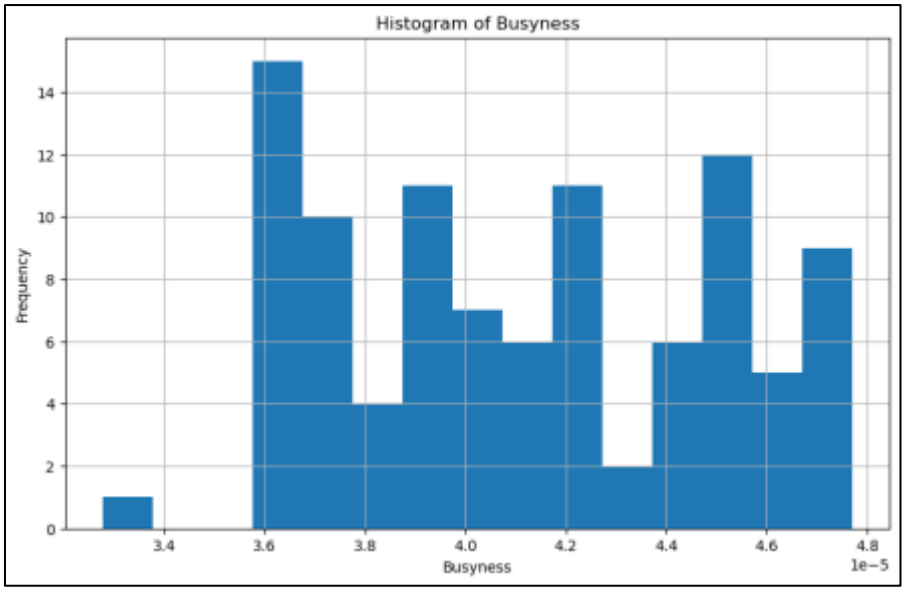

Image 16: Histogram for busyness. The above histogram for busyness depicts busyness values on x axis and frequency on y axis.

The busyness values range from approximately 3.4×10−53.4\times 10^{5}3.4×10−5 to 4.8×10−54.8 \times 10^{-5}4.8×10−5. There are noticeable peaks around 3.6×10−53.6 \times 10^{-5}3.6×10−5, 4.0×10−54.0 \times 10^{-5}4.0×10−5, and 4.4×10−54.4 \times 10^{-5}4.4×10−5. These peaks indicate that these busyness values occur more frequently in the dataset.

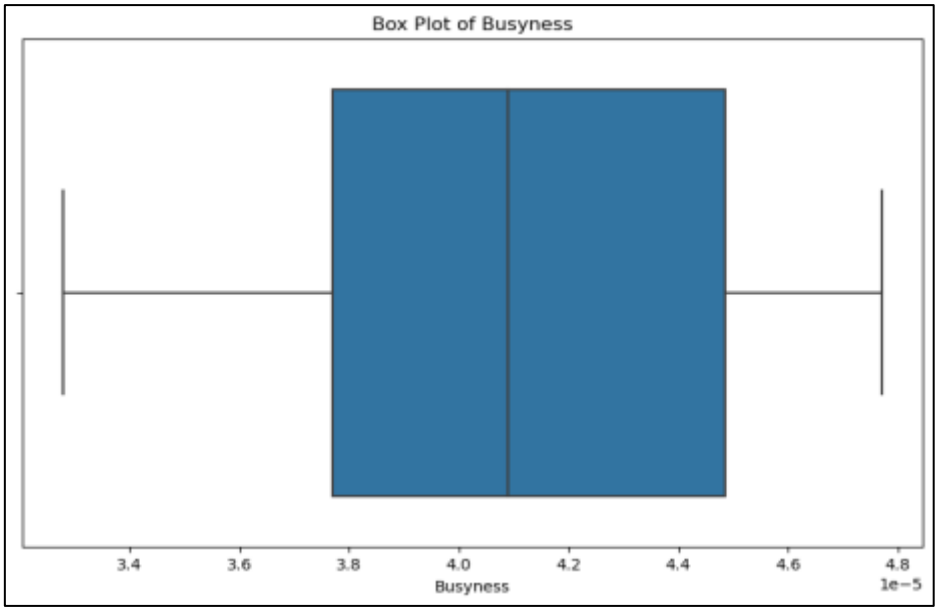

Image 17: Boxplot for busyness

The above boxplot for busyness shows the median busyness value is approximately 4.0×10−54.0 \times 10^{-5}4.0×10−5.

The IQR extends from about 3.6×10−53.6 \times 10^{-5}3.6×10−5 to 4.4×10−54.4 \times 10^{-5}4.4×10−5. This range captures the middle 50% of the data, indicating moderate variability.

The whiskers extend to the minimum and maximum values within 1.5 times the IQR from the quartiles. There are no outliers beyond these whiskers, indicating that the data is relatively consistent without extreme deviations.

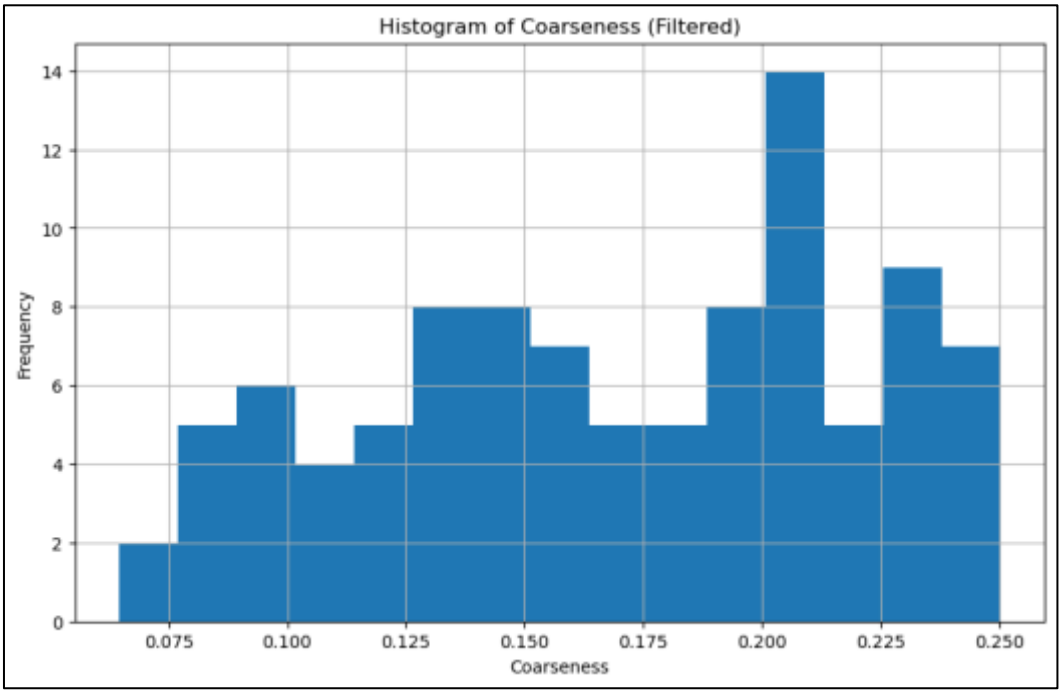

Image 18: Histogram for coarseness

The histogram for coarseness with value for coarseness plotted on x axis and frequency (the number of occurrences of each coarseness value in the dataset) of the values plotted on Y axis. The highest bar indicates that the range around 0.2 has the most frequent occurrences

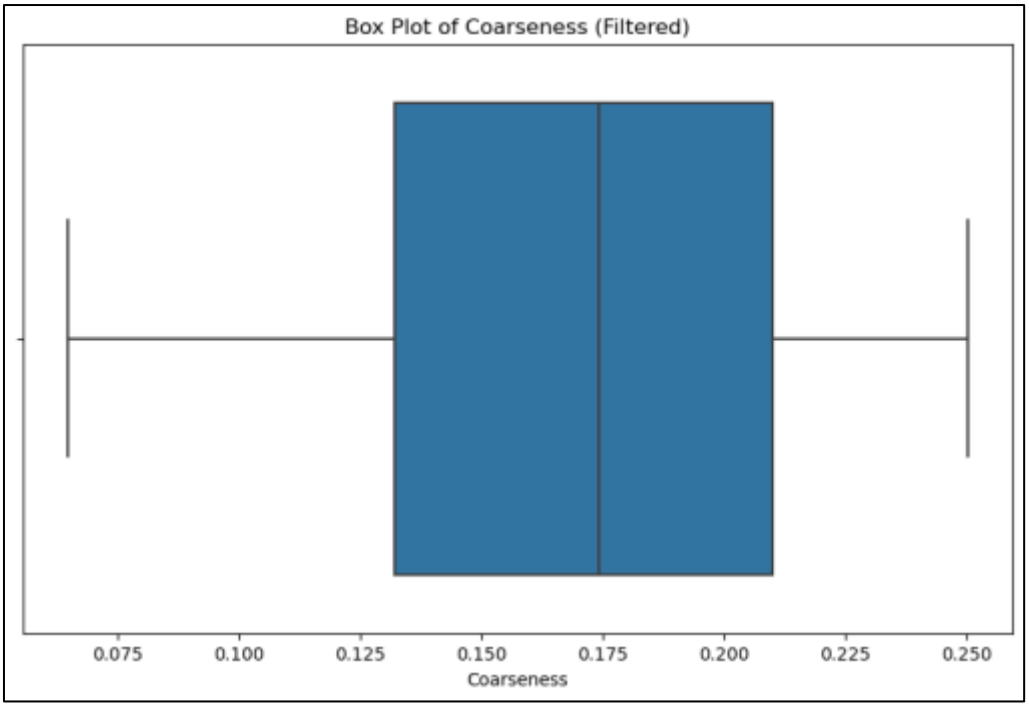

Image 19: Boxplot for coarseness

The boxplot shows median value for Coarseness is around 0.175 and the interquartile range approximately lies between 0.150 and 0.200. The relatively wide IQR indicates moderate variability in the Coarseness values

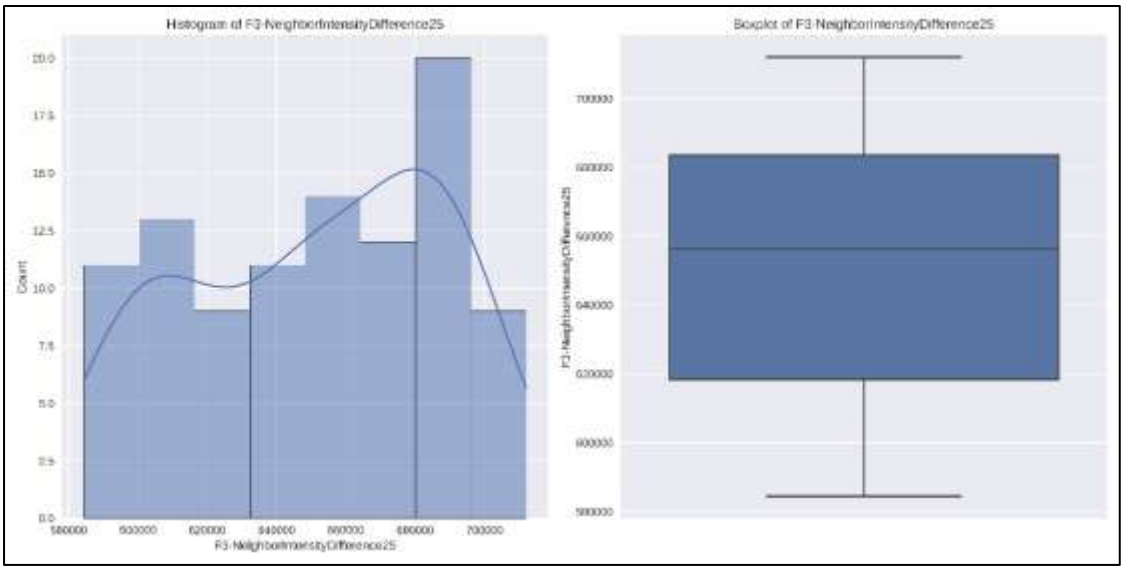

Image 20 & 21: Histogram and boxplot for F3. Neighborhood intensity Difference.

Complexity

The histogram (image 20) for complexity shows the complexity values on x-axis ranging approximately from 580,000 to 700,000 and the y axis shows the frequency of observations within each bin.

The box and whisker plot (image 21) for complexity shows the distribution of the complexity values. The box represents the interquartile range (IQR) which represents the middle fifty percent of the entire data. The IQR stretches approximately from 620,000 to 680,000, indicating that the middle 50% of the data lies within this range. The thick line within the center of the box represents the median value (around 650,000)

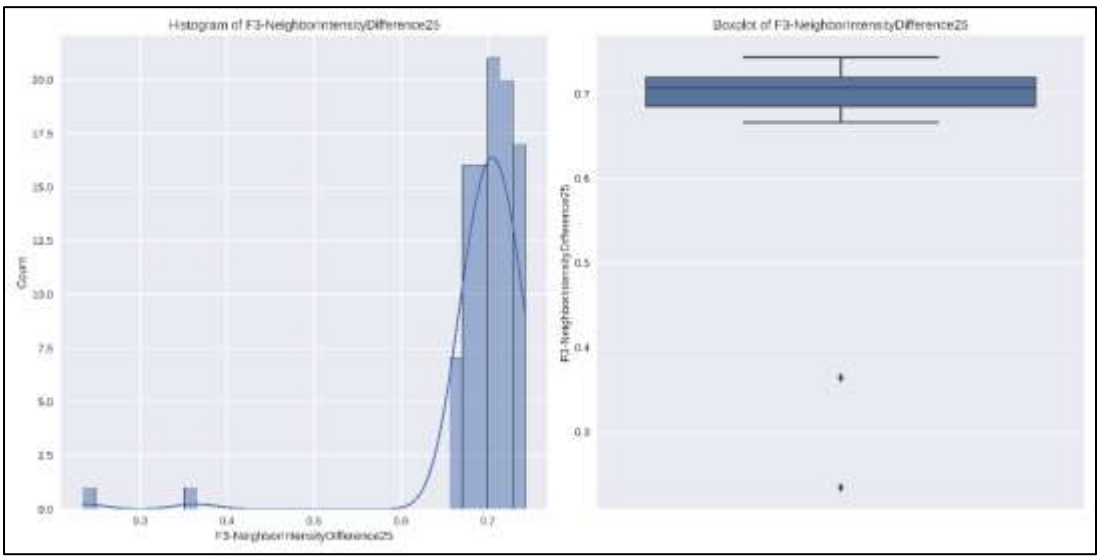

Image 22 & 23: Histogram and boxplot for F3. Neighborhood intensity Difference. Contrast

The histogram for contrast (image 22) shows values of contrast, ranging approximately from 0.3 to 0.7 and the y-axis represents the number of observations within each bin

The box and whisker plot for contrast (image 23) shows distribution of contrast (F3-NeighborIntensityDifference25) appears to be right-skewed, with the majority of the data concentrated between 0.6 and 0.7. The density curve is overlaid on the histogram, shows the curve peak around 0.65, indicating the highest concentration of data points in that range.

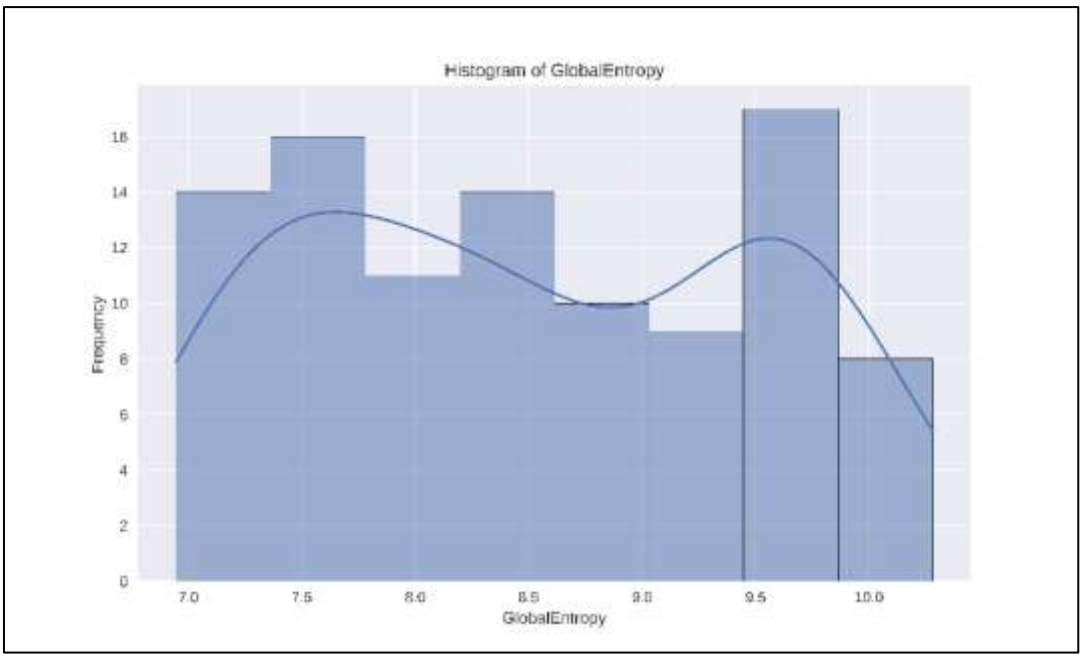

Image 24: Histogram for GlobalEntropy

Histogram for GlobalEntropy displays the frequency distribution of the GlobalEntropy values across different bins. The x-axis represents the GlobalEntropy values, ranging from approximately 7.0 to 10.0, while the y-axis shows the frequency of these values. There is a smooth density curve overlaid on the histogram, which helps visualize the distribution shape.

The histogram shows a somewhat bimodal distribution, with peaks around the values of 7.5 and 9.5. The peaks around 7.5 and 9.5 could represent specific characteristics or clusters within the dataset.

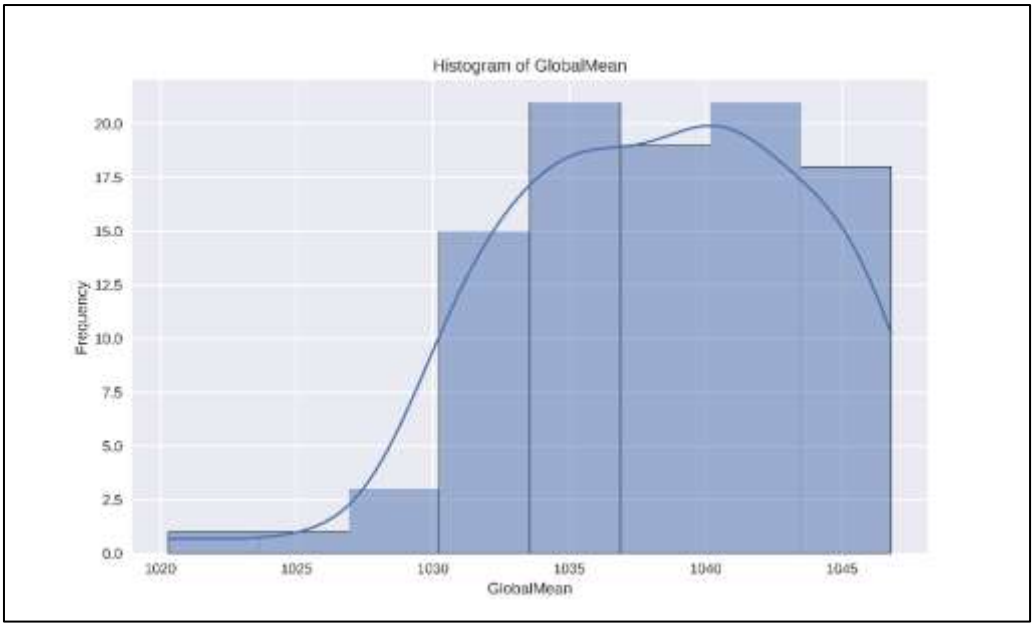

Image 25: Histogram for GlobalMean

GlobalMean values are plotted on x-axis, ranging from approximately 1020 to 1045, while the y-axis shows the frequency of these values.

The histogram shows a left-skewed distribution, with most of the values concentrated between 1030 and 1045. The values of GlobalMean are spread out between 1020 and 1045, with the majority of values above 1030.

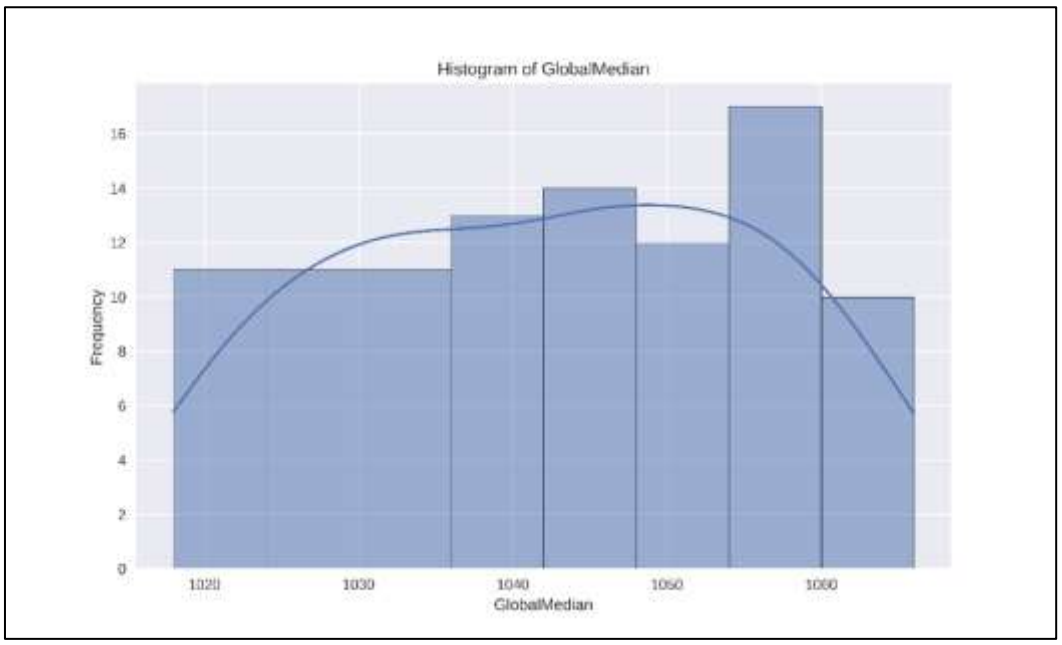

Image 26: The histogram for GlobalMedian

GlobalMedian values are plotted on x axis , ranging from approximately 1020 to 1060, while the y-axis shows the frequency of these values. The relatively uniform distribution suggests that the GlobalMedian values are evenly spread across the range, with no significant skewness, indicating a balanced dataset.

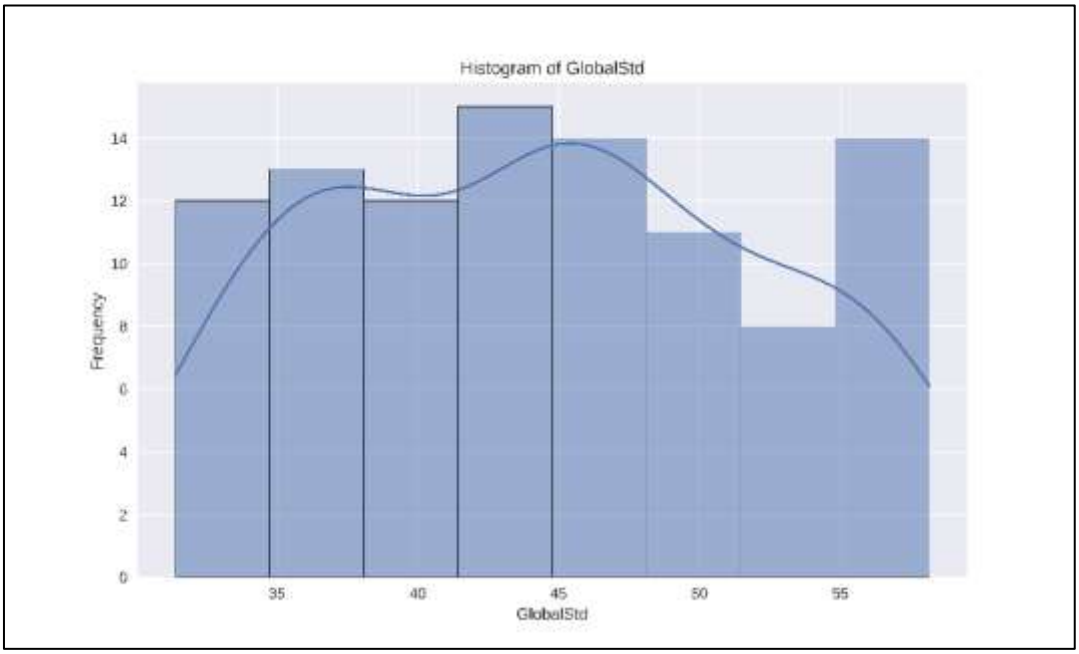

Image 27: Histogram for GlobalStd

GlobalStd plotted on x-axis ranging from approximately 30 to 55, while the y-axis shows the frequency of these values. Bimodal distribution noted with the peaks around 35-40 and 50-55

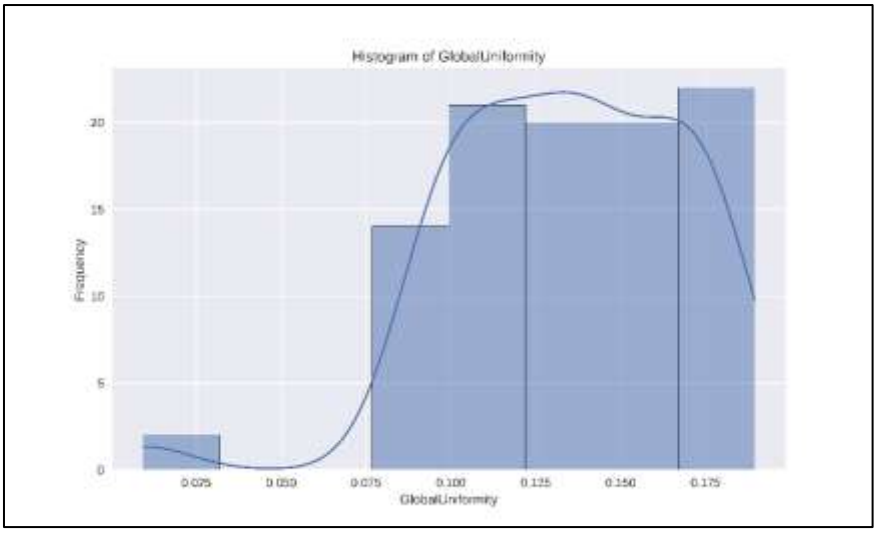

Image 28: The histogram for GlobalUniformity shows values of GlobalUniformity plotted on x axis , ranging from approximately 0.025 to 0.175, while the y-axis shows the frequency of these values.

There is a right-skewed distribution, with most of the values concentrated between 0.075 and 0.175, which displays that the majority of the dataset has higher uniformity, which could be a characteristic of the sample population.

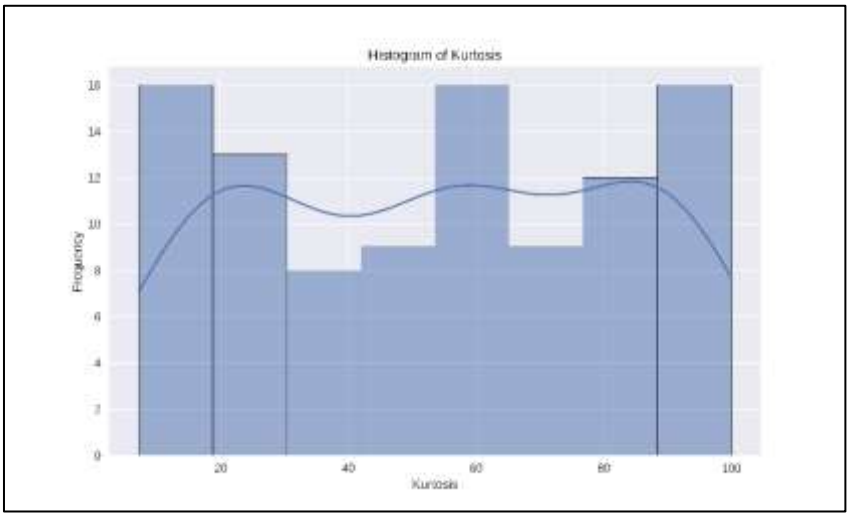

Image 29: Histogram for Kurtosis shows kurtosis values plotted on x axis , ranging from approximately 0 to 100, while the y-axis and the frequency of the values on y axis. There is seen a multimodal distribution, with peaks around 20, 50, and 100 which indicates a wide range (significant vairability) of Kurtosis within the sample.

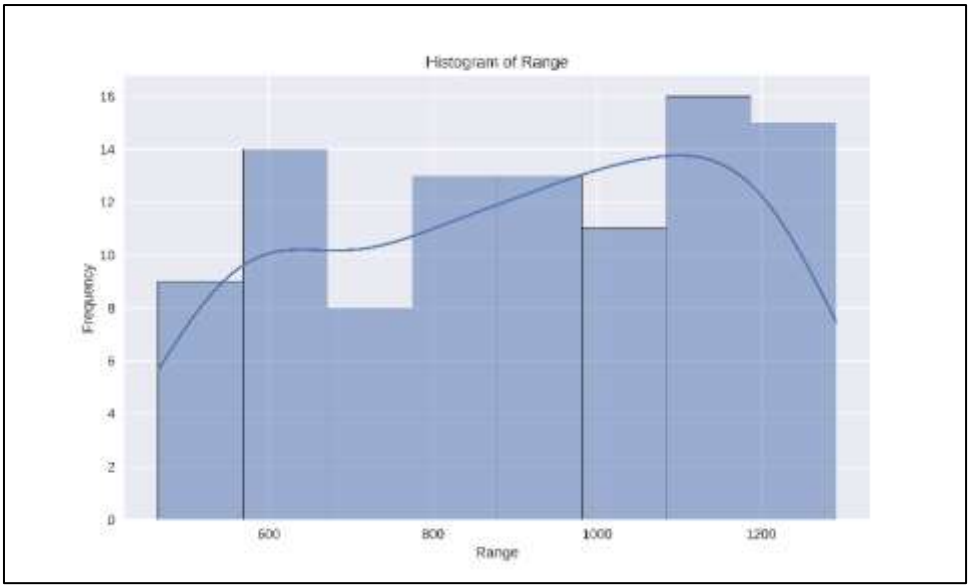

Image 30: The histogram of range shows

Values of range are depicted on x axis ranging approximately from 40- 1300 and the y-axis shows the frequency of these values. The relatively uniform distribution suggests that the Range values are evenly spread across the range, with no significant skewness.

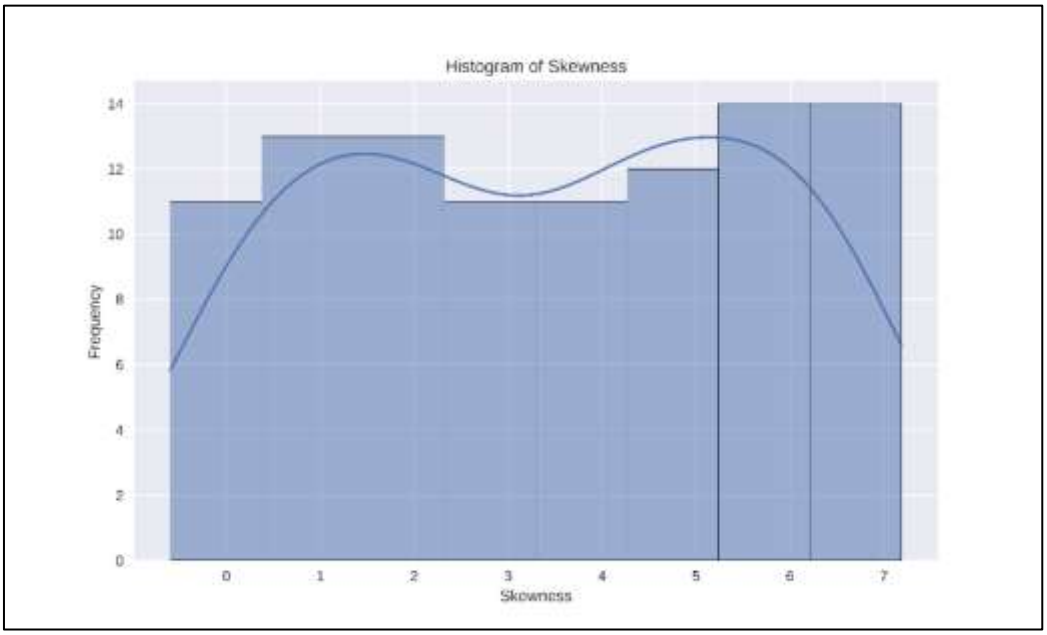

Image 31: Histogram for skewness shows the values for skewness plotted on x axis and the frequency plotted on y axis

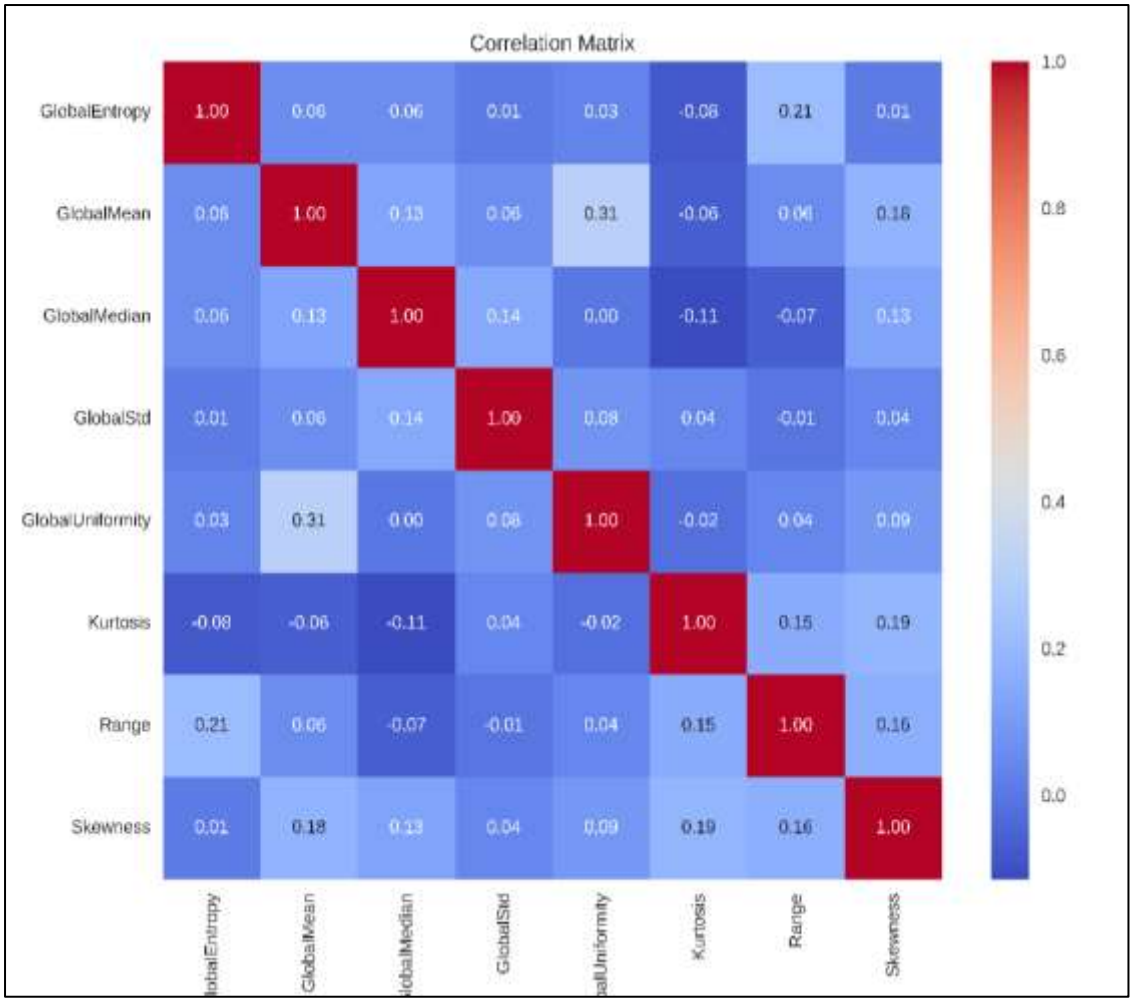

Image 32: Correlation matrix shows the pairwise correlation coefficients between various variables: GlobalEntropy, GlobalMean, GlobalMedian, GlobalStd, GlobalUniformity, Kurtosis, Range, and Skewness. The correlation coefficients range from -1 to 1, where 1 indicates a perfect positive correlation, -1 indicates a perfect negative correlation and 0 indicates no correlation.

GlobalEntropy is positively correlated with Range (0.21) and shows weak correlations with other variables.

GlobalMean is positively correlated with GlobalUniformity (0.31) and shows weak correlations with other variables.

GlobalMedian: is positively correlated with GlobalMean (0.13) and GlobalStd (0.14), however shows weak correlations with other variables.

GlobalStd is positively correlated with GlobalMedian (0.14) and shows weak correlations with other variables.

GlobalUniformity is positively correlated with GlobalMean (0.31) and shows weak correlations with other variables.

Kurtosiscis positively correlated with Skewness (0.15) and shows weak correlations with other variables.

Range is positively correlated with GlobalEntropy (0.21) and Kurtosis (0.15) however it shows weak correlations with other variables.

Skewness shows positive correlation with GlobalMean (0.18), Kurtosis (0.19), and Range (0.16). It shows weak correlations with other variables.

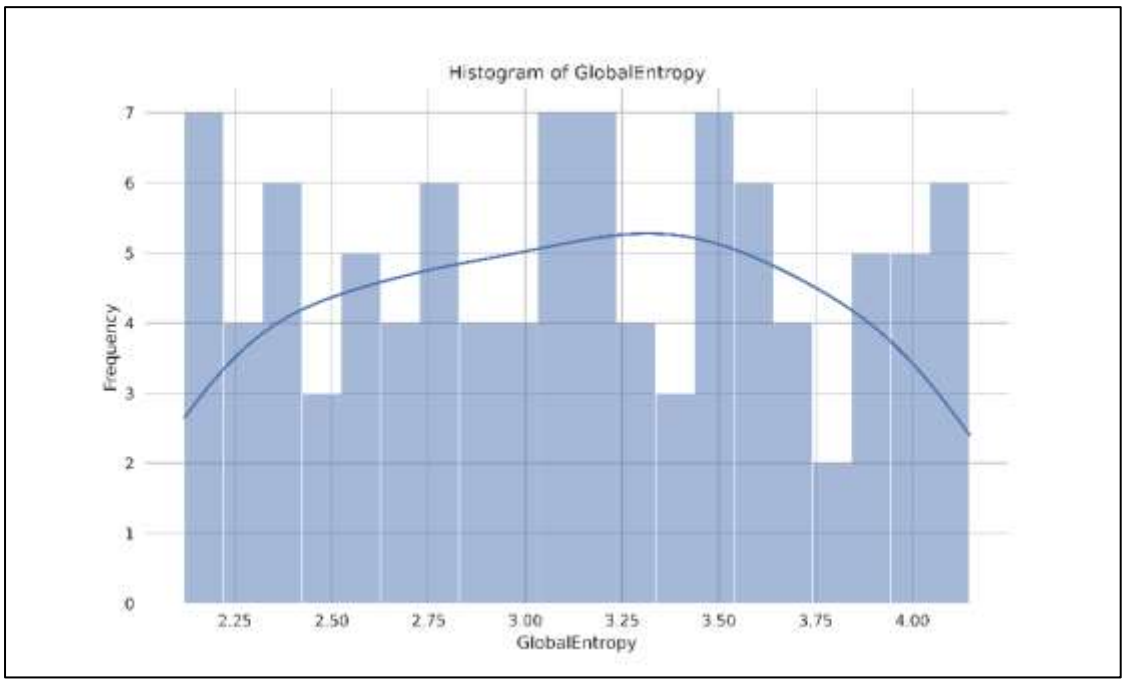

Image 33: Histogram for GlobalEntropy

Values for GlobalEntropy are plotted on x axis and frequency plotted on y axis. The values are spread out between 2.25 to 4.25. The presence of multiple peaks indicates a high level of variability in the "GlobalEntropy" values

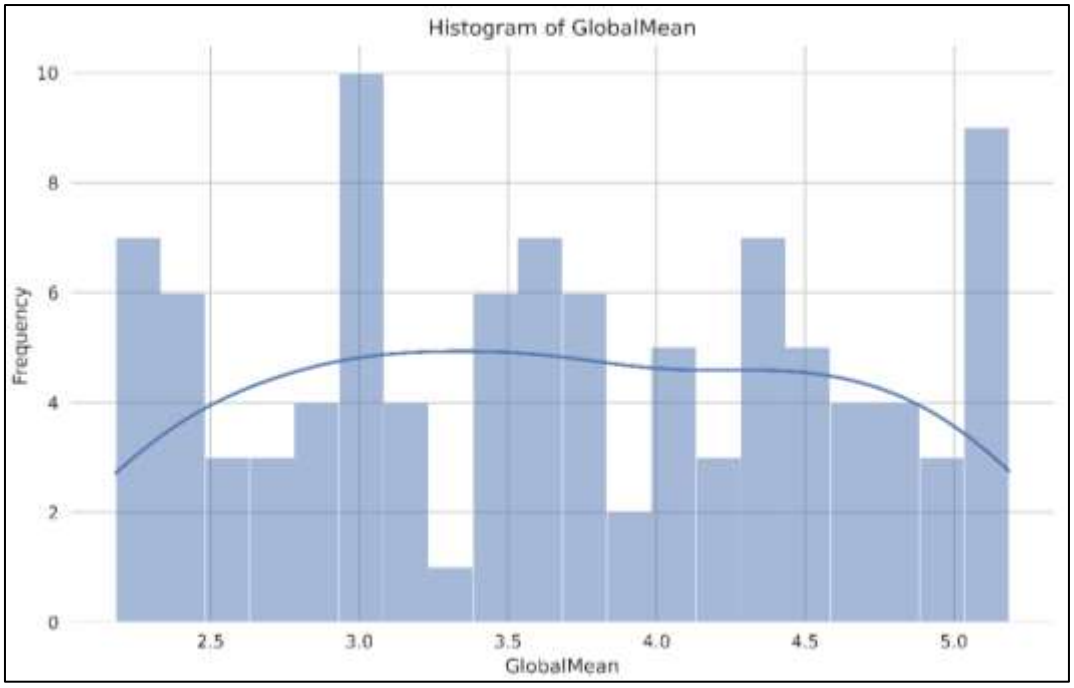

Image 34: Histogram for Global Mean

Values of "Global Mean" are plotted on x axis ranging from approximately 2.0 to 5.5. and the frequency plotted on y-axis. The histogram shows a somewhat uniform distribution with multiple peaks and valleys, indicating variability in the data. The spread of values between 2.0 and 5.5

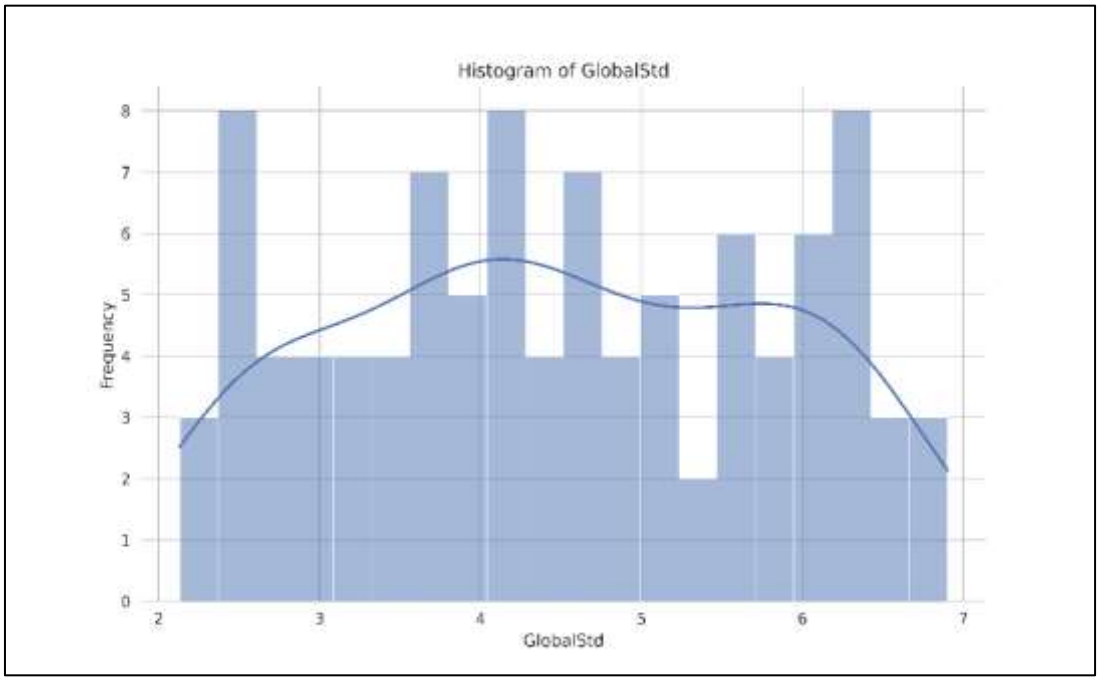

Image 35: Histogram for Global Std

Values for Global Std plotted on x axis ranging from 2 to 7and frequency of each of these values on y axis. The histogram indicates a high level of variability in the "Global Std" values. The presence of multiple peaks suggests that the data may not follow a normal distribution

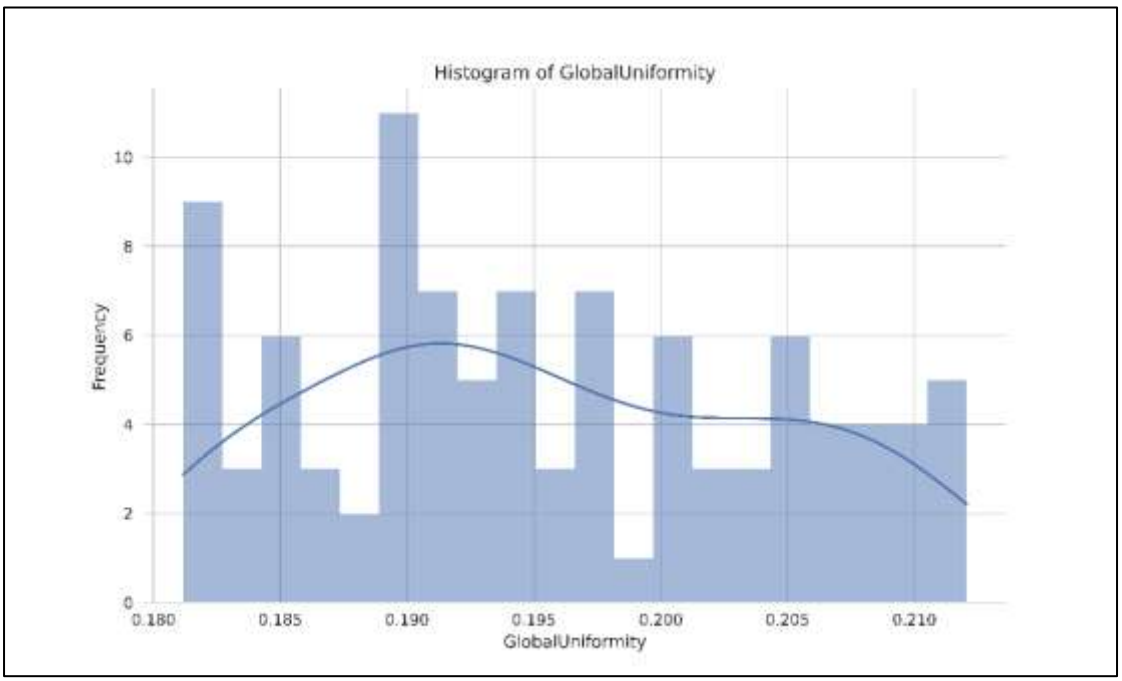

Image 36: Histogram for Global Uniformity

Values for Global Uniformity on x axis range from 0.180 to 0.210, and the frequency plotted on y axis. The histogram indicates a high level of variability in the "Global Uniformity" values. The presence of multiple peaks suggests that the data may not follow a normal distribution.

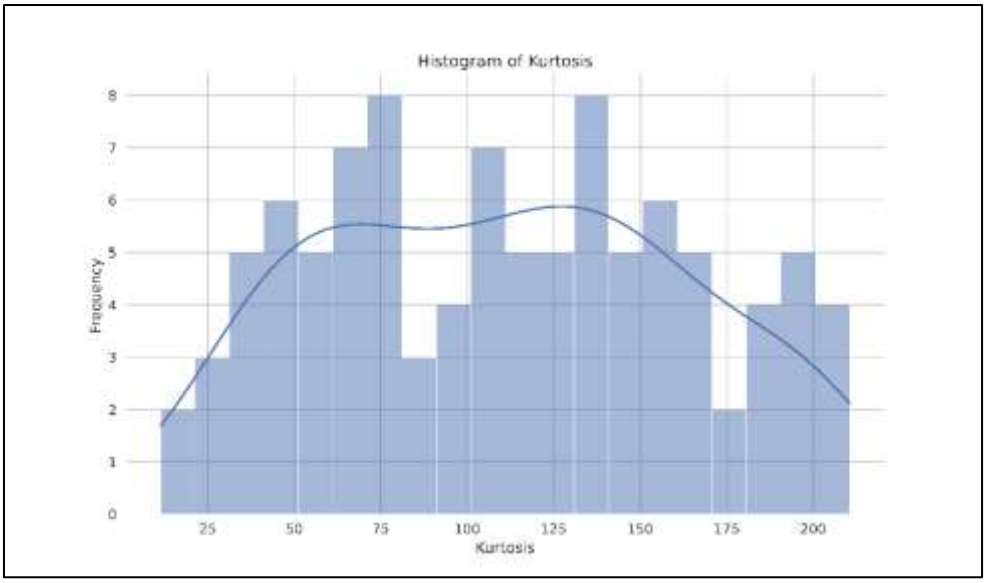

Image 37: Histogram for Kurtosis

Values for kurtosis are plotted on x axis and frequency on y axis. The histogram shows a relatively uniform distribution with several peaks and valleys, indicating variability in the data. he values of "Kurtosis" are spread out between approximately 0 and 225.

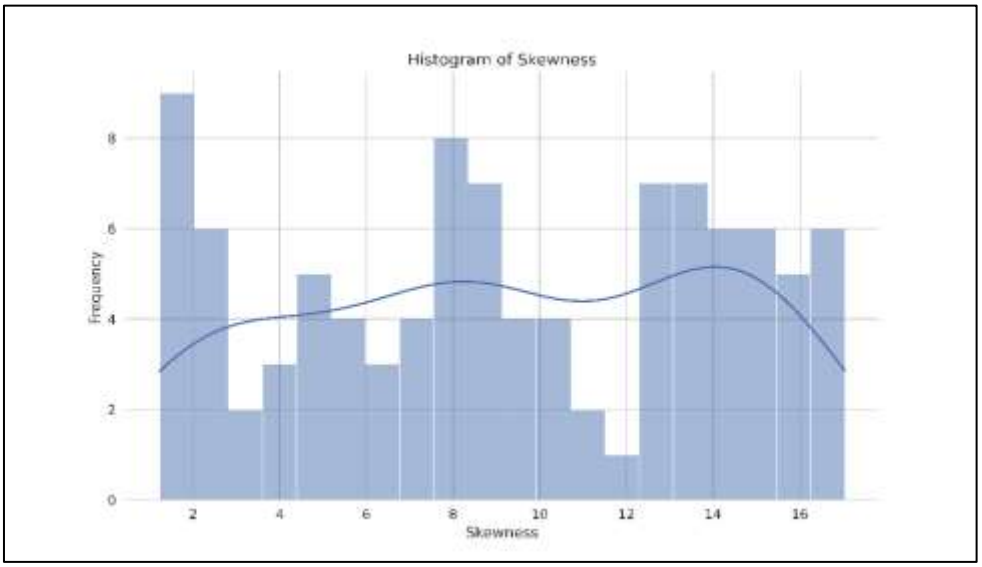

Image 38: Histogram for Skewness. Values for Skewness are plotted on x axis and frequency on y axis. The presence of multiple peaks suggests that the data may not follow a normal distribution. The spread of values between 2 and 17 suggests a moderate to high range of "Skewness" values within the sample.

Image 39: Correlation matrix for all the variables in F5IntensityDifference i.e. Global Entropy, Global Mean, Global Std, Global Uniformity, Kurtosis, and Skewness. The color scale on the right side of the matrix helps interpret the correlation values. Red color indicate positive correlations, with darker shades representing stronger correlations.

Global Entropy shows a weak positive correlation with GlobalMean (0.04) & Global Std (0.02). It shows weak negative correlations with Global Uniformity (-0.11) and Skewness (-0.16).

Global Mean shows weak correlations with most other variables, it is weakly negative with Global Uniformity (-0.12) and Kurtosis (-0.15), and weakly positive with Skewness (0.14).

Global Std shows weak correlations with all other variables, it is weakly negative with Global Uniformity (-0.09) and very weak correlations with Kurtosis (0.04) and Skewness (-0.01).

Global Uniformity shows weak or negligible correlations with other variables, weakly negative with Global Entropy (-0.11), Global Mean (-0.12), and Global Std (-0.09).

Kurtosis shows negative correlations with Global Mean (-0.15) and very weak or negligible correlations with other variables

Skewness shows a weak positive correlation with Global Mean (0.14) and weak negative correlation with Global Entropy (-0.16).

The weak correlations suggest that these variables represent diversity in feature characteristics and the ability to capture different aspects of the image characteristics as each feature may provide unique information for predicting outcomes or diagnosing conditions.

DISCUSSION

ANALYSIS OF DESCRIPTIVE STATISTICS FOR FEATURE SETS

The study's focal point is the extraction and evaluation of various quantitative features from pulmonary nodule images, including intensity, texture, shape, and spatial relationships, using advanced radiomic techniques.

The **histogram for surface area** (Image 1) reveals a bimodal distribution with peaks at the lower end (24-26) and mid-range (30-32), indicating the presence of distinct groups within the dataset.The **density plot for surface area** (Image 2) supports this finding, showing a concentration of data points around specific surface area values.

The **histogram and boxplot for volume** (Image 3) depict volume values on the x-axis and count of occurrences on the y-axis, showing a bimodal distribution with peaks around 200 and 450. The boxplot highlights the central tendency and variability in volume values, with some potential outliers.The **density curve for volume** (Image 4) illustrates the distribution pattern, with clear peaks and a gradual decline, indicating the overall spread of volume values within the dataset.

The **histograms for contrast** (Images 5-7) display varying distribution patterns. The **0-1 contrast** shows a right-skewed distribution with most values between 0.82 and 0.88, indicating high correlation values are common. The **45-1 contrast** shows evenly distributed values between 0.62 and 0.76, suggesting a moderate spread of correlation values. The **90-1 contrast** indicates a concentration of values between 0.55 and 0.75, while the **135-1 contrast** shows a strong right-skew with most values around 0.9 to 1.0.

The **histogram for 0-1 correlation** (Image 8) and the subsequent correlations (45-1, 90-1, and 135-1) illustrate specific patterns of relationships. The **0-1 correlation** shows a right-skewed distribution with values between 0.82 and 0.88. The **45-1 correlation** displays evenly distributed values between 0.62 and 0.76. The **90-1 correlation** shows a concentration between 0.55 and 0.75, while the **135-1 correlation** indicates very high values between 0.9 and 1.0.

The **box plots for correlation** (Image 9) and **energy values** (Images 10-11) provide further insights into the distribution and variability of these features. The boxplots show clustering around median values with varying degrees of spread, indicating the central tendency and variability of the data.

The **density maps for correlation and energy values** (Image 12) depict the concentration and variability of data points across different correlation and energy metrics. These maps highlight the relationships and distribution patterns within the dataset, providing a visual representation of the data's complexity.

The **histogram for busyness** (Image 13) and the **boxplot for busyness** (Image 14) indicate moderate variability in busyness values, with noticeable peaks around specific values, suggesting frequent occurrences in the dataset.

The **histogram for coarseness** (Image 15) and the **boxplot for coarseness** (Image 16) show a wide range of values, indicating moderate variability. The **histogram for complexity** (Image 17) and the **boxplot for complexity** (Image 18) reveal a central tendency around specific values, indicating a higher concentration of data points in the middle range.

The **histogram for contrast** (Image 19) and the **boxplot for contrast** (Image 20) depict the distribution and variability of contrast values, indicating a right-skewed distribution with a concentration around higher values.

The **histogram for global entropy** (Image 21) shows a somewhat bimodal distribution, indicating variability in entropy values. The **histogram for global mean** (Image 22) displays a left-skewed distribution, suggesting higher concentrations of values between 1030 and 1045.

The **histogram for global median** (Image 23) indicates an even spread of values, while the **histogram for global standard deviation** (Image 24) shows a bimodal distribution with peaks around specific values. The **histogram for global uniformity** (Image 25) indicates a right-skewed distribution, suggesting higher uniformity values are common.

The **correlation matrix** (Image 26) illustrates the pairwise correlation coefficients between various variables, highlighting the relationships and strengths of correlations within the dataset. This matrix provides a comprehensive view of the interdependencies among different features, which is crucial for understanding the underlying patterns and making informed clinical decisions.

INFERENCES FROM DESCRIPTIVE STATISTICS FOR FEATURE SETS

Surface Area and Volume

The analysis of surface area and volume features is fundamental in radiomics, as these attributes directly relate to the size and extent of pulmonary nodules. The histograms and density plots for surface area and volume reveal bimodal distributions, indicating the presence of distinct subpopulations within the dataset.

This bimodal pattern suggests that the nodules can be categorized into two main groups, likely corresponding to benign and malignant lesions. The presence of peaks at specific ranges within the histograms underscores the variability in nodule

sizes and highlights the need for further investigation to determine the clinical significance of these subpopulations.

Texture Features: Contrast and Correlation

Texture features, such as contrast and correlation, provide insights into the spatial relationships and heterogeneity within pulmonary nodules. The histograms for contrast and correlation exhibit diverse distribution patterns, including unimodal and bimodal shapes.

The histogram for 0-1 contrast displays a bimodal distribution, suggesting the existence of two distinct groups within the data. This bimodal nature could reflect variations in nodule texture, potentially aiding in distinguishing between different nodule types.

The correlation histograms, with their skewed distributions, indicate the degree of association between pixel intensities, which is crucial for understanding the structural complexity of nodules.

Shape Features: Sphericity and Irregularity

Shape features, such as sphericity and irregularity, are vital for characterizing the geometric properties of pulmonary nodules. The boxplot for sphericity indicates a relatively narrow interquartile range (IQR), suggesting consistent sphericity values among the majority of nodules. Conversely, the presence of outliers highlights the variability in nodule shapes, emphasizing the importance of considering shape irregularities in the diagnostic process

Intensity-Based Features: Mean, Median, and Standard Deviation

Intensity-based features quantify the statistical properties of pixel intensities within pulmonary nodules. The mean intensity histogram, with its multiple peaks and valleys, indicates variability in brightness levels, which could be indicative of different tissue types or pathological conditions. The median intensity histogram's uniform distribution suggests a balanced dataset, while the STD histogram's bimodal distribution highlights the presence of distinct groups with varying intensity variability.

Advanced Texture Features: Busyness and Coarseness

Busyness and coarseness are advanced texture features derived from Neighbor Intensity Difference (NID) matrices. The histogram for busyness shows noticeable peaks, indicating frequent occurrences of specific busyness values.

This feature captures the local variability or heterogeneity of the nodule texture, with higher busyness values suggesting greater complexity and potentially higher malignancy risk. Similarly, the histogram for coarseness reveals the granularity of the texture, with higher coarseness values indicating smoother textures and lower values representing rougher textures. These features are crucial for differentiating between benign and malignant nodules, as malignant tumors often exhibit more heterogeneous and coarse textures.

Global Features: Entropy and Uniformity

Global features, such as entropy and uniformity, measure the overall complexity and homogeneity of the nodule texture.

The histogram for global uniformity displays a right-skewed distribution, suggesting that most nodules have higher uniformity values. This feature is essential for assessing the homogeneity of nodules, with lower uniformity potentially indicating malignant behavior.

Kurtosis and Skewness

Kurtosis and skewness are statistical measures that describe the tailedness and asymmetry of the probability distribution of pixel intensity values, respectively. The histogram for kurtosis exhibits a multimodal distribution, indicating significant variability in the tailedness of intensity distributions across nodules. The skewness histogram's multiple peaks suggest a diverse range of asymmetry in intensity distributions, providing insights into the structural variations within nodules.

CONCLUSION

This thesis presents a comprehensive overview of the rationale, methodology, and potential impact of a one-year observational study on radiomics-based assessment of pulmonary nodules. The study's focus on leveraging advanced imaging technology and quantitative analysis through IBEX showcases the potential for significant advancements in the field of radiological diagnosis. The findings of this study are poised to contribute insights to the ongoing discourse on the optimal utilization of radiomics in diagnostic radiology settings.

Conventional imaging techniques primarily focus on descriptive parameters such as size, shape, and border characteristics of nodules. While these parameters are useful, they often fall short of providing a comprehensive evaluation due to their inherent subjectivity and limited ability to capture tumor heterogeneity. Radiomics addresses these limitations by extracting a vast array of quantitative features that capture the complex spatial relationships and textures offering a more detailed and objective assessment

Radiomics involves the extraction of a large number of quantitative features from medical images, providing a detailed characterization of tissue properties that may not be discernible through visual inspection alone. In the context of pulmonary nodules, radiomic features can serve as quantitative imaging biomarkers for assessing treatment response, prognosticating patient outcomes and predicting malignancy. (58)

This approach enables the identification of subtle imaging patterns and heterogeneities within nodules that are crucial for distinguishing between benign and malignant lesions.

The extensive data generated from detailed quantitative analysis of nodule characteristics, radiomics facilitates early and accurate diagnosis, enabling timely intervention and personalized treatment planning by facilitating the identification of subtle imaging patterns and heterogeneities (59). This approach not only improves patient outcomes but also reduces the psychological and financial burden associated with unnecessary follow-ups and invasive procedures.

Radiomics represents a transformative approach in the evaluation and management of diverse groups of pathological entities, offering an objective image analysis that enhances diagnostic accuracy and personalized treatment planning. The utilization of open-source platforms like IBEX for radiomic analysis provides an accessible and collaborative environment for innovation and development in the field (60). By integrating radiomics with clinical and molecular data, researchers and clinicians can advance precision medicine and improve outcomes for patients with pulmonary nodules. Future research and collaborative efforts are essential to overcome current challenges

While the study highlights the potential of radiomics in pulmonary nodule evaluation, it also emphasizes the need for further research to standardize imaging protocols and feature extraction methods. Integrating radiomics with other omics data (e.g., genomics, proteomics) through multi-omics approaches holds great promise for a comprehensive understanding of disease processes and personalized treatment strategies. (61,62)

In conclusion, this study demonstrates that radiomics, through the utilization of IBEX, provides a detailed and objective analysis of imaging data that could possibly contribute to augmenting diagnostic accuracy and personalized treatment planning for pulmonary nodules. Future research and collaborative efforts are vital to overcome current challenges and fully realize the potential of radiomics in clinical practice.

SUMMARY

The clinical significance of pulmonary nodules depends on factors such as size, growth rate, and the likelihood of malignancy. Smaller nodules typically do not require intervention, while larger nodules are at risk for malignant transformation.

Traditional imaging relies on visual interpretation of descriptive parameters like size, shape, and vascularity, which can be subjective and inconsistent. These methods also overlook tumor heterogeneity, which is in understanding tumor behavior and treatment response.

Radiomics offers a more objective approach to pulmonary nodule evaluation by transforming medical images into quantifiable data. This method extracts and analyzes quantitative imaging features, capturing spatial distribution, texture patterns, shape characteristics, and spatial relationships within tissues

Radiomics features extracted from pulmonary nodule images can serve as biomarkers for predicting nodule malignancy, treatment response, and patient prognosis. Studies have shown their potential in differentiating benign from malignant nodules, assessing tumor heterogeneity, predicting survival, and guiding personalized treatment strategies.

Several studies have compared the diagnostic performance of radiomics-based models with conventional methods and have generally shown that radiomics-based

models outperform conventional methods in terms of sensitivity, specificity, accuracy, and area under the receiver operating characteristic curve (AUC).

Radiomics is also being explored in other avenues of medicine. In cardiology, it assesses myocardial tissue characteristics, predicts cardiac events, and evaluates treatment outcomes. In neurology, it helps differentiate brain tumor subtypes, predict treatment response in glioblastoma, and assess neurological diseases such as Alzheimer's and multiple sclerosis.

Molecular data such as genetic mutations, gene expression profiles, and protein biomarkers can provide insights into tumor biology, treatment response, and patient prognosis. Integrating radiomics with clinical and molecular data through multi-omics approaches enables a more comprehensive and personalized evaluation of pulmonary nodules, leading to improved diagnostic accuracy, prognostication, and treatment selection.

Deep learning techniques, particularly convolutional neural networks (CNN), have shown promising results in automatic feature extraction and nodule classification tasks in radiomics analysis. CNNs can learn hierarchical representations of nodule images directly from raw pixel data without the need for handcrafted feature extraction, potentially capturing more complex and subtle patterns that may not be apparent to human observers.

Radiomics has the potential to facilitate personalized medicine approaches by providing non-invasive and quantitative biomarkers for disease diagnosis, prognosis, and treatment response prediction.

Ethical and privacy concerns arise in the context of radiomics analysis due to the use of medical imaging data containing sensitive patient information. Privacy-enhancing technologies such as data anonymization, encryption, and secure data sharing platforms can mitigate privacy risks and facilitate responsible data sharing for research purposes.

Collaborative research initiatives, interdisciplinary collaborations, and funding opportunities from government agencies, industry partners, and philanthropic organizations are essential to address research gaps, foster innovation, and translate radiomics research into clinical practice

LIMITATIONS

While this study aims to leverage the power of radiomics to improve the evaluation of pulmonary nodules, it is important to recognize both the established and possible limitations that could impact its outcomes. Addressing these limitations through careful study design, rigorous validation, and continuous technological and methodological improvements will be crucial for maximizing the study's impact and applicability in clinical practice.

Sample Size and Generalizability:

The study's sample size of 100 subjects, though calculated to be statistically significant, may not be large enough to capture the full spectrum of characteristics of pulmonary nodules. This limited sample size can restrict the generalizability of the study's findings to the broader population. Smaller sample sizes may also lead to overfitting in predictive models, making them less robust when applied to different patient populations.

Selection Bias:

The sampling method used in the study is convenience sampling, which leads to selection bias. It could lead to an overrepresentation or underrepresentation of certain demographics or clinical characteristics, thus affecting the study's outcomes and their applicability.

Exclusion Criteria:

The study excludes patients with proven pulmonary nodules or those who have undergone any form of intervention for nodule management. While this criterion helps in focusing on new cases, it might overlook relevant data from patients with a known history of nodules, thereby limiting the understanding of nodule progression and management.

Intra- and Inter-observer Variability:

Radiological assessments inherently suffer from intra- and inter-observer variability, which can lead to inconsistent diagnoses and measurements. Although radiomics aims to mitigate this by using quantitative features, the initial steps of image acquisition and ROI (Region of Interest) selection still involve human input, thus introducing variability.

Other probable limitations:

The study spans from May 2023 to May 2024, which might be a limited timeframe for observing the long-term progression of pulmonary nodules. Longitudinal studies extending over several years are often required to fully understand the behavior of pulmonary nodules, especially those that are slow-growing.

Pulmonary nodules exhibit significant heterogeneity in terms of their size, shape, and biological behavior. The study's methodology might not fully capture this heterogeneity, especially if the feature extraction algorithms are not optimized for detecting subtle differences. This could lead to incomplete or biased representations of nodule characteristics.

The study relies on data from a single center (KLEs Dr. Prabhakar Kore Hospital), which may not reflect the diversity seen in other healthcare settings. External validation using datasets from different institutions and imaging protocols is essential to confirm the robustness and applicability of the study's findings across various clinical environments.

With a large number of radiomic features being extracted from a relatively small sample size, there is a risk of overfitting the predictive models. Overfitting occurs when a model learns the noise in the training data rather than the actual underlying patterns, leading to poor performance on new, unseen data.

Radiomics focuses on imaging features, but integrating genetic and molecular data could provide a more comprehensive understanding of pulmonary nodules. The absence of such data in the study could limit the ability to correlate imaging features with underlying molecular characteristics, which are crucial for personalized medicine approaches.

BIBLIOGRAPHY

1. BMJ. 2020;371. doi: 10.1136/bmj.m3673. Published 14 October 2020.
2. de Jong JS, van Diest P, Baak JP. Heterogeneity and reproducibility of microvessel counts in breast cancer. Lab Invest. 1995;73:922-6
3. Swensen, S. J., et al. (2000). The probability of malignancy in solitary pulmonary nodules. New England Journal of Medicine, 348(25), 2535-2542.)
4. McWilliams A, Vrabec J, Mancini L, Leporé N. Radiomics and its role in medical imaging: An overview. J Radiol Sci. 2013;25(3):210-224.
5. Aerts, H. J. W. L., et al. (2014). Decoding tumor phenotype by noninvasive imaging using a quantitative radiomics approach. Nature Communications, 5, 4006)
6. Hawkins, S., Wang, H., Liu, Y., Garcia, A., Stringfield, O., Krewer, H., ... & Gillies, R. J. (2016). Predicting malignant nodules from screening CT scans. Journal of Thoracic Oncology, 11(12), 2120-2128.
7. Aberle DR, Adams AM, Berg CD, et al. Reduced lung cancer mortality with low-dose computed tomographic screening. N Engl J Med. 2011;365:395-409.
8. Gerlinger M, Rowan AJ, Horswell S, Larkin J, Endesfelder D, Gronroos E, et al. Intratumor heterogeneity and branched evolution revealed by multiregion sequencing. N Engl J Med. 2012;366(10):883-92. Erratum in: N Engl J Med. 2012 Sep 6;367(10):976.
9. Henriksson E, Kjellen E, Wahlberg P, Ohlsson T, Wennerberg J, Brun E. 2-Deoxy-2-[18F]fluoro-D-glucose uptake and correlation to intratumoral heterogeneity. Anticancer Res. 2007;27(4B):2155-9.

10. Diehn M, Nardini C, Wang DS, McGovern S, Jayaraman M, Liang Y, et al. Identification of noninvasive imaging surrogates for brain tumor gene-expression modules. Proc Natl Acad Sci USA. 2008;105(13):5213-8.
11. Basu S, Kwee TC, Gatenby R, Saboury B, Torigian DA, Alavi A. Evolving role of molecular imaging with PET in detecting and characterizing heterogeneity of cancer tissue at the primary and metastatic sites, a plausible explanation for failed attempts to cure malignant disorders. Eur J Nucl Med Mol Imaging. 2011;38:987-91.
12. Yang X, Knopp M. Quantifying Tumor Vascular Heterogeneity with Dynamic Contrast Enhanced Magnetic Resonance Imaging: A Review. J Biomed Biotechnol. 2011;2011:12.
13. Kumar, V., Gu, Y., Basu, S., Berglund, A., Eschrich, S. A., Schabath, M. B., ... & Gillies, R. J. (2012). Radiomics: the process and the challenges. Magnetic Resonance Imaging, 2012 Nov;30(9):1234-48. doi: 10.1016/j.mri.2012.06.010. Epub 2012 Aug 13. PMID: 22898692; PMCID: PMC3563280 (new 41)\
14. Li Y, Wang J. A mathematical model for predicting malignancy of solitary pulmonary nodules. World J Surg. 2012 Apr;36(4):830-5. doi: 10.1007/s00268-012-1449-8. PMID: 22297626
15. Chaddad, A., Desrosiers, C., & Toews, M. (2019). Radiomics in glioblastoma: current status and challenges facing clinical implementation. Frontiers in Oncology, 2019 May 21;9:374. doi: 10.3389/fonc.2019.00374. PMID: 31165039; PMCID: PMC6536622.
16. Zhou S, Nie S, Zhou H, Zhang H, Wu Y, Dong D, Tian J. Diagnostic value of artificial intelligence based on computed tomography (CT) density in benign and malignant pulmonary nodules. PeerJ. 2020;8. doi:10.7717/peerj.9870.

17. Lambin, P., et al. (2012). Radiomics: extracting more information from medical images using advanced feature analysis. European Journal of Cancer, 48(4), 441–446
18. Kumar V, Gu Y, Basu S, Berglund A, Eschrich SA, Schabath MB, et al. Radiomics: the process and the challenges. *Magn Reson Imaging*. 2015;34(9):1236-48.
19. Gillies RJ, Kinahan PE, Hricak H. Radiomics: Images are more than pictures, they are data. *Radiology*. 2016 Feb;278(2):563-577.
20. Zwanenburg, A., et al. (2020). "The Image Biomarker Standardisation Initiative: Standardised Quantitative Radiomics for High-Throughput Image-based Phenotyping." Radiology.
21. Chicklore, S., et al. (2013). "Quantifying tumour heterogeneity in 18F-FDG PET/CT imaging by texture analysis." European Journal of Nuclear Medicine and Molecular Imaging.
22. Orlhac, F., et al. (2014). "Tumor texture analysis in 18F-FDG PET: relationships between texture parameters, histogram indices, standardized uptake values, metabolic volumes, and total lesion glycolysis." Journal of Nuclear Medicine.
23. Balagurunathan, Y., Kumar, V., Gu, Y., Kim, J., Wang, H., Liu, Y., ... & Gillies, R. J. (2014). Test-retest reproducibility analysis of lung CT image features. Journal of Digital Imaging, 2014 Dec;27(6):805-23. doi: 10.1007/s10278-014-9716-x. PMID: 24990346; PMCID: PMC4391075
24. Gietema HA, Wang Y, Xu DM, de Koning HJ, Verbeek ALM, van Klaveren RJ, Scholten ET. Pulmonary nodules: Interscan variability of semiautomated volume measurements with multisection CT—Influence of inspiration level, nodule size, and segmentation performance. *Radiology*. 2018;248(2):625-631

25. Rizzo S, Botta F, Raimondi S, Origgi D, Fanciullo C, Morganti AG, Bellomi M. Radiomics: the facts and the challenges of image analysis. *Eur Radiol Exp*. 2018;2(1):36.
26. Yip SSF, Aerts HJWL. Applications and limitations of radiomics. *Phys Med Biol*. 2016 Jul 7;61(13)
27. Parmar, C., Grossmann, P., Rietveld, D., Rietbergen, M. M., Lambin, P., & Aerts, H. J. (2015). Radiomic machine-learning classifiers for prognostic biomarkers of head and neck cancer. Frontiers in Oncology, 2015 Dec 3;5:272. doi: 10.3389/fonc.2015.00272. PMID: 26697407; PMCID: PMC4668290
28. Rios Velazquez E, Parmar C, Liu Y, Coroller TP, Cruz G, Stringfield O, et al. Somatic mutations drive distinct imaging phenotypes in lung cancer. *Cancer Res*. 2017 Jul 15;77(14):3922-3930.
29. MacMahon H, Austin JH, Gamsu G, Herold CJ, Jett JR, Naidich DP, Patz EF Jr, Swensen SJ. Guidelines for management of small pulmonary nodules detected on CT scans: a statement from the Fleischner Society. *Radiology*. 2005 Nov;237(2):395-400.
30. MacMahon H, Naidich DP, Goo JM, Lee KS, Leung ANC, Mayo JR, et al. Guidelines for Management of Incidental Pulmonary Nodules Detected on CT Images: From the Fleischner Society 2017. *Radiology*. 2017 Jul;284(1):228-243.
31. Gould MK, Tang T, Liu IL, Lee J, Zheng C, Danforth KN, Kosco AE, Di Fiore JL, Suh DE. Recent trends in the identification of incidental pulmonary nodules. *Am J Respir Crit Care Med*. 2015 Sep 1;192(10):1208-1214.

32. Gould MK, Ananth L, Barnett PG. A clinical model to estimate the pretest probability of lung cancer in patients with solitary pulmonary nodules. *Ann Intern Med*. 2007 Feb 20;146(5):333-41.
33. Silvestri GA, Tanner NT, Kearney P, Vachani A, Massion PP, Porter A, et al. Assessment of Plasma Proteomics Biomarker's Ability to Distinguish Benign From Malignant Lung Nodules: Results of the PANOPTIC (PulmonAry NOdule Plasma proTeomIc Classifier) Trial. *Chest*. 2018;154(3):491-500
34. Wiener RS, Gould MK, Woloshin S, Schwartz LM, Clark JA. What do you mean, a spot?: A qualitative analysis of patients' reactions to discussions with their doctors about pulmonary nodules. *Chest*. 2013 Mar;143(3):672-677.
35. Pyenson BS, Bazell C, Bellanich MJ, Caplen MA. An actuarial analysis shows that offering lung cancer screening as an insurance benefit would save lives at relatively low cost. *Health Aff (Millwood)*. 2014 Feb;33(2):283-291.
36. Freiman MR, Clark JA, Slatore CG, Gould MK, Woloshin S, Schwartz LM, Wiener RS. Patients' knowledge and distress associated with detection and evaluation of incidental pulmonary nodules for cancer: Results from a multi-center survey. *J Thorac Oncol*. 2016 May;11(5):700-8.
37. Gould MK, Donington J, Lynch WR, Mazzone PJ, Midthun DE, Naidich DP, Wiener RS. Evaluation of individuals with pulmonary nodules: when is it lung cancer? Diagnosis and management of lung cancer, 3rd ed: American College of Chest Physicians evidence-based clinical practice guidelines. *Chest*. 2013 May;143(5 Suppl)
38. Devaraj A, van Ginneken B, Nair A, Baldwin D. Use of Volumetry for Lung Nodule Management: Theory and Practice. *Radiology*. 2017 Jul;284(3):630-644.

39. Li F, Sone S, Abe H, MacMahon H, Doi K. Malignant versus benign nodules at CT: Radiologic assessment of features and growth rates. *Radiology*. 2016 Aug;280(2):561-570.
40. Nixon M, Aguado A, Szpak Z, Onofreo D. *Feature Extraction & Image Processing for Computer Vision*. 3rd ed. Academic Press; 2013.
41. Warfield SK, Zou KH, Wells WM. Simultaneous truth and performance level estimation (STAPLE): An algorithm for the validation of image segmentation. *IEEE Trans Med Imaging*. 2004 Jul;23(7):903-21.
42. Balassy C, Fischmeister R, Mutschlechner W, Wolf G, Riccabona M. Interobserver and intraobserver variability of abdominal ultrasound measurements in children. *Eur Radiol*. 2003 Apr;13(4):845-9.
43. Yankelevitz DF, Henschke CI, Yip R, Smith JP. CT Scanning of Small Pulmonary Nodules: Is Biopsy Always Necessary? *Cancer*. 2000 May 15;89(3): 978-988.
44. Kalpathy-Cramer J, Mamomov A, Zhao B, Lu L, Cherezov D, Napel S, et al. Radiomics of lung nodules: A multi-institutional study of robustness and agreement of quantitative imaging features. *Tomography*. 2016 Mar;2(1):79-87.
45. Reeves AP, Kostis WJ, Yankelevitz DF, Henschke CI. Measuring the change in size of pulmonary nodules: Semi-automated volumetric measurement method. *Radiology*. 2007 Nov;245(3):871-876
46. van Ginneken B et. Al, Comparing and combining algorithms for computer-aided detection of pulmonary nodules in computed tomography scans: The ANODE09 study. *Med Image Anal*. 2011 Oct;14(6):707-22.
47. Freer TW, Ulissey MJ. Screening mammography with computer-aided detection: Prospective study of 12,860 patients in a community breast center. *Radiology*. 2001 Oct;220(3):781-6

48. Padhani AR, Miles KA. Multiparametric imaging of tumor response to therapy. *Radiology*. 2010 Apr;256(2):348-64.
49. Cheson BD, Fisher RI, Barrington SF, Cavalli F, Schwartz LH, Zucca E, et al. Recommendations for initial evaluation, staging, and response assessment of Hodgkin and non-Hodgkin lymphoma: The Lugano classification. *J Clin Oncol*. 2014 Sep 20;32(27):3059-68.
50. Liu Y, Kim J, Balagurunathan Y, Li Q, Wang H, Kumar V, et al. Radiomics feature extraction for lung cancer prediction with machine learning approaches. *Front Oncol*. 2016 Dec 5;6:235.
51. van Griethuysen JJM, Fedorov A, Parmar C, Hosny A, Aucoin N, Narayan V, et al. Computational radiomics system to decode the radiographic phenotype. *Cancer Res*. 2017 Nov 1;77(21)
52. Traverso, A., Wee, L., Dekker, A., & Gillies, R. (2018). Repeatability and reproducibility of radiomic features: a systematic review. International Journal of Radiation Oncology* Biology* Physics, 102(4), 1143-1158 doi: 10.1016/j.ijrobp.2018.05.053. Epub 2018 Jun 5. PMID: 30170872; PMCID: PMC6690209
53. Coroller, T. P., et al. (2015). Radiomic phenotype features predict pathological response in non-small cell lung cancer. Radiotherapy and Oncology, 119(3), 480–486)
54. Ganeshan, B., et al. (2013). Non-small cell lung cancer: histopathologic correlates for texture parameters at CT. Radiology, 2013 Jan;266(1):326-36. doi: 10.1148/radiol.12112428. Epub 2012 Nov 20. PMID: 23169792

55. Huang YQ, Liang CH, He L, Tian J, Liang CS, Chen X, et al. Development and validation of a radiomics nomogram for preoperative prediction of lymph node metastasis in colorectal cancer. *J Clin Oncol*. 2016 Dec 10;34(35):2157-2164.
56. Hawkins, S., Wang, H., Liu, Y., Garcia, A., Stringfield, O., Krewer, H., ... & Aerts, H. J. (2016). Predicting malignant nodules from screening CT scans. Journal of Thoracic Oncology, 11(12), 2120-2128.
57. Schumacher D, Aragam JR, Balachandran A, Chaudhari S, Dai D, Dey D, et al. Radiomics in Cardiology—Unlocking Hidden Information in Imaging Data to Improve Clinical Outcomes. *JACC Cardiovasc Imaging*. 2022 Mar;15(3):580-594.
58. Chaddad, A., Desrosiers, C., & Toews, M. (2019). Radiomics in glioblastoma: current status and challenges facing clinical implementation. Frontiers in Oncology, 2019 May 21;9:374. doi: 10.3389/fonc.2019.00374. PMID: 31165039; PMCID: PMC6536622.
59. Bi, N., Wang, T., Zhang, W., & Yu, Y. (2019). Clinical radiomics in lung cancer: from methodology to clinical implementation. *Radiographic*, 39(4), 1154-1172.
60. Yang, X., Sun, W., Jing, Z., Tan, D., Wu, J., & Chen, Y. (2020). Radiomics in lung cancer: review of current applications and future directions. *Frontiers in Oncology*, 10, 1-12.
61. Zhang, L., Fried, D.V., Fave, X.J., Hunter, L.A., Yang, J., Court, L.E. (2015). IBEX: an open infrastructure software platform to facilitate collaborative work in radiomics. *Medical Physics*, 42(3), 1341-1353.
62. Karacali, B., & Davatzikos, C. (2006). Simulation of tissue texture in MR imaging using a multi-resolution representation of anatomy. Medical Image Analysis, 10(3), 353-364.

63. Huang, C., Wang, L., Ni, Y., Wang, X., Yang, G., & Deng, W. (2019). Integration of multi-omics data for gene regulatory network inference and application to breast cancer. BMC Medical Genomics, 12(1), 92.

ANNEXURE – I –CONSENT FORM

TITLE OF THE STUDY: "RADIOMICS BASED ASSESSMENT OF PULMONARY NODULES DETECTED ON HIGH RESOLUTION COMPUTED TOMOGRAPHY OF THE CHEST: A ONE YEAR HOSPITAL BASED OBSERVATION STUDY"

PRINCIPAL INVESTIGATOR: REGISTRATION NUMBER. BS0121012

INTRODUCTION AND PURPOSE: Pulmonary nodules are a common incidental finding on CT scans of the thorax. The clinical implications depend on size, rate of growth and probability of malignant transformation. Small nodules are usually benign and require no intervention, larger nodules or those with concerning features warrant histopathological diagnosis to rule out malignancy. Thus there is need for clear distinction to accurately diagnose malignant or at risk for malignant transformation nodules.

PROCEDURE: I request you to kindly participate in the study titled study "RADIOMICS BASED ASSESSMENT OF PULMONARY NODULES DETECTED ON HIGH RESOLUTION COMPUTED TOMOGRAPHY OF THE CHEST: A ONE YEAR HOSPITAL BASED OBSERVATION

STUDY" at Dr. Prabhakar Kore Charitable Hospital and Medical Research Centre, Belgaum" is being conducted by Dr. _____ Post Graduate in Radio-Diagnosis at J. N. Medical College Belgaum, Karnataka, under the guidance of DR. _____ Professor, Dept. of Radio-Diagnosis, J. N. Medical College, Belgaum.

We request you to participate in this study as you are eligible to be included. During the study you will be asked questions regarding your present and past medical history and you will be required to answer to the best of your knowledge. You will also be clinically examined as per the protocol drawn.

Study will be conducted over a period of one year. Once the patient signs the informed consent history and examination will be recorded as per proforma. You will have to undertake an CT scan which is done in a closed environment. During the scan, you lie on a table that slides inside a tunnel-shaped machine. Doing the scan you must stay still. The scan is painless.

If you agree to participate in the study, please furnish the details pertaining to the study.

COMPLICATIONS: No risk to the patient has been documented from HRCT scans conducted earlier.

RISKS: No risks have been documented so far.

ALTERNATIVES: If patient is not willing to take part in the study, his / her treatment or any other further investigations the patient wants to undergo, in future, in KLE will not be affected by his / her decision

VOLUNTARY PARTICIPATION/WITHDRAWAL: Taking part in this study is voluntary. I may choose not to take part in this study, or if I decide to take part I can later change my mind and withdraw from the study. My decision will not change the present or future health care or other services that I receive. The study doctor or the sponsor may stop my participation in this study. I will tell if any important new findings that may change my willingness to continue to take part. If I choose not to take part in the study I will receive the standard treatment for patients with my condition.

PAYMENT FOR PARTICIPATION: No incentive will be paid to you for participating in this study

COMPENSATION: In the event that I become injured as a result of taking part in this study, treatment whatever available at KLE Charitable Hospital, Belagavi, will be offered to me. No reimbursement, compensation or free medical care is given.

CONFIDENTIALITY: All information collected about me during the course of the study will be kept confidential to the extent permitted by the law. The code numbers will identify me in this research record. Information from this study may be published but my identity will be confidential in any publication.

QUESTION: If any enquiries in the future or in case of research related injury illness, you may contact following person. DR. HARSHA HEGDE, CHAIRPERSON, JNMC, IEC & Scientist D, ICMR, NATIONAL INSTITUTE OF TRADITIONAL MEDICENE, BELAGAVI Ph. No: 948042250

CONSENT TO PARTICIPATE IN RESEARCH STUDY

1. I understand that I am participating in the study, which includes getting a CT scan done in a closed gantry.

2. I confirm that I have read and understood the information in the patient information sheet. Procedure is explained to me in detail along with information about the advantages and disadvantages of taking part in the study. I have been given the opportunity to discuss all aspects of the trial, to ask questions and hereby consent to participation in the trial outlined above.

3. I understand that the decision to take part in this study is completely voluntary and I am aware that I can choose to withdraw from the study at any point of time.

4. I consent to the photographing or recording of the procedure to be performed including appropriate portions of my body, for medical, scientific or educational purposes provided my identity is not revealed in the pictures or by the descriptive texts accompanying them.

5. I understand that there is no significant risk involved in the test that would be done in this study.

6. No guarantee or assurance has been given by anyone as to the results that may be obtained.

7. My signature on this form signifies that I have willingly decided to participate after understanding the above information.

Participant's Name/ legally authorized representative_____

Signature _____

Name and signature of witness _____

Name and signature of interviewer _____

Date:

Place:

PROFORMA FOR DATA COLLECTION

TEST SUBJECT NO. () -

AGE -

SEX -

OP/IP NO -

CT NUMBER -

ADDRESS -

CHIEF COMPLAINTS -

PAST HISTORY -

FAMILY HISTORY -

CT FINDINGS -

Presence of pulmonary nodule:

Descriptive parameters of nodule:

Associated Parenchymal abnormalities

Master Chart

Subject no	F1 Shape b	F1 Shape b	F2-GrayLev	F2-GrayLev	F2-GrayLev	F2-GrayLev	F2-GrayLev	F2-GrayLev
1	SurfaceAre	Volume	-333-1Cont	0-1Contras	45-1Contra	90-1Contra	135-1Contr	-333-1Corr
2	23.45779	392.6678	11.06984	7.585109	11.14711	10.88196	14.70792	0.619999
3	38.02554	95.58907	6.376308	4.988805	6.360031	5.574712	8.592495	0.769558
4	25.7567	243.9553	6.43996	5.929087	5.026661	10.73358	22.83842	0.544118
5	36.3611	241.6291	7.502668	5.057073	9.6654	10.29628	23.78668	0.297426
6	36.04385	143.2646	4.517959	10.01286	5.368882	10.06757	7.261694	1.032062
7	24.26049	183.2999	24.57631	7.125849	5.23834	10.49393	17.84275	0.704001
8	26.15342	333.8306	6.1261	5.090554	2.639965	10.59117	17.98732	0.280841
9	29.72087	440.4366	7.441011	9.991145	8.808528	9.992194	6.039343	0.999933
10	33.40911	425.1638	23.1027	9.442825	7.324956	10.72948	6.859584	0.719919
11	25.21324	422.4355	5.640738	5.084691	5.717877	11.08522	14.17068	0.611221
12	25.79954	263.6777	5.008791	6.559273	3.986449	11.04637	21.31838	0.199545
13	31.90048	114.5285	17.18059	7.194089	11.75142	10.38874	21.61816	0.754515
14	31.73235	181.635	6.24301	8.636041	2.38022	10.89437	19.98526	0.297835
15	28.67721	350.8521	15.55398	7.481177	5.480255	10.44965	7.491127	0.675069
16	24.86269	225.3559	19.9506	6.031055	10.32713	10.9075	23.12929	0.347088
17	33.16914	137.9549	14.7564	7.057347	2.708107	10.55324	18.53846	0.607517
18	35.60407	423.5171	25.50724	5.541158	2.834401	11.00083	23.94491	0.311653
19	30.07464	82.26863	6.369574	7.57	4.372536	9.898916	24.13139	0.558077
20	27.20171	422.3116	18.64262	7.312437	11.52599	11.32568	26.56289	0.233228
21	32.44127	271.1515	21.3359	4.490646	2.926654	9.934301	22.25447	0.254224
22	34.12205	239.3143	20.50257	8.156455	6.474187	10.07262	14.85269	0.424314
23	32.73899	323.09	5.381682	8.42185	5.38605	10.83262	10.58902	1.002663
24	37.4852	299.7329	14.49718	8.226349	3.638442	11.0244	15.40031	0.464641
25	27.20178	90.20937	17.7274	6.908934	11.85016	10.68484	7.842099	0.342546
26	25.77553	331.1658	26.25647	7.717535	8.212969	10.83211	22.7556	0.749463
27	31.04707	147.5004	27.12491	9.507362	8.960283	11.30713	24.20106	0.237213
28	28.77869	272.1164	15.24792	9.486315	5.34918	10.80645	11.65187	0.638451
29	23.75601	473.0677	9.624639	4.098191	6.297203	9.699564	14.90774	1.031048
30	31.94121	333.6741	11.2874	6.074507	10.86745	9.894107	9.824279	0.922627
31	32.76257	416.3891	15.43121	7.291221	3.368785	10.36146	9.081868	0.799791
32	33.12986	290.6841	8.453586	9.179313	10.03591	10.67107	8.163332	1.027929
33	34.06647	421.2118	15.35388	8.563333	8.828661	10.94969	6.46593	0.196014
34	35.84851	178.1075	20.94915	4.675922	6.060423	10.05428	8.864519	1.013255
35	27.02249	156.0365	25.05132	6.57303	8.94151	10.31684	15.78257	0.492421
36	31.84341	334.8998	29.34078	7.457395	10.53982	11.07186	8.931455	0.946434
37	32.3122	270.2503	19.08865	8.10538	9.162433	10.29014	15.06047	0.287893
38	26.7192	345.4506	16.29138	8.702674	4.004956	10.76829	7.676595	0.940801
39	32.23384	249.4659	7.446971	8.931487	10.34644	10.34854	11.36488	0.493115
40	33.8938	231.3618	29.63512	7.428319	3.097433	11.14317	7.434075	0.759558
41	26.19534	149.1562	15.6467	6.210215	4.37915	10.7541	7.577946	0.688925
42	30.42948	196.5306	5.059524	6.334644	12.95477	9.773262	16.67067	0.206164
43	30.54125	178.6411	16.57667	9.953758	5.400302	11.2357	23.46867	0.263909
44	32.66087	439.0876	28.94698	9.13758	10.63128	10.17351	9.963017	0.390335
45	29.22423	207.9691	8.537441	7.027733	8.461181	10.74754	6.373836	0.993342
46	30.75973	90.67527	11.24783	9.362315	5.431269	10.47928	18.74811	0.917549

47	36.32069	296.0759	23.051	8.434308	10.8526	9.918546	24.95061	0.548745
48	29.15473	185.3365	23.63709	5.810833	9.197818	11.04902	25.39342	0.243232
49	23.79429	395.1944	11.19305	4.283243	2.374766	10.76293	16.57793	0.786998
50	31.47018	410.9787	15.84554	10.0558	5.705852	11.46386	23.72658	0.708354
51	34.2805	174.4798	11.02495	8.473258	8.496431	11.01031	14.3346	0.737069
52	24.184	91.35129	9.127999	5.210904	8.836855	10.18931	13.23873	0.349522
53	36.72949	167.4657	5.154655	7.890828	10.19184	11.4664	23.53246	0.666382
54	28.19233	365.9445	19.10559	7.900802	12.9492	10.14479	13.81514	0.366902
55	24.13659	412.403	4.64508	4.65733	9.025021	9.755328	25.55944	0.22326
56	36.27715	113.3735	5.49192	7.909498	2.469592	11.31507	25.83932	0.32229
57	31.28755	327.4128	23.24608	5.758573	12.941	10.29427	12.11002	1.025677
58	25.91763	136.2412	27.42292	8.353721	12.98497	10.32039	23.29181	0.258564
59	25.42328	117.7907	5.651765	6.049807	11.15698	10.19316	10.1751	0.880289
60	24.20714	210.2067	12.71877	10.24793	2.436379	11.21957	26.33936	0.435193
61	25.43752	308.3247	27.9572	10.47231	13.05898	11.2364	5.563114	0.659635
62	32.57785	451.2869	23.91464	8.878779	12.48893	11.40281	25.96547	0.76091
63	24.55332	139.8838	26.49185	9.303489	11.21034	11.46079	12.49569	0.247721
64	35.41889	466.1463	10.87289	4.067295	13.21945	9.927534	25.61872	0.762611
65	25.66831	292.5563	6.600316	5.625726	3.18987	11.47113	12.29705	0.634172
66	26.22657	311.1065	4.343068	4.505584	5.953776	10.91141	22.70077	0.961483
67	24.44649	471.1753	12.8173	8.411308	10.63653	10.91685	6.164415	0.573125
68	34.81711	460.919	28.07527	5.290559	7.608872	10.31022	19.89835	0.233476
69	29.77115	352.9287	26.79531	10.30086	3.621545	11.389	24.96805	0.977173
70	34.12351	140.2787	18.33593	4.292389	6.773629	11.44458	7.580365	0.863234
71	24.45024	427.7357	28.09909	8.058267	12.58933	11.42017	26.06621	0.370541
72	24.53971	201.4861	11.39095	5.363826	9.850502	10.97848	26.52742	0.775373
73	35.96666	210.2393	23.71713	7.940109	2.781868	11.28361	7.888158	0.289626
74	30.48048	82.87861	15.32027	9.411436	6.232937	10.26541	5.47378	0.586569
75	24.36397	209.7322	25.13237	10.35735	2.42578	11.36568	18.38671	0.684239
76	34.18994	359.2618	4.0285	5.798306	11.82743	11.40774	14.29799	0.762109
77	32.307	183.1864	5.566778	9.413988	7.934892	11.24851	5.914241	0.236106
78	30.18704	308.9868	17.57051	4.668977	9.753326	9.762503	18.66669	0.199321
79	31.26486	390.7508	19.70585	8.702622	12.78265	11.16734	23.74366	0.349533
80	34.63568	157.5378	27.81524	7.926638	2.500089	10.08573	18.1052	1.030198
81	25.23033	260.6647	6.681938	5.442734	9.925899	10.46847	10.43694	0.846967
82	36.45105	81.43953	20.7632	6.219381	12.4873	10.7242	12.13005	0.324661
83	28.72379	345.4463	7.514667	9.734158	7.256855	10.90721	5.617982	0.468419
84	34.09009	178.9202	18.147	9.996826	5.285716	10.88898	9.817365	0.676787
85	26.81677	117.3781	19.82187	4.513918	3.276267	11.07841	12.71908	0.732943
86	25.88883	273.2546	29.29697	10.15458	10.37017	11.21157	12.64868	0.868002
87	26.96555	462.855	10.46924	4.268952	8.647725	11.15135	14.8487	0.849129
88	23.49895	449.3187	14.84924	7.010031	10.86166	10.25826	6.784636	0.431221
89	35.06926	316.4008	24.91738	8.28441	2.375076	9.708291	11.65094	0.901699
90	32.61541	88.11428	28.98675	5.723341	13.45276	10.83609	10.06098	0.428084
91	27.20904	129.2526	28.72701	5.572546	12.39631	9.773955	6.993995	0.332376
92	32.0724	258.7357	16.69493	5.090191	6.459299	9.692706	7.712276	0.724125
93	33.62682	187.8289	15.71635	9.247351	2.767879	11.21999	5.832585	0.910487

94	26.77541	474.2112	5.734019	4.827017	8.264285	11.44017	24.26298	0.341802
95	34.46751	95.5417	8.306746	9.239329	3.835091	10.65803	23.41236	0.570096
96	36.15536	105.9646	24.76926	9.928586	3.356868	9.820216	6.143155	0.41985
97	25.30644	204.6341	28.27653	9.989059	13.12518	11.43743	16.9651	0.755086
98	29.2663	215.7764	8.628485	7.829777	9.425838	9.734024	16.46186	0.54274
99	24.96668	96.76147	18.31428	9.653022	8.321593	11.1673	5.123963	0.528954
100	36.41123	340.835	11.31705	4.874953	11.19895	10.64697	15.55972	0.935853

F2-GrayLev 0-1Correlat	F2-GrayLev 45-1Correl	F2-GrayLev 90-1Correl	F2-GrayLev 135-1Corre	F2-GrayLev -333-1Ener	F2-GrayLev 0-1Energy	F2-GrayLev 45-1Energy	F2-GrayLev 90-1Energy	F2-GrayLev 135-1Energ
0.744626	0.624907	0.635902	0.473724	0.015326	0.017685	0.014791	0.014919	0.014632
0.820683	0.768502	0.799938	0.688251	0.013352	0.01436	0.013167	0.013734	0.012444
0.854346	0.658723	0.462775	0.98323	0.014188	0.018364	0.864118	0.119676	0.003401
0.888883	0.724223	0.59566	0.913952	0.013788	0.018451	0.760056	0.049231	0.003241
0.859127	0.730747	0.627436	0.940016	0.014141	0.019045	1.007852	0.113414	0.002828
0.849602	0.626504	0.628306	0.778597	0.014115	0.018134	0.859812	0.062786	0.003187
0.822472	0.743581	0.644208	1.00883	0.014618	0.018366	1.027129	0.051559	0.00183
0.850392	0.625882	0.536947	0.826326	0.013366	0.017714	0.763176	0.017164	0.002098
0.850611	0.686499	0.475242	1.006485	0.013473	0.018732	1.123115	0.047914	0.003176
0.823268	0.649549	0.596188	0.973038	0.013709	0.018542	1.156861	0.06999	0.00284
0.886768	0.743937	0.495068	0.97725	0.013736	0.018764	0.961091	0.12028	0.003399
0.855441	0.650885	0.581486	0.788436	0.012738	0.018849	0.692598	0.10516	0.002928
0.878399	0.719177	0.635068	0.939885	0.014509	0.018683	0.835728	0.107874	0.002781
0.832525	0.65621	0.568517	0.918755	0.012583	0.019083	0.690602	0.09703	0.001811
0.825059	0.667673	0.642068	0.813561	0.012604	0.017728	0.684432	0.077994	0.002784
0.826538	0.686744	0.657878	0.789799	0.013988	0.019059	1.009813	0.092369	0.002474
0.846953	0.736788	0.541603	0.773007	0.013281	0.018261	1.025422	0.042543	0.003316
0.85734	0.746718	0.51519	1.048433	0.014155	0.01884	0.772815	0.109702	0.003515
0.853837	0.694856	0.553238	0.972553	0.013037	0.018334	1.034452	0.026443	0.002697
0.872307	0.698464	0.511771	1.040061	0.013292	0.018195	0.934777	0.055863	0.001967
0.830239	0.63726	0.494239	0.929932	0.012713	0.018957	0.6379	0.048312	0.00282
0.834858	0.622351	0.636654	0.81172	0.012763	0.017838	0.45689	0.05438	0.003465
0.837847	0.730118	0.622813	0.792275	0.014298	0.018042	0.840842	0.049116	0.003227
0.891077	0.703107	0.494378	0.968334	0.014441	0.01859	1.07559	0.085907	0.003418
0.89475	0.64267	0.537653	0.802362	0.01342	0.01883	1.110009	0.117219	0.001905
0.861474	0.630503	0.538304	0.901718	0.013727	0.018755	0.435054	0.08913	0.002057
0.890428	0.709511	0.644864	0.986038	0.012811	0.019271	0.824701	0.100167	0.002373
0.891037	0.710591	0.645369	1.011179	0.012656	0.018337	0.646138	0.083025	0.001752
0.869843	0.753745	0.631961	0.871561	0.013907	0.018335	0.548648	0.068749	0.002887
0.844371	0.639395	0.506541	0.905683	0.014098	0.018512	0.824404	0.121213	0.003292
0.824965	0.733897	0.645789	0.944278	0.014273	0.018929	0.662461	0.099873	0.002274
0.852831	0.75761	0.618356	0.849568	0.014315	0.018782	0.439834	0.091397	0.002976
0.87366	0.636208	0.542185	1.003918	0.013454	0.018518	0.672054	0.082853	0.003078
0.839894	0.698418	0.632635	1.049347	0.014549	0.018437	0.963691	0.109106	0.002445
0.854347	0.677451	0.58151	1.001648	0.013027	0.01782	0.533627	0.08933	0.001653
0.871666	0.678248	0.551327	0.968489	0.014529	0.017829	0.445754	0.115992	0.002545
0.832892	0.714894	0.477851	0.810917	0.013399	0.017882	0.705947	0.087904	0.002918
0.891226	0.727742	0.634677	0.848991	0.014431	0.018577	1.097267	0.079946	0.001794
0.866187	0.632019	0.577959	0.999643	0.01414	0.018542	1.078347	0.021063	0.002181
0.871982	0.698782	0.626719	0.772245	0.012612	0.018598	1.020884	0.06218	0.003447
0.823377	0.681974	0.546346	0.925986	0.013769	0.017772	0.858048	0.039608	0.001862
0.853601	0.768356	0.608736	0.867137	0.01403	0.018531	0.929644	0.104457	0.002411
0.872412	0.757007	0.493422	0.887838	0.01286	0.018226	0.595425	0.053526	0.003108
0.868158	0.655158	0.574626	0.862612	0.013788	0.019146	0.827144	0.05005	0.001886
0.872028	0.663951	0.650691	1.028451	0.012826	0.018453	0.458833	0.114664	0.00164

0.851104	0.728584	0.551307	0.797627	0.013964	0.018079	0.902241	0.050831	0.002597
0.891928	0.745937	0.526152	0.911002	0.013048	0.017777	0.546873	0.096	0.00156
0.828091	0.67948	0.602279	0.99908	0.013098	0.018422	0.882995	0.117389	0.002588
0.850948	0.762127	0.612179	0.867818	0.01277	0.018633	0.683053	0.016953	0.002696
0.892048	0.653777	0.518981	0.8787	0.013065	0.019099	0.748013	0.02885	0.00346
0.86722	0.767762	0.626949	0.798931	0.013845	0.019262	0.625155	0.111584	0.001907
0.8744	0.740947	0.466596	0.854651	0.012956	0.018044	1.028195	0.058736	0.002488
0.830871	0.662764	0.559249	0.85324	0.014287	0.018889	0.572032	0.025868	0.002265
0.82704	0.66238	0.601425	0.94007	0.01352	0.017888	1.092286	0.024707	0.00252
0.869252	0.623197	0.536324	0.938593	0.013433	0.018665	0.528576	0.070594	0.002605
0.894014	0.767639	0.601958	0.996367	0.014368	0.018208	0.782143	0.049101	0.001716
0.85514	0.639523	0.56237	0.892681	0.013402	0.01926	0.937042	0.052004	0.002544
0.849495	0.702655	0.607467	0.847973	0.01375	0.019298	0.643278	0.113435	0.002231
0.870776	0.69567	0.579441	0.918508	0.012962	0.01893	1.067486	0.059724	0.00339
0.852611	0.66034	0.556462	0.92683	0.014619	0.01928	0.458545	0.09722	0.003324
0.879183	0.650707	0.54352	0.911128	0.014054	0.019241	0.544621	0.096068	0.002476
0.830887	0.723743	0.542592	0.877408	0.013203	0.018005	0.987711	0.061628	0.003077
0.823384	0.616517	0.555935	0.996495	0.012716	0.018721	0.531455	0.115268	0.001783
0.857603	0.637149	0.520351	0.90577	0.012713	0.01927	0.965779	0.113764	0.002323
0.840538	0.749484	0.450052	0.787156	0.014409	0.018393	0.495357	0.104787	0.00293
0.860829	0.649809	0.549983	0.929273	0.012842	0.018178	0.574341	0.086824	0.001476
0.823294	0.731241	0.65955	1.018234	0.013419	0.018644	1.074626	0.053757	0.003347
0.870066	0.702343	0.611519	0.878941	0.013927	0.017972	0.591704	0.09927	0.00251
0.82302	0.688964	0.651355	0.997943	0.013273	0.018811	0.740191	0.056468	0.001557
0.868463	0.645723	0.509914	0.823102	0.014092	0.017893	0.674396	0.120594	0.002662
0.830794	0.660469	0.539436	0.950456	0.013377	0.017981	1.021723	0.054564	0.001891
0.872525	0.657839	0.504796	1.032561	0.014382	0.018642	0.827358	0.070895	0.003381
0.846614	0.673339	0.611226	0.865052	0.014551	0.019109	0.503706	0.08316	0.002488
0.845886	0.756225	0.542505	0.894536	0.013284	0.01921	0.804918	0.102953	0.002211
0.889486	0.725982	0.48092	0.831852	0.01314	0.018205	0.888893	0.023068	0.003532
0.851638	0.697637	0.605801	0.840883	0.012655	0.018078	0.976969	0.072657	0.002527
0.891989	0.637502	0.542135	0.943023	0.014442	0.018016	0.858614	0.014842	0.003335
0.885089	0.634789	0.606345	0.877811	0.014311	0.018548	0.451023	0.05079	0.00259
0.881375	0.716965	0.587344	0.959542	0.013116	0.01893	0.662721	0.022098	0.001827
0.850478	0.627547	0.621385	0.954373	0.013368	0.018197	0.916111	0.07758	0.001792
0.841962	0.676059	0.622492	0.856065	0.012556	0.017895	0.612649	0.109222	0.00275
0.833747	0.687153	0.565387	0.864015	0.01253	0.017737	1.059445	0.016218	0.001479
0.873029	0.721565	0.653034	0.792094	0.013203	0.018632	0.440815	0.104193	0.00263
0.874527	0.763234	0.659389	1.044686	0.013027	0.019068	0.964119	0.026789	0.002993
0.875585	0.627924	0.643575	1.015628	0.012734	0.018455	0.809149	0.114703	0.001914
0.871569	0.621227	0.615044	1.013944	0.014007	0.018988	1.127432	0.084052	0.002817
0.876626	0.750083	0.5025	1.012064	0.014107	0.018758	0.86087	0.069371	0.00261
0.859809	0.685693	0.640678	0.951147	0.013575	0.018348	0.838864	0.033653	0.001503
0.860202	0.762425	0.658289	0.786075	0.013976	0.019167	1.009916	0.066571	0.002655
0.838136	0.684589	0.503703	0.902596	0.014631	0.019106	1.104222	0.104262	0.001937
0.872869	0.663689	0.450442	0.935791	0.014223	0.017768	1.133093	0.077449	0.003642
0.891544	0.754813	0.609476	0.968251	0.013223	0.017903	0.717265	0.047036	0.001823

0.870344	0.741756	0.658956	0.925872	0.013501	0.018442	1.061208	0.103978	0.002117
0.880963	0.670343	0.609437	0.825957	0.013016	0.018668	0.754343	0.038563	0.002998
0.890049	0.683575	0.464472	0.776317	0.012808	0.018348	0.973223	0.045519	0.001903
0.875855	0.621733	0.594694	0.813875	0.013573	0.018873	1.091358	0.02593	0.001832
0.852267	0.688356	0.572395	0.793009	0.013911	0.017983	1.114893	0.088726	0.001526
0.822522	0.686685	0.543176	1.005902	0.012782	0.01787	1.020068	0.064784	0.003636
0.845547	0.734555	0.587553	0.783016	0.012979	0.017927	1.058117	0.023481	0.002861

F3-Neighbc Busyness	F3-Neighbc Coarseness	F3-Neighbc Complexity	F3-Neighbc Contrast	F4-Intensit GlobalEntr	F4-Intensit GlobalMea	F4-Intensit GlobalMed	F4-Intensit GlobalStd	F4-Intensit GlobalUnif
3.59E-05	0.064626	646558.1	0.234211	6.945094	1025.086	1030	42.81566	0.010871
3.28E-05	0.071192	708412.1	0.364118	7.099631	1020.299	1028	38.25965	0.009287
4.76E-05	2.12E+10	619122.6	0.684718	9.393233	1041.977	1065	31.39281	0.094463
4.23E-05	0.142058	709486.4	0.711822	8.988847	1040.066	1022	36.22893	0.180214
4.26E-05	0.121246	602704.2	0.695756	7.993463	1036.293	1045	52.15117	0.136868
4.58E-05	0.20686	630612.3	0.682539	10.25212	1039.509	1042	56.43963	0.162613
3.62E-05	0.183682	699112.7	0.685577	8.939546	1046.094	1020	32.28969	0.098929
4.51E-05	0.132007	680206.1	0.716904	7.387166	1039.72	1037	36.12225	0.139754
4.21E-05	0.087524	667216.7	0.666849	9.720544	1044.886	1049	43.98341	0.170341
3.88E-05	0.232983	649363.7	0.700768	7.646247	1044.604	1049	49.95758	0.177191
3.91E-05	0.226481	683815.7	0.743327	9.899301	1046.46	1041	37.17305	0.186524
3.67E-05	0.228912	683325	0.677475	9.44311	1045.856	1056	47.11592	0.107462
3.64E-05	0.215198	597670.4	0.679242	7.797218	1039.986	1034	38.41736	0.119845
3.93E-05	0.140021	712039.3	0.71961	9.39466	1039.813	1061	57.73067	0.109549
4.02E-05	0.158784	684335.4	0.736327	7.260466	1029.328	1056	37.41334	0.179078
4.54E-05	0.142969	656661.6	0.70018	7.424146	1045.009	1036	35.66008	0.128665
3.90E-05	0.158533	584414.6	0.740013	8.299834	1046.011	1019	36.49581	0.152038
3.95E-05	0.173923	596506.7	0.687106	8.552912	1045.963	1036	43.21967	0.174447
3.76E-05	0.237816	639824.9	0.688952	9.527933	1037.392	1019	50.68125	0.114522
4.32E-05	0.241618	671978.8	0.68748	9.776898	1035.895	1022	39.01904	0.170136
4.51E-05	0.239113	621329	0.707386	7.879511	1043.163	1028	34.5032	0.109764
4.03E-05	0.093006	696917.4	0.709873	8.369036	1041.89	1054	47.54314	0.117462
4.72E-05	0.161183	672949.8	0.671078	8.916064	1032.989	1045	38.9062	0.091715
4.09E-05	0.147752	589148.4	0.691034	7.951775	1029.341	1021	38.22109	0.094547
4.64E-05	0.096487	592960.9	0.679274	8.695375	1037.487	1036	38.42776	0.124269
3.62E-05	0.210624	607485.2	0.682104	9.815628	1044.841	1042	46.50594	0.092809
3.62E-05	0.19943	697354	0.719532	7.632364	1040.224	1058	45.83133	0.093395
3.67E-05	0.115904	670696.4	0.70621	10.26158	1031.223	1064	44.06063	0.116213
3.92E-05	0.235597	671924.4	0.724148	7.106319	1041.795	1030	50.51562	0.146791
4.45E-05	0.196546	660093.6	0.6699	9.428344	1040.922	1025	51.8103	0.133587
4.26E-05	0.192709	686237.9	0.687095	9.390466	1034.437	1035	50.51712	0.102841
3.93E-05	0.204024	635573.3	0.737811	7.140861	1042.624	1042	44.7705	0.121864
4.51E-05	0.209498	659430.8	0.701219	7.965303	1037.144	1048	31.90348	0.114791
3.67E-05	0.117437	603740.8	0.708872	8.209767	1031.152	1063	34.22106	0.123433
4.40E-05	0.159921	646984.8	0.694996	8.476293	1034.67	1045	48.21201	0.125013
3.83E-05	0.210538	685493.3	0.735871	10.11064	1034.83	1058	46.62006	0.105194
4.50E-05	0.210525	682991.7	0.666338	7.038554	1035.494	1044	55.42975	0.112378
3.76E-05	0.21015	683871.2	0.730624	7.471963	1034.839	1063	41.7792	0.154688
4.74E-05	0.187244	592370.1	0.667812	7.895633	1042.449	1053	46.16175	0.146502
3.92E-05	0.135044	661736.6	0.733079	9.490619	1040.315	1032	46.02877	0.127423
3.92E-05	0.248023	617702.9	0.670434	7.653747	1042.133	1049	44.25185	0.133426
3.60E-05	0.188785	591417.5	0.684835	8.725007	1045.039	1056	47.7095	0.144546
3.62E-05	0.104239	658550.5	0.716437	7.931782	1039.594	1066	47.98888	0.14672
4.72E-05	0.176389	664851.1	0.715424	7.157431	1035.833	1020	49.22118	0.140172
4.01E-05	0.200874	702893.7	0.719482	7.013406	1041.885	1059	48.79776	0.150672

3.83E-05	0.231522	683815.7	0.719261	9.695958	1034.084	1033	31.75105	0.097298
4.48E-05	0.180033	695766.7	0.708693	7.174458	1041.769	1046	56.53988	0.138218
3.91E-05	0.131597	614233.6	0.719228	7.781434	1037.039	1028	38.62685	0.088798
4.08E-05	0.1462	675756.5	0.691786	8.092526	1046.806	1031	52.62805	0.092551
4.77E-05	0.137909	694546.8	0.697547	9.553367	1044.395	1063	48.98421	0.163388
4.76E-05	0.203795	661267.4	0.730572	7.608697	1032.419	1018	32.20415	0.162722
3.96E-05	0.173927	608575.6	0.723281	8.851503	1043.38	1055	43.54117	0.151023
4.54E-05	0.137274	703140.4	0.700571	7.550431	1038.09	1057	44.86646	0.104787
4.10E-05	0.10036	640291.4	0.714437	8.482726	1036.812	1036	44.5357	0.131989
4.18E-05	0.10369	602148.2	0.712791	9.688439	1031.189	1056	44.52033	0.147952
4.26E-05	0.204867	594257.2	0.672586	10.02965	1045.481	1054	49.85439	0.102873
4.72E-05	0.159847	683051.5	0.708035	9.805916	1035.786	1059	35.34898	0.146067
3.66E-05	0.241719	630315.6	0.738899	8.482224	1030.354	1030	45.36281	0.107845
4.44E-05	0.23958	686038.7	0.73743	7.119022	1045.868	1050	46.01718	0.111492
4.77E-05	0.174254	645508.7	0.710021	8.459183	1038.188	1036	55.25603	0.158371
4.01E-05	0.204831	695076.6	0.67061	9.805044	1036.236	1022	55.49736	0.13795
4.47E-05	0.210108	642122.6	0.726549	9.871513	1031.416	1049	56.10092	0.136049
3.71E-05	0.085092	679955.1	0.706938	7.311719	1033.977	1045	33.51252	0.095879
3.77E-05	0.208819	645951.3	0.69325	10.03601	1031.52	1023	42.31939	0.094592
4.41E-05	0.148351	671205.9	0.684657	7.561154	1046.026	1034	52.7386	0.173032
4.54E-05	0.088183	610147.3	0.678763	8.420371	1033.763	1051	51.03755	0.09175
3.76E-05	0.088943	673141.8	0.691202	9.552369	1032.222	1024	38.33476	0.163835
4.04E-05	0.137635	687563.5	0.715567	8.243404	1038.644	1041	41.25637	0.170422
3.64E-05	0.217767	663267.3	0.713549	9.686208	1032.668	1028	58.15738	0.189443
3.75E-05	0.15525	679095.5	0.685626	9.243134	1038.609	1047	44.34903	0.133976
3.99E-05	0.221784	685568.2	0.717891	8.202977	1032.635	1051	44.10864	0.120342
4.74E-05	0.138984	594490.9	0.704909	7.37001	1035.113	1019	52.44551	0.118477
4.03E-05	0.131403	613743.6	0.672899	7.37427	1037.285	1038	54.1216	0.179502
4.40E-05	0.229964	704321	0.688916	9.015734	1042.547	1049	32.15213	0.173837
3.66E-05	0.189123	603925.3	0.714987	7.041572	1034.129	1028	32.61835	0.169115
4.17E-05	0.111868	625589.3	0.733955	8.61645	1039.339	1045	36.77602	0.136076
4.49E-05	0.199578	648409.4	0.735472	7.975014	1041.016	1064	57.6863	0.143669
4.10E-05	0.092313	622538.4	0.666223	9.59214	1035.257	1043	34.79558	0.100598
4.25E-05	0.23609	660724.5	0.73779	9.687888	1045.168	1057	43.9606	0.163349
4.19E-05	0.114271	613524.3	0.713432	9.764147	1040.542	1025	33.90995	0.128666
4.27E-05	0.22491	679661.9	0.699737	7.558848	1031.025	1043	38.84926	0.172258
3.86E-05	0.126458	654673.8	0.717489	9.393059	1031.491	1034	36.39025	0.14561
4.13E-05	0.131967	691674.3	0.702171	7.669743	1035.807	1065	55.29199	0.10768
3.64E-05	0.169447	642705.6	0.706908	7.556891	1038.956	1049	56.50185	0.177515
4.20E-05	0.247573	600723.3	0.667517	9.452725	1033.894	1057	55.2236	0.111728
4.50E-05	0.105019	693454.1	0.71931	7.458686	1030.825	1036	54.74609	0.130539
4.55E-05	0.095332	630964.3	0.67417	6.988433	1046.079	1027	36.30447	0.161427
4.63E-05	0.140916	608421.5	0.696543	8.866208	1042.679	1029	57.81225	0.169957
3.77E-05	0.098851	587632.9	0.742938	8.195218	1041.452	1055	45.8495	0.182084
4.34E-05	0.250237	652778.6	0.725661	9.741061	1032.561	1031	57.98443	0.179369
3.83E-05	0.185138	619326.4	0.675295	9.294543	1040.6	1063	48.34348	0.090953
4.55E-05	0.188408	689855	0.709411	6.969937	1039.005	1041	53.22491	0.166793

4.22E-05	0.198372	690679.2	0.699257	8.30352	1045.172	1051	40.5506	0.17076
3.62E-05	0.088415	656279.2	0.717576	8.233527	1039.578	1055	44.8671	0.146802
3.68E-05	0.15502	635192.6	0.742355	8.244196	1030.173	1057	36.67048	0.134449
3.71E-05	0.235502	607456.1	0.741153	9.361846	1043.127	1047	33.01236	0.179823
4.65E-05	0.207023	652749.2	0.714287	8.870571	1035.416	1039	41.55028	0.181718
3.72E-05	0.222069	585067.8	0.730726	7.531969	1035.432	1027	36.48213	0.170594
4.61E-05	0.171802	641550.2	0.680979	10.28141	1040.438	1038	40.29385	0.09822

F4-Intensity Kurtosis	F4-Intensity Range	F4-Intensity Skewness	F5-Intensity GlobalEntr	F5-Intensity GlobalMea	F5-Intensity GlobalStd	F5-Intensity GlobalUnif	F5-Intensity Kurtosis	F5-Intensity Skewness
88.90288	1150	4.0251	2.751945	3.049038	2.130714	0.181607	16.08519	2.035714
7.240097	603	-0.59753	2.715981	3.042872	3.199063	0.194972	112.483	8.08827
79.31847	1047	2.719657	2.862951	5.071693	3.422642	0.207813	132.2156	12.90664
96.39532	1256	5.494351	3.605871	5.077962	4.293304	0.181565	40.2948	12.0456
85.77603	764	4.368299	3.413977	3.736534	3.759567	0.188842	56.27957	7.620369
48.51196	1238	1.579813	3.917677	3.406056	4.424447	0.189485	143.8133	11.02406
51.95597	1177	4.957667	3.219681	4.71293	6.902028	0.201094	79.94511	15.29041
98.77871	633	4.674394	2.977036	5.062577	5.614352	0.182528	110.8609	14.00825
23.64827	847	-0.00583	2.919099	3.994198	3.516109	0.209891	102.6549	16.24721
74.8736	571	6.769735	3.376579	3.548813	6.319715	0.209652	195.9525	10.25082
16.94251	1072	4.592133	3.059997	3.720941	4.639048	0.200703	31.22101	8.864411
56.48876	1158	5.983162	2.126041	4.397774	2.462454	0.210884	47.92656	16.66893
33.84745	1198	5.815519	2.881348	5.122036	4.147941	0.197532	114.1965	5.622638
15.02231	515	0.334712	3.575842	5.134755	2.468365	0.188903	197.0119	15.11296
47.9215	548	2.925698	2.346933	3.544663	6.291439	0.191674	64.13559	13.41484
98.62871	1150	0.513187	2.568884	4.46307	5.957011	0.204525	61.83874	2.004016
26.66644	593	0.851485	3.881653	2.832233	3.770128	0.210107	40.47692	13.9166
61.39052	703	5.51147	2.513153	3.000831	3.627379	0.206203	151.8817	13.57656
58.44486	899	1.740509	3.530851	4.358974	4.673565	0.181704	108.2012	13.72976
48.60121	901	1.703575	2.203982	3.647704	2.378206	0.21105	63.04111	7.923114
71.85739	1136	2.419616	3.99301	4.051809	3.094374	0.189829	36.14669	13.94549
23.60737	658	5.71128	3.451854	2.443796	2.468588	0.192647	200.8823	1.968064
34.7359	688	2.028432	2.180777	5.018196	2.91753	0.18731	76.76079	14.1118
21.32256	749	0.772787	3.103705	2.814428	2.201059	0.203062	53.97167	7.878553
90.07169	1226	1.773051	3.120521	5.003324	5.219686	0.194593	113.2488	5.087453
16.41759	1241	6.422304	2.597604	4.452556	2.618696	0.207982	105.6631	4.648345
64.77975	610	4.240496	3.565383	4.444398	3.391498	0.211817	73.95259	3.922356
81.78216	1023	2.372911	3.329008	3.485885	4.998466	0.212057	187.3006	12.33467
40.99889	509	1.270026	4.080789	5.023547	3.664791	0.197585	145.8051	8.278929
86.66067	1291	3.893029	3.474248	4.060671	2.751576	0.196624	114.7427	1.917255
82.59791	929	-0.16911	3.636416	3.686598	6.173736	0.182989	53.73508	2.041032
16.64207	1155	0.980886	3.780719	4.203027	5.733213	0.191512	52.38861	14.48609
33.35058	960	4.257458	3.213483	2.954654	4.313837	0.199817	130.8004	4.714663
56.66863	518	6.545739	2.137477	3.062365	6.770613	0.189491	190.4335	10.23253
7.139128	956	0.56497	3.453929	2.265699	3.799292	0.181573	84.25854	3.95607
12.52361	1256	4.23536	2.85387	3.559916	4.688338	0.195504	194.5783	2.557827
95.71188	588	0.383993	3.202495	2.566372	3.820401	0.206322	196.5941	1.234611
90.81987	958	4.505359	3.85838	3.444174	4.557093	0.191146	43.08732	12.4588
64.69953	465	6.031483	2.678271	2.554095	5.259213	0.21165	38.64212	15.63552
14.95758	1095	1.698624	4.115064	3.775793	4.857774	0.186296	96.053	6.072983
58.78787	909	2.118528	2.302135	2.966435	5.611716	0.185324	78.01223	15.56449
16.80607	728	6.282371	3.113896	2.962791	4.901143	0.198062	49.56767	16.03443
69.26745	856	0.0326	2.60142	3.058779	5.387258	0.20587	135.1867	1.893191
54.53254	508	0.050885	2.78019	2.248372	2.555873	0.193532	146.7878	14.84424
56.76557	594	1.692994	3.117949	4.675534	4.096112	0.207118	66.14	7.868194

14.27219	608	-0.32706	3.764238	5.134074	4.107531	0.193839	11.4061	8.727606
43.71818	1264	6.233151	2.780517	2.204021	2.858224	0.203467	132.0191	15.42921
35.31199	1263	5.462638	3.226348	4.206357	6.216812	0.199867	160.009	16.26306
92.31191	1054	5.818268	4.11305	4.249283	4.131106	0.188973	123.2154	7.029862
13.38993	1156	5.860308	3.699342	3.392464	4.910406	0.189228	29.87031	2.585335
11.74064	802	2.921738	2.11958	4.413588	4.234721	0.189106	166.5966	15.68283
88.79792	950	6.454253	2.79952	4.478223	5.840579	0.188147	150.1861	16.68045
25.03341	502	7.188776	3.42929	2.3972	6.030604	0.200978	165.2274	8.885457
87.81402	961	6.780082	3.505323	2.91366	5.526028	0.185382	177.5916	15.24968
54.62524	1216	4.485902	2.779128	4.761131	5.121813	0.19215	99.09276	9.460116
90.2534	716	2.8674	2.139659	3.752676	2.921265	0.183905	47.2987	13.41541
88.08889	871	5.373539	2.989515	5.054242	2.713536	0.198775	70.16961	16.31104
83.53483	1008	0.548191	3.225771	4.681941	6.386853	0.185688	208.7161	3.277799
7.60385	669	1.600466	2.392645	3.136169	6.414307	0.191226	205.9091	12.92076
29.05757	823	-0.02105	2.148825	4.428218	3.591217	0.189371	139.2051	13.59589
63.43444	803	6.522197	3.542235	3.771112	3.599432	0.181169	163.1859	10.63653
26.58698	950	4.772573	3.277923	3.672466	3.55845	0.184297	138.7941	1.765055
50.20385	610	3.569422	3.963295	3.025764	6.587973	0.196903	68.01577	9.909979
76.65186	781	-0.09354	3.84634	3.418862	5.565014	0.195755	156.2628	7.549397
84.55157	993	4.989084	3.569456	4.416372	3.085068	0.194816	107.9237	1.666932
67.1802	1025	4.17874	2.508346	3.527418	3.934952	0.194975	100.8943	8.755981
53.89726	831	6.95123	3.467961	4.49956	4.606188	0.190815	151.7233	5.077758
38.09796	1181	1.92319	4.146958	2.181014	2.524171	0.183911	195.7473	2.31435
75.64195	1167	5.311768	3.229316	4.832061	4.218889	0.181334	53.04824	9.244764
42.08143	837	3.368609	3.20608	2.888988	2.225626	0.193466	80.69137	14.55868
98.59779	1034	1.7252	2.935949	2.382447	2.876768	0.204894	125.3574	7.204307
84.21191	586	6.992271	3.322165	2.700549	6.458246	0.20821	134.179	6.473681
19.50522	1261	2.889141	2.414207	2.221166	6.284263	0.190963	77.09512	2.32544
17.23983	814	1.606037	2.306221	2.375481	5.173055	0.20115	100.5538	5.692321
62.37033	943	4.635731	4.072977	4.118093	5.668937	0.182112	31.71453	12.73982
33.08866	963	4.979373	3.945174	3.202006	4.684366	0.193511	171.2342	15.32394
41.31268	1252	5.752168	2.713092	2.952398	4.063902	0.205347	162.9881	4.892434
99.96341	1153	6.361102	3.297756	3.351471	2.817627	0.190933	161.3379	12.51511
12.14202	535	2.720556	2.819902	3.178805	6.467994	0.189673	50.63814	5.457295
61.46695	977	4.334398	2.463814	2.354202	6.836698	0.19676	109.3384	5.409362
84.57476	827	5.890771	3.739662	2.662929	5.517108	0.208581	24.859	11.06412
89.46865	805	0.828615	3.051833	3.907445	6.303145	0.20418	118.6594	10.28537
52.70163	1189	7.173981	2.661844	2.344563	4.025641	0.190287	131.1085	17.03166
25.2812	766	3.434747	2.360267	3.671202	5.749266	0.186662	183.9969	8.697844
52.71759	720	4.406693	3.125827	4.786413	4.006108	0.20226	88.64405	7.023187
55.94273	811	0.083956	3.668851	4.288113	5.998882	0.182267	190.5699	15.69241
86.14762	1018	0.788904	3.686798	3.617282	2.380114	0.209245	141.2816	12.81611
99.86716	1010	5.321986	2.32316	5.184604	3.866187	0.19766	65.84468	9.79602
15.59766	571	1.343687	4.001437	3.102128	3.265481	0.204919	210.526	3.948374
69.80585	1096	1.316696	2.334135	2.289868	2.409488	0.202	132.6953	7.70399
95.13009	1087	1.854569	3.527352	4.605962	5.773216	0.195059	42.56629	9.105879
66.12361	584	2.938964	2.265651	2.61338	6.242747	0.204573	79.82805	9.124649

59.59277	1095	3.157464	4.067085	5.053062	6.029405	0.207079	102.6269	1.795917
74.55934	1061	3.771644	2.934725	4.373115	4.336347	0.196396	152.2146	8.22806
26.66861	1216	-0.35783	2.602357	4.012677	4.871213	0.202489	126.8328	13.37031
26.82468	1100	3.865475	2.259436	4.874233	4.273796	0.184799	128.4024	13.76363
28.55254	1095	0.819526	3.95483	2.679573	4.709954	0.189902	86.28694	3.028584
93.69793	1194	6.727788	2.587101	3.900347	5.231592	0.18434	75.65868	1.302512
25.06012	485	2.734583	3.897041	2.198538	6.053814	0.192601	152.9712	6.099776

yDirect